Spin-orbit coupling effects, interactions and superconducting transport in nanostructures

Inaugural-Dissertation

zur Erlangung des Doktorgrades der
Mathematisch-Naturwissenschaftlichen Fakultät
der Heinrich-Heine-Universität Düsseldorf

vorgelegt von

Andreas Schulz

aus Leverkusen-Schlebusch

Düsseldorf, Mai 2010

Aus dem Institut für Theoretische Physik IV
der Heinrich-Heine-Universität Düsseldorf

Referent: Prof. Dr. Reinhold Egger
Koreferent: Prof. Dr. Dagmar Bruß

Tag der mündlichen Prüfung:

This thesis is based on the following original articles:

- Chapter 2

  Effective low-energy theory and spectral function of interacting carbon nanotubes with spin-orbit coupling,
  Andreas Schulz, A. De Martino, Reinhold Egger, (arXiv:1003.3495, Submitted to Phys. Rev. B)

- Chapter 3

  Low-energy theory and RKKY interaction for interacting quantum wires,
  Andreas Schulz, A. De Martino, Reinhold Egger, Phys. Rev. B **79**, 205432 (2009)

- Chapter 4

  Critical Josephson current through a bistable single-molecule junction,
  Andreas Schulz, Alex Zazunov, Reinhold Egger, Phys. Rev. B **79**, 184517 (2009)

- Chapter 5

  Josephson-current induced conformational switching of a molecular quantum dot,
  A. Zazunov, A. Schulz, R. Egger, Phys. Rev. Lett. **102**, 047002 (2009)

The following article was not included in this thesis

- *Electron-electron interaction effects in quantum point contacts*,
  A.M. Lunde, A. De Martino, A. Schulz, R. Egger, K. Flensberg, New J. Phys. **11**, 023031 (2009)

Summary

In the present thesis we study the electronic properties of several low dimensional nanoscale systems. In the first part, we focus on the combined effect of spin-orbit coupling (SOI) and Coulomb interaction in carbon nanotubes (CNTs) as well as quantum wires. We derive low energy theories for both systems, using the bosonization technique and obtain analytic expressions for the correlation functions that allow us to compute basically all observables of interest. We first focus on CNTs and show that a four channel Luttinger liquid theory can still be applied when SOI effects are taken into account. Compared to previous formulations, the low-energy Hamiltonian is characterized by different Luttinger parameters and plasmon velocities. Notably, the charge and spin modes are coupled. Our theory allows us to compute an asymptotically exact expression for the spectral function of a metallic carbon nanotube. We find modifications to the previously predicted structure of the spectral function that can in principle be tested by photoemission spectroscopy experiments. We develop a very similar low energy description for an interacting quantum wire subject to Rashba spin-orbit coupling (RSOC). We derive a two component Luttinger liquid Hamiltonian in the presence of RSOC, taking into account all e-e interaction processes allowed by the conservation of total momentum. The effective low energy Hamiltonian includes an additional perturbation due to intraband backscattering processes with band flip. Within a one-loop RG scheme, this perturbation is marginally irrelevant. The fixed point model is then still a two channel Luttinger liquid, albeit with a non standard form due to SOI. Again, the charge and spin mode are coupled. Using our low energy theory, we address the problem of the RKKY interaction in an interacting Rashba wire. The coupling of spin and charge modes due to SO effects implies several modifications, e.g. the explicit dependence of the power-law decay exponent of the RKKY Hamiltonian on both RSOC and interaction strength and an anisotropic range function.

In the second part of this thesis we focus on the study of superconducting transport in a quantum dot Josephson junctions coupled to a two-level system, which serves as a simple model for a conformational degree of freedom of a molecular dot or a break junction. We first address the limit of weak coupling to the leads and calculate the critical current through the junction perturbatively to lowest non-vanishing order in the tunneling couplings, allowing for arbitrary charging energy U and TLS parameters. We show that the critical current can change by orders of magnitude due to the two-level system. In particular, the π-junction behavior, generally present for strong interactions, can be completely suppressed.

We also study the influence of the Josephson current on the state of the TLS in the regime of weak charging energy. Within a wide range of parameters, our calculations predict that the TLS is quite sensitive to a variation of the phase difference φ across the junction. Conformational changes, up to a a complete reversal, can be induced by varying φ. This allows for the dissipationless control (including switching) of the TLS.

Contents

1. Introduction

The subject of this thesis is the study of the electronic properties of a number of low dimensional systems. The typical size of those nanoscale or mesoscopic systems is of the order of a few up to hundreds of nanometers. Situated between the microscopic world of atoms and the macroscopic world, they can be thought of as being so small that quantum effects dominate their behaviour, but large enough that it is not feasible to describe them taking every single particle into account. Due to their size, interactions quite often play an important role. Interactions will also be the recurrent theme or unifying principle of this thesis. While electrons in an ordinary three dimensional metal can be viewed as if they they where effectively free, this often changes when electronic motion is bounded in one, two or three spatial dimensions, forming 2-dimensional electron gases, quantum wires or quantum dots, respectively. In such systems, the effects of electron-electron interactions manifest in various ways.

In one-dimensional systems, interactions often induce Luttinger-liquid behaviour. In quantum dots, a charging energy has to paid in order to place two electrons on the dot, causing e.g. Coulomb-blockade phenomena or the reversal of the supercurrent through a quantum dot , to name but a few.

Interacting one-dimensional metals subject to spin-orbit interaction

First we will focus on one dimensional systems. Constraining electrons to (effectively) one dimension can cause them to loose their "individuality" and the *low-energy* physics is then dominated by collective excitations. At the heart of this astonishing phenomenon is the different way in which electron-electron *interactions* work in one dimension. At least as surprising as the emergence of collective behaviour is the fact that these excitations can be grouped into those that carry the charge- and those that carry the spin degrees of freedom (which are properties of each individual electron in higher dimensions) and that those excitations *travel at different speeds*, a phenomenon dubbed *spin-charge-separation*. Counter to intuition, the reduction of (geometric) dimensionality does not make the physics simpler, but very different (or, to paraphrase P.W. Anderson: Sometimes even *less* is different).

This behaviour has been both theoretically predicted, as well as experimentally observed in several effectively one-dimensional nanoscale systems, two of which are carbon nanotubes and quantum wires. Carbon nanotubes are large molecules made up of carbon atoms that are arranged in a cylindrical structure. They can be thought of as graphene sheets rolled into a tube. Quantum wires can be fabricated e.g. by constraining electronic motion within two-dimensional interfaces in semiconductor heterostructures (e.g.

by application of gate electrodes). Common to both systems is that the confinement of the transverse coordinate leads to a discretization of the momentum in the transverse, but not the longitudinal direction. At low temperatures, all but the lowest "band" is occupied (the others are said to be "frozen out") and the system is an effectively one-dimensional one. The interaction between electrons in such effectively one-dimensional systems then gives rise to the aforementioned collective excitations.

The effect of another quantum phenomenon, namely the coupling between spin- and orbital angular momenta, in such one-dimensional, strongly-correlated systems, has recently attracted much interest. While *spin-orbit coupling* (SOI) is a one-body coupling and Coulomb interaction is a two-particle interaction, the study of their *combined* effect has produced a considerable body of theoretical and experimental research, motivated both by the challenge to research as well as possible technological applications, e.g. the possibility of electronic control over spin degrees of freedom.

One could phrase the question as follows: "If SOI couples the spin and the momentum of the individual electrons, and long-ranged Coulomb interactions cause collective phenomena in one-dimensional systems, especially spin-charge separation, what happens if both are combined?"

In the first part of this thesis, we will focus on that question. We shall present effective low-energy theories for carbon nanotubes and quantum wires subject to spin-orbit coupling in the second and third chapter, respectively. Despite the differences (e.g. in geometry and number of quantum labels) of the two systems, we find that within our approximations, the theoretical models describing them are very similar.

Each theory leads to a modified *Luttinger-liquid* description (see below) of the system, in which the spin and charge degrees of freedom are manifestly coupled and spin-charge separation is broken.

Our theory allows us to study the spectral properties of carbon nanotubes and we find modifications to the previously predicted structure of the spectral function due to the coupling. Those additional features could, in principle, be experimentally observed.

In the third chapter, we apply our formalism to the study of the effective interaction between magnetic (spin $\frac{1}{2}$) impurities in the wire. We find modifications in the range function of the interaction that depend on the combined effects of spin-orbit and electron-electron interactions. In the limits of vanishing SOI or Coulomb interaction, our theory recovers the results of previous works that studied the two effects separately. We mention that chapter three builds upon Ref. [23], where the crucial Eq. (3.30) was derived. We provide an abbreviated derivation to provide necessary context.

Quantum-dot Josephson junctions coupled to a two-level system

If two superconductors are electrically connected by a weak link, e.g., a tunnel barrier or a single molecule, a dissipationless current can flow, carried by (Cooper) pairs of electrons with twice the elementary charge and opposite momenta. This current is not driven by an externally applied voltage, but by the difference between the phases of the superconducting order parameter in the bulk electrodes (or leads).

The ongoing research on such *Josephson junctions* is driven by substantial interest to experimental and theoretical solid state physics, as well as the promise of technological innovation. In situations where a single level or *quantum dot*, is available for tunneling into and out of the insulating region, the relation between the current and the phase difference can be strongly affected. For example, when the Coulomb interaction on the dot is large enough to be relevant, the current can be reversed by tuning a gate voltage applied to the dot, an effect commonly referred to as π-phase behaviour.

In the fourth and fifth chapter, we investigate the effect of a two-level system (TLS), representing a simple model for the conformational degree of freedom of the contacting molecule, coupled to the charge of the quantum dot.

In the fourth chapter, we focus on the case where the coupling to the leads is weak compared to the superconducting gap and Coulomb repulsion is strong. We derive the critical current by perturbation theory to lowest non-vanishing order in the tunneling amplitude and find that the π-junction behaviour can be strongly affected, even completely suppressed by the coupling to the two-level system.

In the last chapter of this thesis, we take the opposite viewpoint and focus on the influence of the Josephson current on the two state system in the limit of weak or vanishing Coulomb repulsion. We find that the Josephson current can induce changes in the state of the TLS, suggesting the possibility of dissipationless switching of the conformational degree of freedom. Throughout this thesis, we use $\hbar = e = k_B = 1$, unless noted otherwise.

2. Low-energy theory and spectral function of interacting CNTs with SOI

2.1. Introduction

Carbon nanotubes have been the subject of intense theoretical and experimental activity in recent years due to their exotic properties. Particularly fascinating from a theoretical physicist point of view is the fact that electrons of the conducting π-band of long CNTs can be described as Luttinger liquid, an electronic phase that arises due to interactions in (effectively) one-dimensional electron systems. Luttinger liquids share few of the properties of the Fermi-liquid, their higher dimensional counterpart.

The effects of electron-electron interactions in dimensions higher than one can be described by Landau's Fermi-liquid theory. It states that the properties of a system of interacting electrons remain similar to those of a system of free fermion particles. Interactions in fact essentially only "dress" electrons by a cloud of density fluctuations. The resulting "quasiparticles" can be considered as basically free. The physical principle which underlies this picture is the so-called principle of adiabatic continuity.

In one dimension, however, Fermi-liquid theory breaks down. One can easily imagine that in one dimension, interactions have much more drastic effects compared to higher dimensions. An electron that tries to propagate in a 1D system cannot do so without pushing its neighbors due to electron-electron interactions. Consequently, only collective excitations, namely density fluctuations, the so-called plasmons, can exist. This somewhat pictorial argument illustrates that in one dimension the concept of individual quasiparticles doesn't work.

It makes even less sense, if one considers fermions with spin. Since only collective excitations can exist, an individual fermionic excitation splits into a density fluctuation carrying charge, and another carrying spin. Since those fluctuations generally have different velocities, an individual electron will 'break' into a spin-density wave and a charge-density wave, an effect called *spin-charge separation* (SCS). Another exotic property of an interacting, one-dimensional metal is that because the density waves are gapless bosonic modes, correlation functions decay as power laws with exponents depending on the interaction.

These properties are the defining features of the so-called Luttinger-liquid (see, for example [1]). The individual electron in a Luttinger liquid is expressed as superposition of

bosonic excitations, the density fluctuations. The mathematical tool that allows the mapping between fermionic single particle operators and bosonic fields is called bosonization.

Luttinger liquid (LL) behavior has been predicted e.g. for metallic single-wall nanotubes (SWNTs) [2]. Experimental evidence for this strongly correlated phase has been reported using quantum transport [3] and photoemission spectroscopy [4].

Recent advances in the fabrication of single-wall carbon nanotubes (SWNTs) have allowed to study ultraclean samples where the effects of the spin-orbit interaction (SOI) can be clearly observed [5]. SOI effects [6] are of great interest in the field of spintronics, and a detailed understanding of such couplings in SWNTs is both of fundamental and of technological interest, e.g., concerning a spin-qubit proposal based on nanotube dots [7]. The SOI in carbon nanotubes arises predominantly from the interplay of atomic SO coupling and curvature-induced hybridization (see below), and the bandstructure of spin-orbit coupled SWNTs has been clarified [8–14, 16, 17].

In this chapter we shall address the question of how the LL theory of interacting electrons in SWNTs [2] is modified when the SOI is taken into account.

The chapter is structured as follows: We will illustrate the derivation of an effective one-dimensional model [16] for the π electrons of a CNT that addresses SO-effects under a lowest-order $k \cdot p$ scheme in section 2.2. This model was originally proposed to explain experimentally observed asymmetries between electron and hole dispersion.

We will first focus on the simpler case of a nanotube without SOI and curvature effects for the benefit of the reader. We derive the $k \cdot p$ - Hamiltonian for a clean graphene sheet in Sec. 2.2.1 and show how the CNT dispersion readily emerges from this 2D system by imposing boundary conditions. Next, we focus on curvature and SO-effects in nanotubes. In Sec. 2.2.2, we briefly illustrate the derivation of the model of Ref. [16] and show how the curvature-assisted SOI contributions, especially the recently proposed "diagonal" terms, emerge in second order perturbation theory. This noninteracting model is the basis for our low-energy effective theory, which addresses SOI and electron-electron interaction effects in CNTs.

In section 2.3, we will linearize the dispersion relation of the model derived in the previous section around the Fermi points. We obtain a low-energy effective Hamiltonian, which can be written as a massless, one-dimensional Dirac Hamiltonian. This Hamiltonian is the kinetic part of a four-channel Luttinger model. In the next step, we will include electron-electron interactions into the model.

In section 2.4, we will map the fermionic model to a massless, bosonic theory using the bosonization technique. We shall derive our bosonic theory in some detail, first, in order to keep the treatment as self-contained as possible, and furthermore to establish a formalism that we can readily use in chapter 3. In the first subsection, we will map the fermionic Hamiltonian to a bosonic one, using two identities derived in Appendix B, which will be form the basis of our further treatment. This subsection also illustrates why bosonization such a popular technique in the cases it is applicable: While it is a formidable task to find exact, non-perturbative solutions to interacting fermionic models, especially strongly correlated ones, the corresponding bosonic model is exactly solvable. We represent the model in terms of total and relative charge and spin density modes, obtaining

a four-channel LL, in which charge- and spin-sectors are coupled. This Hamiltonian can be expressed in terms of its normal modes. In section 2.5, we use the transformation employed to diagonalize the Hamiltonian in order to obtain a general expression for two-point correlation functions, using the functional integral formalism (see also Appendix A). This expression allows us to readily compute basically all observables of interest and applies, with very few modifications, also to the model studied in the next chapter, despite the differences between both systems.

As an application, we compute the spectral function, which is the main result of this chapter. The combined effects of SOI and electron-electron interaction, more specifically, the broken spin-charge separation, cause modifications with respect to the standard case that should in principle be accessible to experiment. We give some conclusions in section 2.6.

For the interested reader, we establish a "bosonization dictionary" in Appendix B, i.e., we derive the core identities used in the first two chapters of this thesis while illustrating that the mapping from the fermionic to the bosonic theory does indeed produce the correct correlation functions and commutation relations.

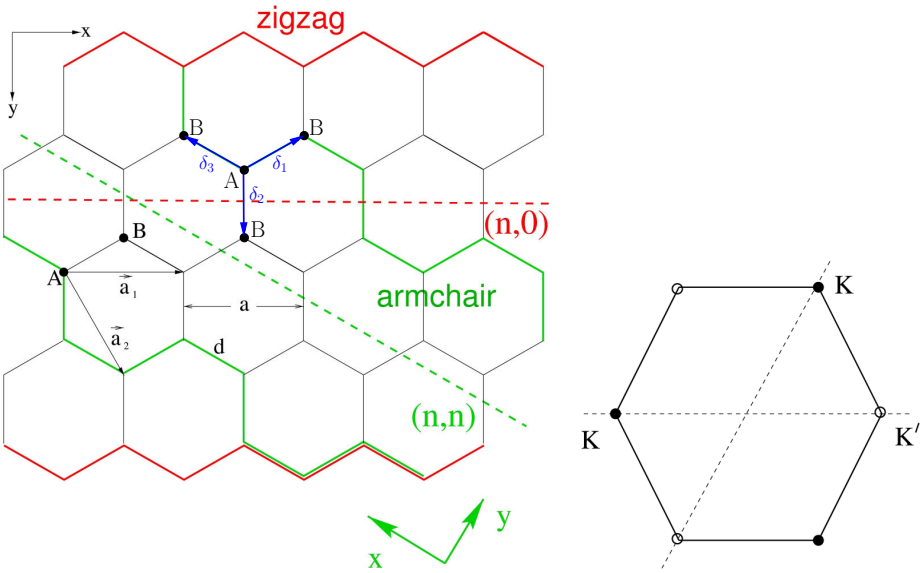

Figure 2.1: Graphene lattice and reciprocal lattice

2.2. Microscopic model for the CNT

In this section, we address the band structure of a metallic (n,m) SWNT. For completeness, we will first address the CNT without taking SOI and curvature effects into account in section 2.2.1. Starting from a simple tight-binding model on the lattice, we derive a single-particle continuum Hamiltonian for π electrons in flat graphene (cf. Eq.(2.3)) under a lowest order $k \cdot p$ scheme. Last, we shall show how the "wrapping" of the graphene sheet to a cylinder is described mathematically by imposing periodic boundary conditions around the SWNT circumference. Those boundary conditions imply a quantization of the transverse momentum, $k_\perp R = n \in \mathbb{Z}$ of the 2D graphene Hamiltonian, resulting in an effective 1D model .

In section 2.2.2, we will incorporate curvature and SOI effects into the model. We shall briefly illustrate the perturbative calculations of Ref. [16, 17], resulting in an effective SO Hamiltonian for π electrons derived in Ref. [16].

2.2.1. Carbon nanotubes without SOI and curvature

A carbon nanotube can be seen as a graphene sheet rolled into a cylinder. The left figure in Fig. 2.1 depicts the lattice structure of a 2D graphene sheet: The basis (unit cell) contains two atoms (leading to two sublattices A and B) and the basis vectors are given by

$$\vec{a}_1 = a\,(1,0)\,, \qquad \vec{a}_2 = a\left(\frac{1}{2}, -\frac{\sqrt{3}}{2}\right),$$

where $a = \sqrt{3}d$, and the interatomic distance is $d = 0.14$ nm. The sites of sublattice A are represented by the lattice vector $\vec{R} = n_1\vec{a}_1 + n_2\vec{a}_2$ and the three nearest neighboring atoms

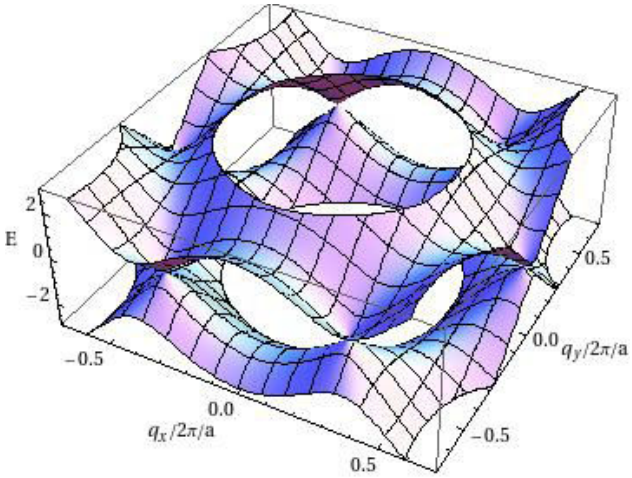

Figure 2.2: Dispersion of Graphene in the TB-model

on sublattice B are connected to the atom on sublattice A by the vectors

$$\vec{\delta}_{1/2} = \frac{a}{\sqrt{3}}\left(\pm\frac{\sqrt{3}}{2}, \frac{1}{2}\right), \quad \vec{\delta}_3 = \frac{a}{\sqrt{3}}(0,-1).$$

The reciprocal lattice is also a hexagonal lattice (cf. Fig. 2.1) with two distinguished points at the corners of the first Brillouin zone

$$K \to \vec{K}_1 = -\frac{4\pi}{3a}(1,0),$$
$$K' \to \vec{K}_2 = -\vec{K}_1.$$

There are numerous ways of wrapping a graphene sheet onto a cylinder, specified by the (n,m) indices. When rolling the graphene sheet, the atom at $\vec{L}[n,m] = n\vec{a}_1 + m\vec{a}_2$ has to coincide with the one at the origin. The angle between $\vec{L}[n,m]$ and $\vec{a}_1$ is the so-called *chiral angle* θ. For "zigzag" tubes $(n,0)$, $\theta = 0$, while for "armchair", (n,n), $\theta = \frac{\pi}{6}$, see Fig. 2.1. *Chiral* nanotubes have a chiral angle θ between 0 and 30 degrees.

Graphene: From tight-binding to Dirac-Weyl Hamiltonian

We start from the well-known tight-binding Hamiltonian for the graphene honeycomb lattice describing hopping of an electron at site $\vec{R} \equiv \vec{R}_A$ on sublattice A to it's nearest neighbors on sublattice B, where $\vec{R}_B = \vec{R} + \vec{\delta}_{l=1,2,3}$

$$H_0 = -t\sum_{\vec{R}}\sum_{\vec{\delta}}\left(c^{\dagger}_{\vec{R}+\vec{\delta},B}c_{\vec{R},A} + h.c.\right), \tag{2.1}$$

where $c_{\vec{R},A}$ creates an electron in sublattice A at site $\vec{R}$ in the p_z -orbital. The p_x, p_y and s -orbitals are hybridized and do not contribute to electron transport.

We then switch to a continuum description utilizing the so-called $k \cdot p$ scheme by expanding the electron operators near the (Dirac) K points

$$c_{\vec{R},p} \simeq e^{i\vec{K}\cdot\vec{R}}\psi_{1,p}\left(\vec{R}\right) + e^{-i\vec{K}\cdot\vec{R}}\psi_{2,p}\left(\vec{R}\right), \tag{2.2}$$

where $p = A,B$ denotes the sublattice and the valley index $\alpha = 1,2 = \pm$ denotes the Dirac points K and K'.

Note that since K and K' are proportional to the inverse of the lattice spacing a, the factors $e^{i\vec{K}\cdot\vec{R}}$ vary rapidly on the order of a scale of a, while the operators $\psi_{\alpha,p}\left(\vec{R}\right)$ can be regarded as *slowly varying* on the same scale. Hence, their (discrete) argument $\vec{R}$ can be treated as a *continuous variable*, i.e. the $\psi_{\alpha,p}\left(\vec{R}\right)$ can be considered as differentiable field operators that can be expanded in a Taylor series

$$\psi_{\alpha,p}\left(\vec{R}+\vec{\delta}\right) = \left[1 + \left(\vec{\delta}\cdot\vec{\nabla}\right) + \left(\vec{\delta}\cdot\vec{\nabla}\right)^2 + ...\right]\psi_{\alpha,p}\left(\vec{R}\right).$$

Furthermore, we can replace the sum by an integral in Eq.(2.2), i.e. $\sum_{\vec{R}} ... \to \int d^2\vec{R}....$ Substituting Eq. (2.2) into H_0 and summing over $\vec{\delta}$, we obtain

$$H_0 = v\sum_{\alpha=\pm}\int d^2\vec{R}\ \begin{pmatrix}\psi^\dagger_{\alpha,A} & \psi^\dagger_{\alpha,B}\end{pmatrix}\underbrace{\begin{pmatrix}0 & -\alpha i\partial_x + \partial_y\\ -\alpha i\partial_x - \partial_y & 0\end{pmatrix}}_{\equiv \mathscr{H}_0(\partial_x,\,\partial_y)}\begin{pmatrix}\psi_{\alpha,A}\\ \psi_{\alpha,B}\end{pmatrix}, \tag{2.3}$$

where $v = \frac{a\sqrt{3}}{2}t$ and we used the identities $\sum_{\vec{\delta}} e^{\pm i\vec{K}\cdot\vec{\delta}}\left(i\vec{\delta}\cdot\vec{q}\right) = -\frac{a\sqrt{3}}{2}\left(\pm q_x + i q_y\right)$ and $\sum_{\vec{\delta}} e^{i\vec{K}\cdot\vec{\delta}} = 1$ and their respective counterparts is coordinate space. The terms with factors $e^{\pm i2\vec{K}\vec{R}}$ vanish upon integration, because they vary rapidly on scale of a, while $\psi_{\alpha,p}$ does not. $\mathscr{H}_0$ has the form of a Dirac-Weyl Hamiltonian. The spectrum of $H_0\left(\vec{k}\right)$is conical,

$$E_0^{(\pm)}(q_x,q_y) \equiv \pm v\sqrt{q_x^2+q_y^2}. \tag{2.4}$$

which is a good approximation to the dispersion of the tight-binding model (see Fig. 2.2) up to energies of the order of $1eV$.

Wrapping the graphene sheet

We wrap the graphene sheet to a cylinder of radius $R = \frac{2\pi}{L}$ [1] along the chiral vector $\vec{L}$ with length $L = \left|\vec{L}\right|$. This imposes periodic boundary conditions $c_{\vec{R}+\vec{L},p} \overset{!}{=} c_{\vec{R},p}$ around the

[1] where $0 \le x < L = 2\pi R$ is the circumferential direction.

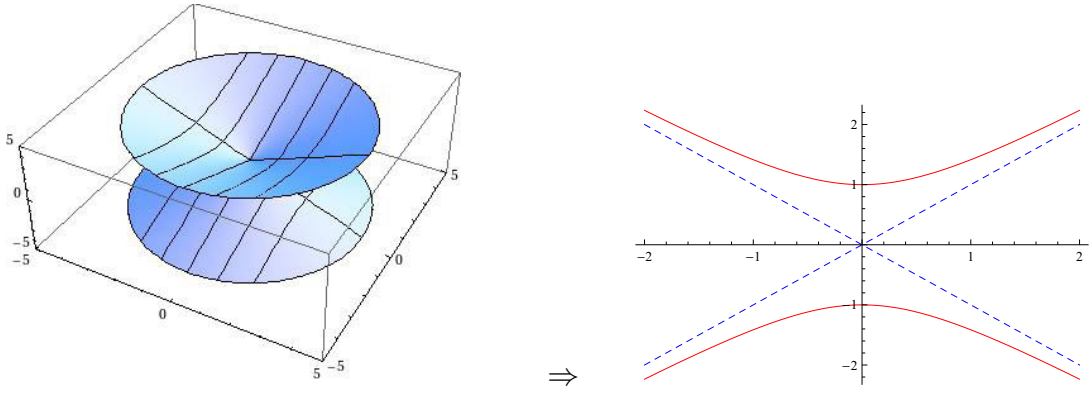

Figure 2.3: Rolling the tube

circumference leading to[2] (cf. Eq.(2.2))

$$\begin{aligned}\psi_{\alpha,p}\left(\vec{R}+\vec{L}\right) &\stackrel{!}{=} e^{-i\alpha\vec{K}\cdot\vec{L}}\psi_{\alpha,p}\left(\vec{R}\right)\\ &= e^{-i\alpha\frac{2\pi}{3}\nu}\psi_{\alpha,p}\left(\vec{R}\right),\end{aligned} \tag{2.5}$$

where $\nu = (2n+m)\ mod\, 3 = 0, \pm 1$. The fermionic operators describing electrons on the surface of the tube become effective 1D-operators:

$$\Psi_{\alpha p}(x,y) = \frac{1}{\sqrt{2\pi R}} e^{i q_x x}\psi_{\alpha p}(y),$$

because the transverse momenta q_x are quantized due to the periodic b.c.[3]

$$q_x^{(n,\nu)} = \frac{2\pi}{L}\left(n - \alpha\frac{\nu}{3}\right). \tag{2.6}$$

The single-particle Hamiltonian of the nanotube is now simply given $q_x^{(n,\nu)}$ into Eq.(2.3) Inserting the quantized coordinate q_x into Eq.(2.3) yields the spectrum of the effective 1D-model given by

$$E_0^{(\pm,n,\alpha)}(q_y) \equiv \pm\nu\sqrt{\left(\frac{2\pi}{L}\right)^2\left(n-\alpha\frac{\nu}{3}\right)^2 + q_y^2}, \tag{2.7}$$

which can be visualized easily (cf. Fig. 2.3) by conical sections. Note that even for the lowest band, $n = 0$, there is a band gap if $\nu = \pm 1$ and no bandgap for $\nu = 0$ (cf. right figure in Fig.2.3). Such nanotubes are respectively called *semiconducting* or *metallic*.

The "new" x- coordinate wraps around the tube counterclockwise with respect to the tube axis, described by the chiral angle $\theta = \tan^{-1}[\sqrt{3}m/(2n+m)]$. The tube radius is

[2] $\vec{K}\cdot\vec{L} = \frac{2\pi}{3a}(2n+m)$

[3] The integer n, specifying the transverse momentum, should not be confused with the wrapping index n.

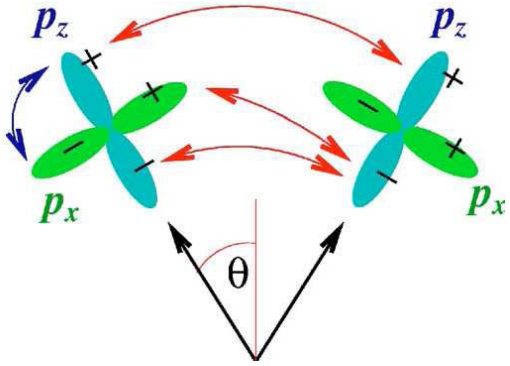

Figure 2.4: Sketch of the relevant orbitals. Figure taken from [13].

$R = \frac{L}{2\pi} = \frac{a}{2\pi}\sqrt{n^2+nm+m^2} \simeq 0.0391\sqrt{n^2+nm+m^2}$ nm. Note that a *chiral nanotube* (i.e. for $\theta \neq 0°, 30°$), is not inversion symmetric, since the "wrapping direction" of the new coordinate x changes if the longitudinal y coordinate is inverted.

Note that now that we have rolled the graphene sheet, there is a transverse direction and we shall change notation to reflect that fact

$$q_x, q_y \to k_\perp, k.$$

2.2.2. Carbon nanotube with SOI

Perturbations due to curvature and SOC

The single-particle Hamiltonian H_0 neglects the effects due to curvature of the nanotube surface. Furthermore, the effect of atomic spin-orbit interaction is not included.

Treating both as small perturbations, Ref. [16, 17] recently computed corrections to H_0 by using degenerate second order perturbation theory. We shall illustrate their findings following Ref. [17], a detailed derivation can be found e.g. in Ref. [16]. Special emphasis shall be put on the *curvature-assisted* SOI arising from a combination of both effects. While one resulting term was already derived by e.g. Ref. [8], a SOI-contribution that is diagonal in the sublattice index was not previously predicted. As we shall see in later sections, this contribution is crucial to our low-energy treatment of a CNT.

In flat graphene, there is no hybridization between p_z- and the s, p_x, p_y-orbitals at adjacent sites. This is because the Hamiltonian is invariant under reflection in the graphene (x, y) plane, while the p_z orbital is odd under the same transformation and the other orbitals are even. Curvature due to rolling the graphene sheet into a nanotube breaks that symmetry, cf. Fig. 2.4. The p_z orbitals are then "miss aligned" with respect to the s, p_x, p_y at adjacent sites and the matrix elements describing hopping between p_z-orbitals on one site (say at $\vec{R}_A$) into an s, p_x or p_y - orbital at the three *adjacent sites* (i.e. at $\vec{R}_B = \vec{R}_A + \vec{\delta}$) are now finite.

This is expressed by the operator H_{curv}, which, to leading order in $\frac{a}{R}$, reads (cf. [17])

$$H_{curv} = \sum_{\sigma=\uparrow,\downarrow} \sum_{\vec{R}_A,\vec{\delta}} \sum_{l=s,x,y} g_l\left(\vec{\delta}\right)\left[c^{\dagger}_{z\sigma}\left(\vec{R}_A\right) c_{l\sigma}\left(\vec{R}_A+\vec{\delta}\right)\right.$$
$$\left. -(-1)^{\delta_{l,s}} c^{\dagger}_{l\sigma}\left(\vec{R}_A\right) c_{z\sigma}\left(\vec{R}_A+\vec{\delta}\right)+h.c.\right].$$

The parameters $g_l\left(\vec{\delta}\right)$ are of the order $\frac{a}{R}$ (the angle between the surface normals at two neighboring carbon atoms on the CNT) and can be computed from geometric considerations [16, 17].

Consider next the spin-orbit Hamiltonian given by $H_{SO} = V_{SO}\sum_{\vec{R}} \vec{L}_{\vec{R}} \cdot \vec{S}_{\vec{R}}$, where $\vec{L}_{\vec{R}}$ ($\vec{S}_{\vec{R}}$) is the atomic orbital (spin-) angular momentum at site $\vec{R}$. Its tight-binding Hamiltonian can be expressed as (cf. [17])

$$H_{SO} = V_{SO} \sum_{\vec{r}=\vec{R}_{A/B}} \sum_{\sigma=\uparrow,\downarrow} \left(c^{\dagger}_{z\sigma}\left(\vec{r}\right)\left(i\sigma_3\right)_{\sigma,\sigma'} c_{x,\sigma'}\left(\vec{r}\right)\right)+h.c.,$$

where $c_{(x,y,z),\sigma}\left(\vec{r}\right)$ destroys an electron in the $p_{x,y,z}$ orbital at site $\vec{r}$ and σ_3 is the third Pauli-matrix. Note that H_{SO} contains hopping between p_z and $p_{x,y}$-bands at the *same* lattice site.

It is obvious that SOC does not contribute to corrections to the π-bands in first order perturbation theory, since it causes *interband transitions* from π to σ bands (p_z to p_x, p_y or s-orbitals). The next-leading order contribution (to the effective SOC) is given by the second-order perturbation Hamiltonian:

$$H^{\alpha,(2)}_{C-SO} = H_{curv}\frac{\mathscr{P}^{\alpha}}{E^{\alpha,(0)}-\hat{H}^{\alpha,(0)}}H_{SO},$$

where $H^{\alpha,(0)}$ describes the $\sigma-$ and $\pi-$bands without both curvature and SOC. The projector $\mathscr{P}^{\alpha} = 1-\sum_{\sigma}\left|\psi^{(\alpha)}_{0,\sigma}\right\rangle\left\langle\psi^{(\alpha)}_{0,\sigma}\right| = \sum_{\sigma}\left|\psi^{(-\alpha)}_{0,\sigma}\right\rangle\left\langle\psi^{(-\alpha)}_{0,\sigma}\right|$, where $\left|\psi^{(\alpha)}_{0,\sigma}\right\rangle$ are eigenstates of $H^{\alpha,(0)}$, excludes states corresponding to $E^{\alpha,(0)}$ from the summation (inserting resolutions of unity over intermediate states of the unperturbed Hamiltonian then gives the usual second order-formula). Let us mention in passing that those eigenstates are not states localized on one particular sublattice, but are linear combinations of such states. Hence, $\mathscr{P}^{\alpha}$ will contain terms that conserve the sublattice-index, as well as terms that flip it.

Summarizing, we can say that:

- H_{SO} describes interband coupling that preserve sublattice index ($\pi_A \longleftrightarrow \sigma_A$ and $\pi_B \longleftrightarrow \sigma_B$). Its coupling constant is V_{SO}.

- H_{curv} describes interband coupling that exchange sublattice index ($\pi_A \rightarrow \sigma_B$ and $\pi_B \rightarrow \sigma_A$). Its coupling constant is $\frac{a}{R}$

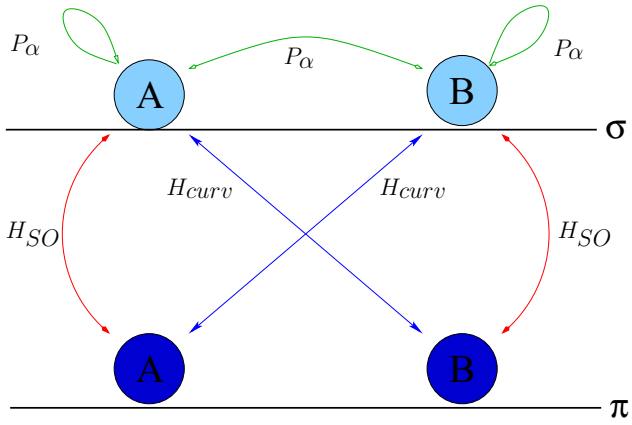

Figure 2.5: Schematic of second order processes. Red and blue lines denote interband transitions (between π and σ bands) due to SOC and curvature, respectively. Green lines denote symbolize interband "transitions".

- $\frac{\mathscr{P}^\alpha}{E^{(0)}-H^{\alpha,(0)}}$ contains terms ("$\rightleftharpoons$") that may exchange ($\sigma_{A/B} \overset{\mathscr{P}^\alpha}{\rightleftharpoons} \sigma_{B/A}$) or preserve ($\sigma_{A/B} \overset{\mathscr{P}^\alpha}{\rightleftharpoons} \sigma_{A/B}$) sublattice index.

This can be visualized by Fig. 2.5. The possible processes due to $H^{\alpha,(2)}_{C-SOC}$ are then:

1. An interband transition from π to σ that preserves sublattice index, due to SOC, an intraband "transition" that also preserves sublattice index, followed by a transition from σ back to π band due to H_{curv} which flips the sublattice index.

$$\pi_A \overset{H_{SO}}{\longleftrightarrow} \sigma_A \rightleftharpoons \sigma_A \overset{H_{curv}}{\longleftrightarrow} \pi_B \tag{2.8}$$

   This "off-diagonal" curvature-assisted SOC transition is proportional to $V_{SO}\frac{a}{R}$.

2. The same process as before, but with an intermediate change of sublattice index due to a intraband "transition":

$$\pi_A \overset{H_{SO}}{\longleftrightarrow} \sigma_A \rightleftharpoons \sigma_B \overset{H_{curv}}{\longleftrightarrow} \pi_A \tag{2.9}$$

   This "diagonal" curvature-assisted SOC transition is also proportional to $V_{SO}\frac{a}{R}$.

The term $H^{\alpha,(2)}_{SO-SO} = H_{SO}\frac{\mathscr{P}^\alpha}{E^{(0)}-\hat{H}^{\alpha,(0)}}H_{SO}$ is small compared to $H^{\alpha,(2)}_{C-SO}$ according to Ref. [17] and shall be disregarded here. Similarly, one may construct second-order curvature corrections $H^{\alpha,(2)}_{curv} = H_{curv}\frac{\mathscr{P}^\alpha}{E^{(0)}-H^{\alpha,(0)}}H_{curv}$ that lead to processes

$$\pi_A \overset{H_{curv}}{\longleftrightarrow} \sigma_A \rightleftharpoons \sigma_A \overset{H_{curv}}{\longleftrightarrow} \pi_B \tag{2.10}$$

which are proportional to $\left(\frac{a}{R}\right)^2$. The final result of this analysis is the following effective SO Hamiltonian for π electrons [16]

$$H_0^{(\alpha,\sigma)}(k) = \begin{pmatrix} \alpha\sigma E_{\rm SO} & -\alpha\hbar v_F[\phi_\perp + i(k+\alpha\phi_\parallel)] \\ -\alpha\hbar v_F[\phi_\perp - i(k+\alpha\phi_\parallel)] & \alpha\sigma E_{\rm SO} \end{pmatrix}. \tag{2.11}$$

Using the parameter estimates of Ref. [16], the diagonal term arising from Eq.(2.9) is

$$E_{\rm SO}[\text{meV}] \simeq -\frac{0.135\cos(3\theta)}{R[\text{nm}]}. \tag{2.12}$$

Writing $\phi_\perp = \phi_{\perp,\rm SO} + \phi_{\perp,\rm cur}$, the SOI (cf. Eq. (2.8)) corresponds to a spin-dependent shift of the transverse momentum [5, 13, 16],

$$\phi_{\perp,\rm SO}[\text{nm}^{-1}] \simeq \alpha\sigma\frac{2.7\times10^{-4}}{R[\text{nm}]}, \tag{2.13}$$

while curvature effects [16, 18] give (cf. Eq.(2.10))

$$\phi_{\perp,\rm cur}[\text{nm}^{-1}] \simeq \frac{0.011\cos(3\theta)}{(R[\text{nm}])^2}, \tag{2.14}$$

$$\phi_\parallel[\text{nm}^{-1}] \simeq \frac{0.045\sin(3\theta)}{(R[\text{nm}])^2}. \tag{2.15}$$

It is worth pointing out that for zigzag nanotubes, the effect of curvature assisted SOI is strongest and that it vanishes for armchair nanotubes.

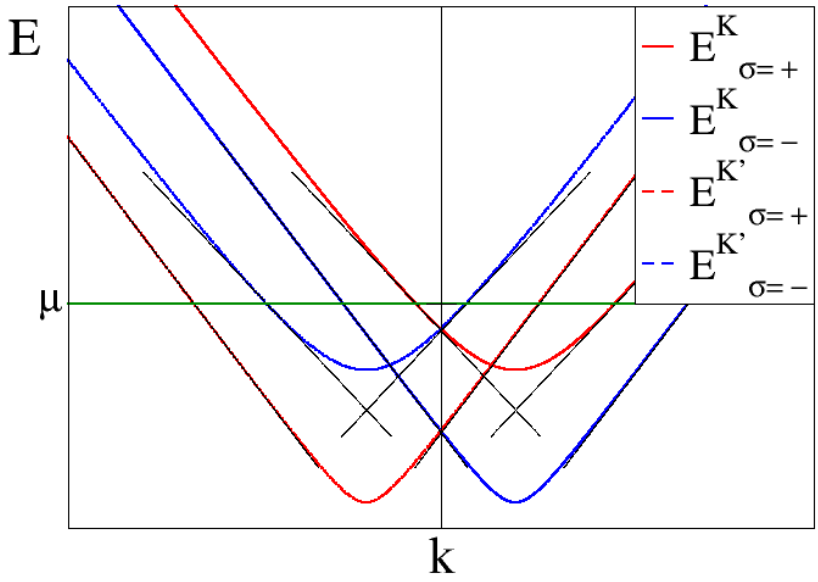

Figure 2.6: Dispersion for metallic ($\nu = 0$) nanotube.

2.3. Luttinger model for the interacting CNT

In our low-energy theory, we assume a Fermi energy $E_F > 0$ but small enough such that only the $n = 0$ band has to be taken into account. All other bands are then separated by an energy gap $\approx \hbar v_F/R \approx 1$ eV, where $v_F \approx 8 \times 10^5$ m/s. The dispersion relation obtained from Eq. (2.11) is

$$E_{\pm}^{(\alpha,\sigma)}(k) = \alpha\sigma E_{\mathrm{SO}} \pm \hbar v_F \sqrt{\phi_{\perp}^2 + (k + \alpha\phi_{\parallel})^2}, \tag{2.16}$$

where the Kramers degeneracy is reflected in $E_{\pm}^{(\alpha,\sigma)}(k) = E_{\pm}^{(-\alpha,-\sigma)}(-k)$, see Fig. 2.6. Since $E_F > 0$, only the conduction bands (positive sign) are kept, and the Fermi momenta $k_{r\alpha\sigma}^{(F)}$ for right- and left-movers ($r = R/L = \pm$) follow from $E_{+}^{(\alpha,\sigma)}\left(k_{r\alpha\sigma}^{(F)}\right) = E_F$, $k_{r\alpha\sigma}^{(F)} \approx r(E_F - \alpha\sigma E_{\mathrm{SO}})/\hbar v_F - \alpha\phi_{\parallel}$. Under a low-energy approach, we linearize the dispersion relation around the Fermi points, always assuming that E_F is sufficiently far away from the band bottom:

$$E_{+}^{(\alpha,\sigma)}(k_{r\alpha\sigma}^{(F)} + q) - E_F = \hbar r\, v_{\alpha,\sigma}\, q + \mathscr{O}\left(q^2\right), \tag{2.17}$$

The 1D Fermi velocities $v_{\alpha,\sigma} = \hbar^{-1}\partial_k E_{+}^{(\alpha,\sigma)}\left(k = k_{+,\alpha\sigma}^{(F)}\right)$ then take only two different values, $v_A \equiv v_{-,\uparrow} = v_{+,\downarrow}$ and $v_B \equiv v_{+,\uparrow} = v_{-,\downarrow}$. We mention in passing that R/L movers

have pairwise identical velocities only in the absence of trigonal warping and orbital magnetic fields [19] or transverse fields [20], as assumed here. The fermionic single-particle Hamiltonian can then be written in the language of second quantization as:

$$\begin{aligned} H_0 &= \sum_{\alpha r \sigma} \int \frac{dk}{2\pi} E_+^{(\alpha,\sigma)}(k)\, c_{\alpha\sigma}^\dagger(k)\, c_{\alpha\sigma}(k) \\ &\simeq \hbar \sum_{\alpha r \sigma} \int_{-\Lambda}^{+\Lambda} \frac{dq}{2\pi}\, (r v_{\alpha,\sigma} q)\, c_{\alpha\sigma r}^\dagger(q)\, c_{\alpha\sigma r}(q) \end{aligned} \tag{2.18}$$

where the operator $c_{\alpha\sigma r}(q) \equiv c_{\alpha\sigma}\left(k_{\alpha\sigma r}^{(F)} + q\right)$ obeys the canonic anti-commutation relations $\left\{c_{\alpha\sigma r}(q), c_{\alpha'\sigma' r'}^\dagger(q')\right\} = 2\pi\delta_{\alpha,\alpha'}\delta_{\sigma,\sigma'}\delta_{r,r'}\delta(q-q')$ and the momentum-cutoff Λ has been included to mimic the finite bandwidth. Note that $q \ll k_{r\alpha\sigma}^{(F)}$. Lastly, we write H_0 in coordinate space for later reference (from now on, we set $\hbar = 1$ again)

$$H_0 = \sum_{\alpha r \sigma} \int dx\, \psi_{\alpha r\sigma}^\dagger\, (-i r v_{\alpha\sigma}\, \partial_x)\, \psi_{\alpha r\sigma}, \tag{2.19}$$

where we defined the field operator

$$\psi_{\alpha r\sigma}(x) = \int_{-\Lambda}^{+\Lambda} \frac{dq}{2\pi}\, e^{iqx} c_{\alpha\sigma r}(q),$$

that obeys anti-commutation relations $\left\{\psi_{\alpha\sigma r}(x), \psi_{\alpha'\sigma' r'}^\dagger(x')\right\} = \delta_{\alpha,\alpha'}\delta_{\sigma,\sigma'}\delta_{r,r'}\delta(x-x')$.

2.3.1. Including Interaction

Electrons in carbon nanotubes interact via Coulomb repulsion. We include only the important *forward scattering* processes (in the literature, those are often denoted as g_4-process), since electron-electron backscattering effects in SWNTs are tiny and disregarded here [2].

Forward scattering means that each of the two electrons that are scattered is transfered from a state on one branch of the linearized dispersion[4] (cf. Fig. 2.6) into another state on the same branch. Consequently, the interaction Hamiltonian for processes of this type contains only products of the type $\rho_\nu \rho_\mu = \psi_\nu^\dagger \psi_\nu \, \psi_\mu^\dagger \psi_\mu$, where ν, μ denote the respective Fermi-momenta. Such products also lead to a convenient form after bosonization, see section 2.4.

Processes that scatter an electron from, say, a branch on the right side of the dispersion to one on the left (and also do conserve total momentum), are called *backscattering* processes. If such processes turn out to be relevant, the model cannot be described as a Luttinger liquid.

In-depth analysis of the relevance of such processes in CNTs has been performed and shall not be repeated here. Moreover, we stay away from half-filling such that Umklapp scattering processes also play no role. The interaction Hamiltonian for forward-scattering processes in a CNT can be written as.

$$H_I^{(F)} = \frac{V_0}{2} \sum_{\alpha\sigma r} \sum_{\alpha'\sigma' r'} \int dx \, \rho_{\alpha\sigma r}(x) \, \rho_{\alpha'\sigma' r'}(x) \tag{2.20}$$

where[5] $\rho_{\alpha\sigma r} =: \psi^\dagger_{\alpha\sigma r} \psi_{\alpha\sigma r} :$ and V_0 denotes the zero-momentum Fourier-component of the interaction potential. For a detailed explanation of electron-electron interaction in 1D-systems, see [1, 21], for a rigorous (RG-) treatment of interaction-, especially the relevance of backscattering-processes in CNTs, cf. [2].

[4] In dimensions higher than one the Fermi-surface, is a continuum. E.g. in 2D, a free electron at low temperature is restricted to states close to the Fermi-energy E_F and the modulus of its momentum $\vec{k}_1$ has to be close to k_F: $\left|\vec{k}_1\right| \simeq k_F$. Its direction, however, is not fixed by any constraint. Also, it can only be scattered into a state with momentum $\vec{k}_2$ where $\left|\vec{k}_2\right| \simeq k_F$. Since the direction of both momenta is not restricted, the modulus of the transfered momentum $\vec{q} \equiv \vec{k}_1 - \vec{k}_2$ can be in a continuous range between zero and $2k_F$. In 1D, the Fermi-surface becomes a set of discrete points and this freedom to "play with the angles" is lost. An electron can only be scattered out of a region close to one Fermi-Point into a region close to another. For a single-branch model, e.g., the transfered momentum q can only be zero (forward scattering) or $2k_F$(backscattering).

[5] The normal ordering of two operators amounts to subtracting the vacuum expectation value $: AB := AB - \langle AB \rangle$.

2.4. Bosonization

Diagonalizing (and thereby solving) a single-particle fermionic Hamiltonian is always possible, since it is bilinear in fermionic operators. The interaction terms, however, are *quartic* in fermion operators, and therefore non-perturbative analytic solutions to interacting problems are scarce. The so called Luttinger-liquids (to which our model belongs) are a class of interacting models that can be mapped to a simpler, noninteracting model. Using abelian bosonization [1], which allows for a nonperturbative inclusion of interactions, we are able to map the contributions from both the single-particle Hamiltonian and the interactions[6]:

$$\begin{aligned} H_0^{(F)} + H_I^{(F)} = & \sum_{\alpha r \sigma} \int dx : \psi^\dagger_{\alpha\sigma r} \left(-irv_{\alpha\sigma}\,\partial_x\right) \psi_{\alpha\sigma r} : \\ & + \frac{V_0}{2} \sum_{\alpha\sigma r} \sum_{\alpha'\sigma' r'} \int dx \, : \psi^\dagger_{\alpha\sigma r} \psi_{\alpha\sigma r} : (x) : \psi^\dagger_{\alpha'\sigma' r'} \psi_{\alpha'\sigma' r'} : (x) \end{aligned} \tag{2.21}$$

to a bosonic Gaussian (i.e. quadratic) field theory, which is *exactly* solvable.

2.4.1. Chiral fields and the bosonic Hamiltonian

At the heart of the bosonization technique is the notion that fermionic operators $\psi_{\alpha\sigma r}(x)$ can be written in terms of (*chiral*) bosonic fields $\phi_{\alpha\sigma r}(x)$ and *Klein factors* $\eta_{\alpha\sigma r}$ (see below):

$$\psi_{\alpha\sigma r}(x) = \frac{\eta_{\alpha\sigma r}}{\sqrt{2\pi\kappa}} e^{ir\sqrt{4\pi}\,\phi_{\alpha\sigma r}(x)} \tag{2.22}$$

where the $\phi_{\alpha\sigma r}$ satisfy the following commutation relations:

$$\left[\phi_{\alpha\sigma r}(x), \phi_{\alpha'\sigma' r'}(y)\right] = \frac{i}{4}\, r\, \delta_{r,r'} \delta_{\alpha,\alpha'} \delta_{\sigma,\sigma'} \mathrm{sign}\,(x-y)\,. \tag{2.23}$$

The Klein factors $\eta_{n,r}$, $\eta^\dagger_{n,r}$ in Eq. (2.22) are hermitian and obey a Clifford algebra:

$$\begin{aligned} \eta^\dagger_{n,r} &= \eta_{n,r}\,, \\ \left\{\eta_{n,r}, \eta_{n',r'}\right\} &= 2\delta_{n,n'}\delta_{r,r'}\,. \end{aligned} \tag{2.24}$$

They ensure the correct *anti*commutation relations between different species of fermions, which cannot be achieved by combinations of bosonic operators. Already for a single species, this problem would arise, since right and left moving bosons commute (cf. Eq. 2.23). In the thermodynamic limit though, the Klein factors can be neglected when computing correlation functions.

[6] H_0 can, up to an irrelevant shift, be written in terms of the *normal ordered* field operators.

The factor κ in Eq. (2.22) is a short-distance cutoff which is of the order of the lattice constant a. It represents a *microscopic* length scale, as for example a lattice spacing, and should consequently be seen as infinitesimal compared to any *macroscopic* distance.

A detailed proof that Eq. (2.22) is indeed an operator identity is beyond the scope of this thesis. It can be found, for example, in [21]. In App.B. we show explicitly that the r.h.s. of Eq. (2.22) generates the same correlation functions and commutation relations as the l.h.s.

The density of fermions of species α, σ, r is defined as $\tilde{\rho}_{\alpha\sigma r}(x) \equiv \lim_{x\to x'} \psi^\dagger_{\alpha\sigma r}(x)\,\psi_{\alpha\sigma r}(x')$. Due to the unbounded spectrum, this expression will contain a divergent part. With the help of the so-called *point-splitting* technique (cf. App. B), $\tilde{\rho}_{\alpha\sigma r}(x)$ can be separated into a regular and a singular part. One can then define the regular part as the normal ordered density and show that

$$\rho_{\alpha\sigma r} \equiv :\psi^\dagger_{\alpha\sigma r}\psi_{\alpha\sigma r}: (x) = \frac{1}{\sqrt{\pi}}\partial_x\phi_{\alpha\sigma r}. \tag{2.25}$$

Consequently, the bosonized counterpart of the interaction Hamiltonian is quadratic in (derivatives) of bosonic fields. Using the same technique (again, cf. App. B), one can compute the kinetic energy densities

$$:\psi^\dagger_{\alpha\sigma r}(-ir\partial_x)\,\psi_{\alpha\sigma r}: (x) = (\partial_x\phi_{\alpha\sigma r})^2, \tag{2.26}$$

which is *equally quadratic* in derivatives of bosonic field. Inserting Eq. (2.25) into Eq. (2.20) one obtains[7]

$$H = \sum_{\alpha,\sigma,r}\sum_{\alpha',\sigma',r'}\int dx\,(\partial_x\phi_{\alpha\sigma r})\left[v_{\alpha\sigma}\delta_{\alpha,\alpha'}\delta_{\sigma,\sigma'} + \frac{V_0}{2\pi}\right](\partial_x\phi_{\alpha'\sigma'r'}). \tag{2.27}$$

We obtained a gaussian field theory, which can be exactly solved. For convenience, we will first re-write it in a different basis of bosonic fields.

2.4.2. Normal-mode representation

We employ the boson fields $\phi_\gamma(x)$ with $\gamma = c+, c-, s+, s-$, representing the total and relative charge and spin density modes, and their conjugate momentum fields $\Pi_\gamma(x) = -\partial_x\theta_\gamma$, where θ_γ are the dual fields. These fields are conveniently combined into the vectors $\vec{\Phi}_a(x) = (\phi_{c+}, \theta_{c+}, \phi_{s-}, \theta_{s-})^T$ and $\vec{\Phi}_b(x) = (\phi_{c-}, \theta_{c-}, \phi_{s+}, \theta_{s+})^T$ (see below). A qualitative understanding of the physical meaning of these fields can be gained by noticing that they are (anti-) symmetric linear combinations of the chiral fields $\phi_{\alpha,r,\sigma}$ of Eq. (2.22)

[7] Note that using the Heisenberg equation of motion $\partial_t\phi_{n,r} = i[\phi_{n,r}, H_0]$ together with the commutation relations for the chiral fields, one obtains $\left(\partial_x + \frac{r}{v_n}\partial_t\right)\phi_{n,r}(x,t) = 0$, which makes the term *chiral* fields clear: right/left-moving bosons only depend on $(x \mp v_n t)$: $\phi_{n,r}(x,t) = \phi_{n,r}(x - r v_n t)$.

with respect to the α, σ, r quantum numbers, which is encoded by the transformation:

$$\begin{aligned}\phi_{\alpha\sigma r} &= \frac{1}{4}\left\{\left[\left(\phi_{c_+}+r\theta_{c_+}\right)+\alpha\left(\phi_{c_-}+r\theta_{c_-}\right)\right]+\sigma\left[\left(\phi_{s_+}+r\theta_{s_+}\right)+\alpha\left(\phi_{s_-}+r\theta_{s_-}\right)\right]\right\}\\ &\equiv \frac{1}{4}\vec{n}_{\alpha\sigma r}\cdot\left(\vec{\phi}_a+\alpha\vec{\phi}_b\right)\end{aligned} \tag{2.28}$$

where $\vec{n}_{\alpha\sigma r}=\begin{pmatrix}1, & r, & \alpha\sigma, & \alpha\sigma r\end{pmatrix}$. From Eq. (2.23) one straightforwardly obtains the commutation relations for the new fields:

$$\begin{aligned}\left[\phi_\gamma(x),\theta_{\gamma'}(y)\right] &= \frac{i}{2}\delta_{\gamma,\gamma'}\mathrm{sign}(x-y)\\ \left[\phi_\gamma(x),\Pi_{\gamma'}(y)\right] &= i\delta_{\gamma,\gamma'}\delta(x-y).\end{aligned}$$

Note that interaction only affects the total charge density mode[8]. The low-energy Hamiltonian of a spin-orbit-coupled interacting metallic SWNT then reads

$$H=\frac{v}{2}\int dx\begin{pmatrix}\partial_x\vec{\Phi}_a\\ \partial_x\vec{\Phi}_b\end{pmatrix}^T\begin{pmatrix}h(K) & 0\\ 0 & h(1)\end{pmatrix}\begin{pmatrix}\partial_x\vec{\Phi}_a\\ \partial_x\vec{\Phi}_b\end{pmatrix} \tag{2.29}$$

with the K-dependent matrix

$$h(K)=\begin{pmatrix}\frac{1}{K^2} & 0 & \delta & 0\\ 0 & 1 & 0 & \delta\\ \delta & 0 & 1 & 0\\ 0 & \delta & 0 & 1\end{pmatrix},$$

where we introduced the mean velocity $v=(v_A+v_B)/2$ and the dimensionless difference $\delta=(v_A-v_B)/(2v)$. The important electron-electron forward scattering effects are parametrized by the standard LL parameter $K\equiv K_{c+}=\frac{1}{\sqrt{1+\frac{2V_0}{\pi v}}}$, where $K=1$ for noninteracting electrons but $K\approx 0.2\ldots0.4$ for SWNTs deposited on insulating substrates (or for suspended SWNTs) due to the long-ranged Coulomb interaction [2–4].

The above representation shows that SOI breaks spin-charge separation since spin and charge modes are coupled for $\delta\neq 0$, as can be seen from the expressions for $h(K)$ and $\vec{\Phi}_{a/b}$. Notably, the modes $\vec{\Phi}_a$ and $\vec{\Phi}_b$ decouple, and interactions ($K\neq 1$) only affect the $\vec{\Phi}_a$ sector. In each sector, the Hamiltonian is then formally identical to the one for a semiconductor wire with Rashba SOI in the absence of backscattering [22, 23].

Parameter estimates can be obtained from Eq. (2.16) together with Eqs. (2.13-2.15) yields

$$\begin{aligned}\frac{v}{v_F} &\simeq 1-\frac{0.01(R[\mathrm{nm}])^2+17\cos^2(3\theta)}{(E_F[\mathrm{meV}])^2\,(R[\mathrm{nm}])^4},\\ \delta &\simeq \frac{0.83\cos(3\theta)}{(E_F[\mathrm{meV}])^2}R[\mathrm{nm}])^3.\end{aligned} \tag{2.30}$$

[8] Since $\phi_{c_+}=\frac{1}{2}\sum_{\alpha\sigma r}\phi_{\alpha\sigma r}$

The renormalization of v away from v_F goes always downwards, but the quantitative shift is small. The asymmetry parameter δ effectively parametrizes the SOI strength and is more important in what follows. For fixed E_F and R, it is maximal for $\theta = 0$ (zig-zag tube) and vanishes for $\theta = \pi/6$ (armchair tube). Moreover, δ increases for smaller tube radius, but the continuum description underlying our approach eventually breaks down for $R \leq 0.4$ nm. Since E_F should at the same time be sufficiently far above the band bottom in Eq. (2.16), in practice this leads to rather small values, $\delta \leq 0.05$. Nonetheless, we show below that observable consequences do arise.

Diagonalization

Equation (2.29) can be diagonalized by the linear transformation [24] $\hat{\vec{\Phi}}_a = V_a \vec{\Phi}_a$ and $\hat{\vec{\Phi}}_b = V_b \vec{\Phi}_b$, with the 4×4 matrix

$$V_a = \begin{pmatrix} \cos\eta & 0 & -\frac{\sin\eta}{y} & 0 \\ 0 & \cos\eta & 0 & -y\sin\eta \\ y\sin\eta & 0 & \cos\eta & 0 \\ 0 & \frac{\sin\eta}{y} & 0 & \cos\eta \end{pmatrix}, \tag{2.31}$$

where

$$y = \sqrt{(1+K^{-2})/2}, \quad \tan(2\eta) = \frac{2\delta y}{y^2-1}. \tag{2.32}$$

V_b is as in Eq. (2.31) with $K = 1$, i.e., $y = 1$ and $\eta = \pi/4$. In terms of the new field vectors $\hat{\vec{\Phi}}_\rho = \left(\hat{\phi}_{+,\rho}, \hat{\theta}_{+,\rho}, \hat{\phi}_{-,\rho}, \hat{\theta}_{-,\rho}\right)^T$ with mutually dual boson fields $\hat{\phi}_{j\rho}$ and $\hat{\theta}_{j\rho}$ for each set $(j = \pm, \rho = a/b = \pm)$, the diagonalized Hamiltonian is seen to describe an unconventional four-channel Luttinger liquid,

$$H = \sum_{j,\rho} \frac{v_{j\rho}}{2} \int dx \left(\frac{1}{K_{j\rho}} (\partial_x \hat{\phi}_{j\rho})^2 + K_{j\rho} (\partial_x \hat{\theta}_{j\rho})^2 \right). \tag{2.33}$$

The interacting sector corresponds to $\rho = a$, where the effective LL parameters $K_{\pm,a}$ and the plasmon velocities $v_{\pm,a}$ are

$$\begin{aligned} K_{\pm,a} &= y^{\mp 1} \sqrt{\frac{3 + K^{-2} \pm \Delta}{3K^{-2} + 1 \pm \Delta}}, \\ \frac{v_{\pm,a}}{v} &= \sqrt{y^2 + \delta^2 \pm \Delta/2}, \\ \Delta &= \sqrt{(K^{-2}-1)^2 + (4\delta y)^2} \end{aligned} \tag{2.34}$$

with y in Eq. (2.32). For $\rho = b$, the noninteracting values apply, $K_{\pm,b} = 1$ and $v_{\pm,b} = v\,(1 \pm \delta)$. Note that the above expressions recover the LL theory for $\delta = 0$ [2], where $v_{j\rho} = v_F/K_{j\rho}$ with $K_{j\rho} = 1$ except for $K_{+,a} = K$.

2.5. Physical quantities and spectral function

Within the framework of the LL Hamiltonian (2.33), using the bosonized form of the electron field operator $\psi_{\alpha\sigma r}(x,t)$ and the transformation (2.31), it is possible to obtain exact results for all observables of interest.

In particular, arbitrary correlation functions of exponentials of the boson fields[9], so called *vertex operators* can be calculated using the functional integral formalism (The interested reader may refer to Appendix A) .

In this model, a generic vertex-operator two-point function factors into an interacting (subscript $\rho = "a" = +$) and a noninteracting part (subscript $\rho = "0" = "b" = -$). Specifying the vertex-operator by index-vectors $\vec{n}_{\rho=\pm} = \begin{pmatrix} n_{\phi_{c_\pm}} & n_{\theta_{c_\pm}} & n_{\phi_{s_\mp}} & n_{\theta_{s_\mp}} \end{pmatrix}$, the two-point function reads (cf. Eq.(A.20-A.21))

$$\begin{aligned}
&\left\langle T_t\, e^{i\sqrt{4\pi}\left(\vec{n}_a\cdot\vec{\Phi}_a(\vec{x}_1)+\vec{n}_b\cdot\vec{\Phi}_b(\vec{x}_1)\right)} e^{i\sqrt{4\pi}\left(\vec{m}_a\cdot\vec{\Phi}_a(\vec{x}_2)+\vec{m}_b\cdot\vec{\Phi}_b(\vec{x}_2)\right)}\right\rangle \\
&= \delta_{\vec{n}_a,-\vec{m}_a}\delta_{\vec{n}_b,-\vec{m}_b} \\
&\times \prod_{j=\pm,\rho=a,b}\prod_{\mu=\pm}\left[\frac{v_{j,\rho}\beta}{-i\kappa\mu\pi}\sinh\left(\frac{\pi}{v_{j,\rho}\beta}\left(x_{12}+\mu\left(v_{j,\rho}t_{12}-i\kappa\, sign\,(t)\right)\right)\right)\right]^{-\Gamma_{j,\rho;\mu}},
\end{aligned} \tag{2.35}$$

where the exponent (cf. Eq.(A.21))

$$\Gamma_{j,\rho;\mu}\left(\vec{n}_\rho\right) \equiv \left(\hat{n}_{\phi_{j,\rho}} K_{j,\rho}^{\frac{1}{2}} - \mu\, \hat{n}_{\theta_{j,\rho}} K_{j,\rho}^{-\frac{1}{2}}\right)^2, \tag{2.36}$$

of each of each of the normal modes is given as bilinear form in the (transformed) index vectors $\vec{n}_\rho \xrightarrow{V} \hat{\vec{n}}_\rho = V_\rho \vec{n}_\rho$ resulting in

$$\Gamma_{+,\rho;\mu} = \left[\cos\left(\eta_\rho\right)\left(\sqrt{K_{+,\rho}}n_{\phi_{c_\rho}} - \frac{\mu\, n_{\theta_{c_\rho}}}{\sqrt{K_{+,\rho}}}\right) + \sin\left(\eta_\rho\right)\left(y\sqrt{K_{+,\rho}}n_{\phi_{s_{\overline{\rho}}}} - \frac{\mu\, n_{\theta_{s_{\overline{\rho}}}}}{y\sqrt{K_{+,\rho}}}\right)\right]^2, \tag{2.37}$$

$$\Gamma_{-,\rho;\mu} = \left[\cos\left(\eta_\rho\right)\left(\sqrt{K_{-,\rho}}n_{\phi_{s_{\overline{\rho}}}} - \frac{\mu\, n_{\theta_{s_{\overline{\rho}}}}}{\sqrt{K_{-,\rho}}}\right) - \sin\left(\eta_\rho\right)\left(\frac{\sqrt{K_{-,\rho}}}{y}n_{\phi_{c_\rho}} - \frac{\mu\, y\, n_{\theta_{c_\rho}}}{\sqrt{K_{-,\rho}}}\right)\right]^2. \tag{2.38}$$

With the general expression Eq. (2.35) and Eqs. (2.37, 2.38), we can calculate all correlation function straightforwardly.

[9] Consider, e.g. the expression of the electron field operator in Eq.(2.22) in terms of the previously introduced total and relative charge (spin) fields:

$$\begin{aligned}
\psi_{\alpha\sigma r} &= \frac{\eta_{\alpha\sigma r}}{\sqrt{2\pi\gamma}} e^{ir\sqrt{4\pi}\frac{1}{4}\left\{\left[\left(\phi_{c_+}+r\theta_{c_+}\right)+\alpha\left(\phi_{c_-}+r\theta_{c_-}\right)\right]+\sigma\left[\left(\phi_{s_+}+r\theta_{s_+}\right)+\alpha\left(\phi_{s_-}+r\theta_{s_-}\right)\right]\right\}} \\
&= \frac{\eta_{\alpha\sigma r}}{\sqrt{2\pi\gamma}} e^{ir\sqrt{4\pi}\frac{1}{4}\vec{n}_{\alpha\sigma r}\cdot\left(\vec{\phi}_a+\alpha\vec{\phi}_b\right)}
\end{aligned}$$

2.5.1. Spectral function

As an important application, we will first discuss the *spectral function* for an $r = R/L$ moving electron with spin σ near the K point $\alpha = \pm$, which is defined as

$$A_{r\alpha\sigma}(q,\omega) = -\frac{1}{\pi}\,\mathrm{Im}\,G^{\mathrm{ret}}_{r\alpha\sigma}(q,\omega), \tag{2.39}$$

with the Fourier transform of the single-particle retarded Green's function

$$G^{\mathrm{ret}}_{r\alpha\sigma}(x,t) = -i\Theta(t)\left[\left\langle \Psi_{r\alpha\sigma}(x,t)\Psi^{\dagger}_{r\alpha\sigma}(0,0)\right\rangle + \mathrm{c.c.}\right],$$

where Θ is the Heaviside function and the momentum q is measured with respect to the relative Fermi momentum $k^{(F)}_{r\alpha\sigma}$.

After some algebra, Eq. (2.39) follows in closed form, which we specify in the zero-temperature limit now. With the short-distance cutoff (lattice spacing) $a_0 \approx 0.246$ nm, we find

$$\begin{aligned} A_{r\alpha\sigma}(q,\omega) &\propto \int_{-\infty}^{\infty} dx \int_{-\infty}^{\infty} dt\; e^{-i[qx-\omega t]} \\ &\times \left[\prod_{j,\rho}\prod_{\mu=\pm}\left(1 + i\frac{v_{j\rho}t + \mu r x}{\kappa}\right)^{-\Gamma^{(\alpha\sigma)}_{j,\rho;\mu}} + (x,t)\to(-x,-t)\right] \end{aligned} \tag{2.40}$$

where the exponents for $j = \pm$ and $\mu = \pm$ are given by (see Eq. (2.35-2.38) and Eq. (2.32)

$$\begin{aligned} \Gamma^{(\alpha\sigma)}_{j,a;\mu} &= \frac{1}{16}\Big[\cos(\eta)\left(K^{1/2}_{j,a} - \mu K^{-1/2}_{j,a}\right) \\ &+ \alpha\sigma j \sin(\eta)\left(y^{j}K^{1/2}_{j,a} - \mu y^{-j}K^{-1/2}_{j,a}\right)\Big]^2, \\ \Gamma^{(\alpha\sigma)}_{j,b;\mu} &= \frac{1}{2}\delta_{j,\alpha\sigma}\delta_{\mu,-}. \end{aligned} \tag{2.41}$$

The remaining Fourier integrals are difficult to perform exactly. We here follow Ref. [1] and focus on the analytic structure of the spectral function, which can be obtained by the power counting technique and Jordan's lemma. Up to an overall prefactor, the spectral function exhibits power-law singularities close to the lines $\omega = \pm v_{j\rho}q$. These singularities are captured by the approximate form

$$\begin{aligned} A_{r\alpha\sigma}(q,\omega) &\approx \left(\prod_{j,\mu}\left|\omega + \mu r v_{j,a}q\right|^{\Gamma^{(\alpha\sigma)}-1-\Gamma^{(\alpha\sigma)}_{j,a;\mu}}\right) \\ &\times \left|\omega - r(1+\alpha\sigma\delta)vq\right|^{\Gamma^{(\alpha\sigma)}-3/2} \\ &\times \left[\Theta(\omega - r\bar{v}q) + \Theta(-\omega - r v_{-a}q)\right], \end{aligned} \tag{2.42}$$

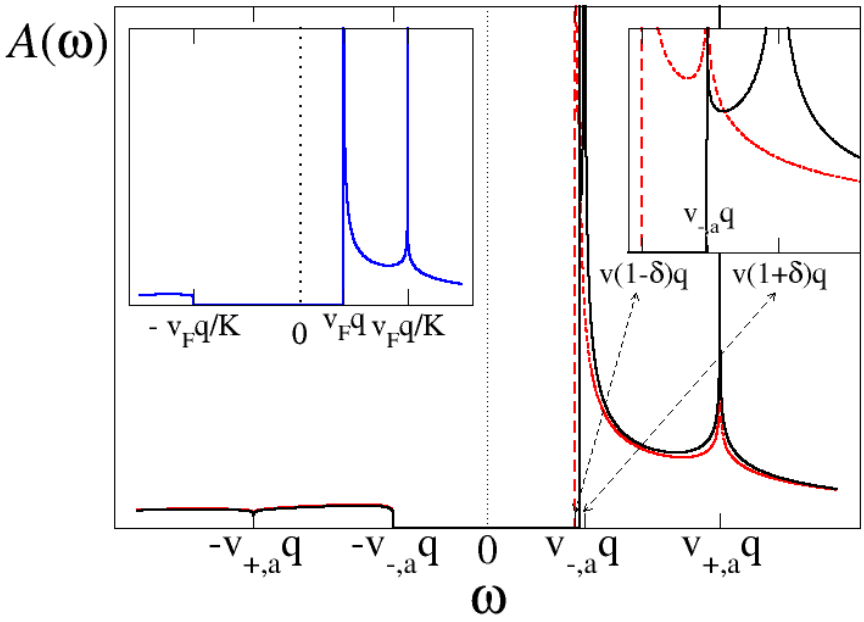

Figure 2.7: Spectral function (2.42) for a right-mover in an interacting SWNT with LL parameter $K = 0.4$ and SOI parameter $\delta = 0.05$, shown in arbitrary units as function of ω for given wavevector $q > 0$. The black solid curve is for $\alpha\sigma = +1$, while the red dashed curve is for $\alpha\sigma = -$. Note that $A_{R\alpha\sigma}(q,\omega) = 0$ for $-v_{-,a}q < \omega < \bar{v}q$. Right inset: Magnified view around $\omega \approx v_{-,a}q$. Left inset: Same as main panel but without SOI ($\delta = 0$). Shifts of the positions of the singularities due to the shifts of Fermi momenta are not included in the figure since each spectral function $A_{r\alpha\sigma}(q,\omega)$ is evaluated at momentum q relative to the *respective* Fermi momentum.

where $\bar{v} = \min[v_{-,a}, (1+\alpha\sigma\delta)v]$ and

$$\Gamma^{(\alpha\sigma)} = \sum_{j\rho\mu} \Gamma^{(\alpha\sigma)}_{j\rho\mu}. \tag{2.43}$$

We stress that Eq. (2.42) is asymptotically exact: it has the same analytic structure and the same exponents of the power laws at the singular lines $\omega = \pm v_{j\rho}q$ as the exact spectral function. Away from the singularities, however, it only serves illustrative purposes.

The spectral function Eq. (2.42) is depicted in the main panel of Fig. 2.7 for fixed wavevector $q > 0$ as a function of frequency ω, taking $K = 0.4$ and $\delta = 0.05$. Compared to the well-known spectral function in the absence of SOI ($\delta = 0$), see left inset of Fig. 2.7 and Refs. [1, 25], additional structure can be observed for $\delta \neq 0$.

- First, the singular feature around $\omega = v_{-,a}q$ splits into two different power-law singularities when $\delta \neq 0$, see the right inset of Fig. 2.7 for a magnified view. For

large q, the corresponding frequency differences ($\propto 2\delta q$) are in the meV regime and can be resolved even for the rather small δ expected here.

- Second, for $-v_{+,a}q < \omega < -v_{-,a}q$, the spectral function is finite (albeit small) when $\delta \neq 0$. Note that for $\delta = 0$, the respective velocities are $v_{+,a} = v_F/K$ and $v_{-,a} = v_F$, implying a large frequency window where this effect may take place.

These predictions for the spectral function could be detected by photoemission spectroscopy.

Many standard quantum transport properties, however, will hardly show an effect due to the SOI. For instance, the tunneling density of states [here summed over (r,α,σ)]

$$\nu(\omega) = -\frac{1}{\pi}\sum_{r\alpha\sigma}\mathrm{Im}\int dt\; e^{i\omega t}G^{\mathrm{ret}}_{r\alpha\sigma}(0,t)$$

exhibits power-law scaling with ω for low frequencies, $\nu(\omega) \propto \omega^{\gamma-1}$. The exponent γ is the smaller of the quantities $\Gamma^{(\pm)}$ in Eq. (2.43). This exponent is analytic in δ, and the smallness of δ then implies that the tunneling density of states in SWNTs will be very close to the one in the absence of SOI.

Relation to quantum wires with Rasba SOI

Let us also briefly comment on the relation of our results to the LL theory for semiconductor quantum wires with Rashba SOI [22, 26–31]. We shall see in chapter 3, that despite the differences between the two systems, the bosonic Hamiltonian is structurally very similar. Indeed, the "interacting" sector $\rho = a$ in Eqs. (2.29) coincides with Eqs. (3.30) when electron-electron backscattering can be neglected and the exponents of the spectral function for this model of a quantum wire with Rashba SOI could be obtained by multiplying the exponents of the interacting (noninteracting) sector derived above by a factor of two (zero). The presence of the "noninteracting" sector $\rho = b$ in our model for the CNT, however, causes the additional structure, i.e. the splitting in the singular feature around $\omega = v_{-,a}q$ in the spectral function. Moreover, while backscattering in semiconductor wires is an irrelevant perturbation in the renormalization group sense (cf. chapter 3, [22, 23]), it nonetheless causes a renormalization of the LL parameters and the plasmon velocities. Such renormalization effects are negligible in SWNTs. The finite spectral weight in the region $-v_{+,a}q < \omega < -v_{-,a}q$, however, is a feature common to both theories and is caused by the breaking of $SU(2)$-spin symmetry, which manifests as a Luttinger-parameter $K_{-,a} \neq 1$ in the (diagonalized) bosonic model. This feature would also appear in the theory for the quantum wire with RSOC when backscattering is taken into account.

2.6. Conclusion

To conclude, in this chapter we have studied spin-orbit interaction effects on the effective low-energy theory of an interacting metallic single-wall carbon nanotube. We have

shown that a four-channel Luttinger liquid theory remains applicable, but compared to the previous formulation without spin-orbit coupling [2], all four channels are now characterized by different Luttinger liquid parameters and plasmon velocities, reflecting the broken spin SU(2) symmetry. While the theory remains exactly solvable, the decoupled plasmon modes do not correspond to spin and charge anymore and spin-charge separation in the usual sense is broken.

As an application of our theory, we have discussed in detail the spectral function, which can directly be probed experimentally for SWNTs [4]. We show how its analytic structure changes from the established spinful LL behavior [1, 25] when SOI effects are taken into account. The predicted deviations are small but should be observable. Furthermore, we have computed the tunneling density of states, and found that it is only weakly affected by SOI. This implies that also most transport observables in long nanotubes are only weakly affected due to the smallness of the spin-orbit coupling. The low-energy theory we have formulated here is formally very similar to the LL description of 1D interacting semiconductor wires including the Rashba SOI [22, 28] (cf. chapter 3) and effects on observables involving spin-spin correlations (e.g. RKKY interaction) could readily be obtained within the framework presented here.

3. Low-energy theory and RKKY interaction for interacting quantum wires with Rashba SOI

3.1. Introduction

In the last decade there have been tremendous advances in the field of spintronics. The term spintronics refers to electronic devices that exploit the spin rather than the charge degree of freedom of electrons [32]. One proposal for such a device, the spintronic field effect transistor (spin-FET) was made by Datta and Das [33]. The physical effect exploited in this device is based on the Rashba coupling [34]. This is a spin-orbit coupling that occurs in a two dimensional electron gas (2DEG) and arises due to inversion asymmetry of the confinement potential forming the 2DEG. Rashba spin-orbit coupling (RSOC) causes the electron spin to precess as the electron moves in a semiconductor heterostructure. This intrinsic coupling can be tuned by applying an external electric field which allows one to vary the precession length. In the presence of source and drain contacts that can inject and absorb electrons with only one specific spin orientation, one could modulate the current by varying the precession length. In order to ensure that interference effects do not smear out the current modulation, it is necessary to confine electron motion to one dimension, i.e. to realize a quantum wire. Thus, the gate-tunable Rashba spin-orbit interaction (see below) of strength α allows for a purely electrical manipulation of the spin-dependent current. The confinement however has a price.

The first problem that arises when confining electrons in a 2DEG to one spatial dimension is a band mixing due to the Rashba term. Those band mixing effects will be discussed in Sec. 3.2. There it will be shown that they can be incorporated into the description of the noninteracting quantum wire under certain approximations (see [35]).

The second problem is that interacting 1D electrons often exhibit Luttinger liquid rather than Fermi liquid behaviour. As was stated in the introduction to the first chapter, this state of matter has a number of interesting features, such as power-law correlations and the phenomenon of "spin-charge separation", which refers to the fact that interactions renormalize the velocity of the charge- but not the spin-plasmon [1].

Spin transport in one-dimensional (1D) quantum wires continues to be a topic of much interest in solid-state and nanoscale physics, offering interesting fundamental questions as

well as technological applications. Motivated mainly by the question of how the Rashba spin precession and Datta-Das oscillations in spin-dependent transport are affected by e-e interactions, Rashba SOI effects on electronic transport in interacting quantum wires have been studied in recent papers [27, 35–41]. In effect, however, all those works only took e-e forward scattering processes into account. Because of the Rashba SOI, one obtains a modified LL phase with broken spin-charge separation [37, 38], leading to a drastic influence on observables such as the spectral function or the tunneling density of states. Moroz *et al.* argued that e-e backscattering processes are irrelevant in the renormalization group (RG) sense, and hence can be omitted in a low-energy theory [37, 38]. Unfortunately, their theory relies on an incorrect spin assignment of the subbands [35, 36], which then invalidates several aspects of their treatment of interaction processes.

The possibility that e-e backscattering processes become relevant (in the RG sense) in a Rashba quantum wire was raised in Ref. [30], where a spin gap (see Sec. 3.3.2) was found under a weak-coupling two-loop RG scheme. If valid, this result has important consequences for the physics of such systems, and would drive them into a spin-density-wave type state. Our approach below is different to theirs in that we include the Rashba coupling α in the single-particle sector from the outset, i.e., in a nonperturbative manner, whereas Ref. [30] start from a strict 1D single-band model and assume both α and the e-e interaction as weak coupling constants flowing under the RG. The important difference to Ref. [30] is that by including the SOI in the single-particle sector, our approach naturally takes into account that certain interaction processes are not allowed (for not too small α), since they would break conservation of total momentum. The one-loop RG flow then turns out to be equivalent to a Kosterlitz-Thouless flow, and for the initial values realized in this problem, e-e backscattering processes are always irrelevant.

This chapter is structured as follows: In the first part (Sec.3.2-3.4) we investigate how the Luttinger-liquid physics emerges in an interacting quantum wire in the presence of RSOC, taking explicitly into account the combined effects of spin-orbit coupling and the transverse confinement in a two-band approximation (see also [23]).

In section 3.2, we discuss the bandstructure of the noninteracting "Rashba quantum wire" (cf. also [35, 42–46]). First, we will derive the Hamiltonian for a noninteracting quantum wire with Rashba-spin orbit coupling. We will treat the band mixing term in a two band approximation (assuming only the lowest (spinful) band is occupied) and diagonalize the Hamiltonian to obtain the dispersion relation and the eigenvectors. Next we will linearize the dispersion relation around the Fermi-points to obtain a low-energy effective Hamiltonian which can be written as a massless, one-dimensional Dirac Hamiltonian in second quantization. The bandstructure at low energy scales is characterized by two velocities [19],

$$v_{A,B} = v_F(1 \pm \delta), \quad \delta(\alpha) \propto \alpha^4. \tag{3.1}$$

These reduce to a single Fermi velocity v_F in the absence of Rashba SOI ($\delta = 0$ for $\alpha = 0$), but they will be different for $\alpha \neq 0$, reflecting the broken spin $SU(2)$ invariance in a spin-orbit coupled system. The small-α dependence $\delta \propto \alpha^4$ follows for the model below and has also been reported in Ref. [39]. Therefore, the velocity splitting (3.1) is typically weak. While a similar velocity splitting also happens in a magnetic Zeeman

field (without SOI) [47], the underlying physics is different since time-reversal symmetry is not broken by SOI. The Hamiltonian we obtain in this subsection is the kinetic part of a two-component Luttinger liquid. We will explicitly take into account the spin structure of the wave function resulting from the combined effects of RSOC and the transverse confinement in the 2D fermion operators. The resulting model holds (within the limitations of the underlying assumptions) for arbitrary spin-orbit coupling strengths.

In section 3.3, we will include electron-electron interactions into the system using the 2D-field operators derived in chapter 2. First, we will reduce the generic interaction Hamiltonian to a form that contains only processes allowed by momentum-conservation, which dominate the low-energy properties of the system. Next, we will approximate the matrix elements of the interaction, assuming that the wire width is small enough to neglect the dependence of the pair potential on the transverse coordinate. Within this approximation, one can neglect exchange integral-contributions to the coupling terms. The resulting effective, low energy Hamiltonian is a two-component Luttinger-liquid.

Using renormalization group (RG) techniques (cf. [1, 21, 23]) we will examine the relevance of an interaction term g_F that arises due to RSOC, which is peculiar and can not be treated within the Luttinger-liquid framework. We present the one-loop RG-equations and use the coupling constants obtained in Sec. 3.3.1 to determine the fixed point of the RG-flow. We will come to the conclusion that the interaction term g_F is marginally irrelevant. Thus, the model we study flows to the two component Luttinger-liquid fixed point. We will also derive the renormalized coupling constants which lead to a non-standard form of the fixed point model.

In section 3.4, we will map the fermionic model to a massless, bosonic theory using the bosonization technique. The bosonized form of the Hamiltonian (cf. Eq. (3.30)) is a spinless, two component Luttinger-model with a coupling term that connects the total and the relative charge sector, due to the effect of the velocity mismatch.

In the second part of this chapter, we present a generalized correlation function in Sec. 3.5.2 derived from the normal-mode representation of the bosonic Hamiltonian presented inSec. 3.5.1, and we compute charge- and spin density correlation functions in Sec. 3.5.3.

The theory allows us to derive two-particle density-density correlation functions (Sec. 3.5.3) and in Section 3.6, we use these results to addess the problem of the Ruderman-Kittel-Kasuya-Yosida (RKKY) interaction [48, 49], i.e. the effective interaction between two spin-$1/2$ magnetic impurities, $\mathbf{\Sigma}_{1,2}$, separated by a distance x . The RKKY interaction is mediated by the conduction electrons in the quantum wire which are exchange-coupled (with coupling J) to the impurity spins. In the absence of both the e-e interaction and the SOI, one finds an isotropic exchange (Heisenberg) Hamiltonian [49],

$$H_{\mathrm{RKKY}} = -J^2 F_{\mathrm{ex}}(x)\, \mathbf{\Sigma}_1 \cdot \mathbf{\Sigma}_2, \quad F_{\mathrm{ex}}(x) \propto \frac{\cos(2k_F x)}{|x|}, \tag{3.2}$$

where the $2k_F$-oscillatory RKKY range function $F_{\mathrm{ex}}(x)$ is specified for the 1D case. When the spin $SU(2)$ symmetry is broken by the SOI, spin precession sets in and the RKKY interaction is generally of a more complicated (twisted) form. For a noninteracting Rashba

quantum wire, it has indeed been established [50–52] that the RKKY interaction becomes anisotropic and thus has a tensorial character.On the other hand, in the presence of e-e interactions but without SOI, the range function has been shown [53] to exhibit a slow power-law decay, $F_{\mathrm{ex}}(x) \propto \cos(2k_F x)|x|^{-\eta}$, with an interaction-dependent exponent $\eta < 1$. The RKKY interaction in interacting quantum wires with SOI has not been studied before.

Let us briefly summarize the main points of this chapter. We present the effective low-energy theory of an interacting Rashba wire (cf. Eq. (3.30)), with the velocities and dimensionless interaction parameters given in (3.1). Previous theories did not fully account for the interplay of e-e backscattering processes with the broken $SU(2)$ invariance due to spin-orbit effects, which lead to, among other notable modifications, to $K_s < 1$. This implies, e.g. that the power-law decay exponent of the RKKY-interaction in an interacting Rashba-wire explicitly depends on both RSOC and interaction strength. Furthermore, the inclusion of RSOC into the interacting model leads to an anisotropic range function, cf. (3.44). Throughout the chapter we use units where $\hbar = 1$.

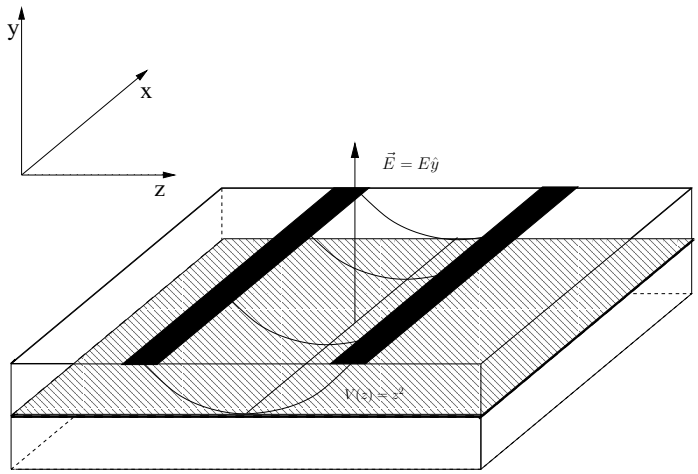

Figure 3.1: Two dimensional electron gas, schematic. Black stripes represent gate electrodes.

3.2. Single-particle description

In this section we shall derive an effective low-energy Hamiltonian for a quantum wire with spin-orbit (SO) coupling. Spin-orbit coupling (SOC) is a relativistic effect. It is a correction term to Pauli equation, which arises when expanding Dirac equation in powers of the fine-structure constant. The general form of the spin-orbit contribution to the Hamiltonian is:

$$H_{SO} \sim \left(\vec{p} \times \vec{E}\right) \cdot \vec{S}. \tag{3.3}$$

We consider a quantum wire electrostatically confined in the z-direction within the 2DEG (xz-plane, see Fig. 3.1) by a harmonic potential, $V_c(z) = m\omega^2 z^2/2$, where m is the effective mass. The noninteracting problem is then defined by the single-particle Hamiltonian [34, 35, 42, 43, 45]

$$\begin{aligned} H_{\rm sp} &= \frac{1}{2m}\left(p_x^2 + p_z^2\right) + V_c(z) + \alpha\left(\sigma_z p_x - \sigma_x p_z\right), \\ &= \left[\frac{p_x^2}{2m} + \alpha\sigma_z p_x\right] + \left[\frac{p_z^2}{2m} + \frac{m\omega^2}{2} z^2\right] - \alpha\,\sigma_x p_z. \end{aligned} \tag{3.4}$$

where α is the Rashba coupling and the Pauli matrices $\sigma_{x,z}$ act in spin space. For $\alpha = 0$, the transverse part of the Hamiltonian can be diagonalized in terms of the familiar 1D harmonic oscillator eigenstates (Hermite functions) $H_n(z)$, with $n = 0, 1, 2, \ldots$ labeling the subbands (channels). Eigenstates of Eq. (3.4) have conserved longitudinal momentum $p_x = k$, and with the z-direction as spin quantization axis, $\sigma_z|\sigma\rangle = \sigma|\sigma\rangle$ with $\sigma = \uparrow, \downarrow = \pm$, the $\sigma_x p_z$ term implies mixing of adjacent subbands with associated spin flips. Retaining only the lowest ($n = 0$) subband from the outset thus excludes spin relaxation. We follow

Ref. [35] and keep the two lowest bands, $n=0$ and $n=1$. The higher subbands $n\geq 2$ yield only tiny corrections, which can in principle be included as in Ref. [45]. The resulting 4×4 matrix representing $H_{\rm sp}$ in this truncated Hilbert space is readily diagonalized and yields four energy bands. We choose the Fermi energy such that only the lower two bands, labeled by $s=\pm$, are occupied, and arrive at a reduced two-band model, where the quantum number $s=\pm$ replaces the spin quantum number. The dispersion relation is

$$E_s(k)=\omega+\frac{k^2}{2m}-\sqrt{\left(\frac{\omega}{2}+s\alpha k\right)^2+\frac{m\omega\alpha^2}{2}}, \tag{3.5}$$

with eigenfunctions $\sim e^{ikx}\phi_{k,s}(z)$. The resulting asymmetric energy bands (3.5) are shown in Fig. 3.1. The transverse spinors are given by

$$\begin{aligned}\phi_{k,+}(z) &= \begin{pmatrix} i\cos[\theta_+(k)]H_1(z)\\ \sin[\theta_+(k)]H_0(z)\end{pmatrix},\\ \phi_{k,-}(z) &= \begin{pmatrix} \sin[\theta_-(k)]H_0(z)\\ i\cos[\theta_-(k)]H_1(z)\end{pmatrix},\end{aligned} \tag{3.6}$$

with k-dependent spin rotation angles (we take $0\leq\theta_s(k)\leq\pi/2$)

$$\theta_s(k)=\frac{1}{2}\cot^{-1}\left(\frac{-2sk-\omega/\alpha}{\sqrt{2m\omega}}\right)=\theta_{-s}(-k). \tag{3.7}$$

As a result of subband mixing, the two spinor components of $\phi_{k,s}(z)$ carry a different z-dependence. They are therefore not just the result of a $SU(2)$ rotation. For $\alpha=0$, we recover $\theta_s=\pi/2$, corresponding to the usual spin up and down eigenstates, with $H_0(z)$ as transverse wavefunction; the $s=+$ ($s=-$) component then describes the $\sigma=\downarrow$ ($\sigma=\uparrow$) spin eigenstate. However, for $\alpha\neq 0$, a peculiar implication of the Rashba SOI follows.From Eq. (3.7) we have $\lim_{k\to\pm\infty}\theta_s(k)=(1\pm s)\pi/4$, such that both $s=\pm$ states have (approximately) spin $\sigma=\downarrow$ for $k\to\infty$ but $\sigma=\uparrow$ for $k\to-\infty$; the product of spin and chirality thus always approaches $\sigma{\rm sgn}(k)=-1$. Moreover, under the time-reversal transformation, $\mathscr{T}=i\sigma_y\mathscr{C}$ with the complex conjugation operator $\mathscr{C}$, the two subbands are exchanged,

$$e^{-ikx}\phi_{-k,-s}(z)=s\mathscr{T}[e^{ikx}\phi_{k,s}(z)],\quad E_{-s}(-k)=E_s(k). \tag{3.8}$$

Time-reversal symmetry, preserved in the truncated description, makes this two-band model of a Rashba quantum wire qualitatively different from Zeeman-spin-split models [47].

In the next step, since we are interested in the low-energy physics, we linearize the dispersion relation around the Fermi points $\pm k_F^{(A,B)}$, see Fig. 3.2, which results in two velocities v_A and v_B, see Eq. (3.1). The linearization of the dispersion relation of multi-band quantum wires around the Fermi level is known to be an excellent approximation for weak e-e interactions [1]. Explicit values for δ in Eq. (3.1) can be derived from Eq. (3.5), and we find $\delta(\alpha)\propto\alpha^4$ for $\alpha\to 0$, in accordance with previous estimates [39].

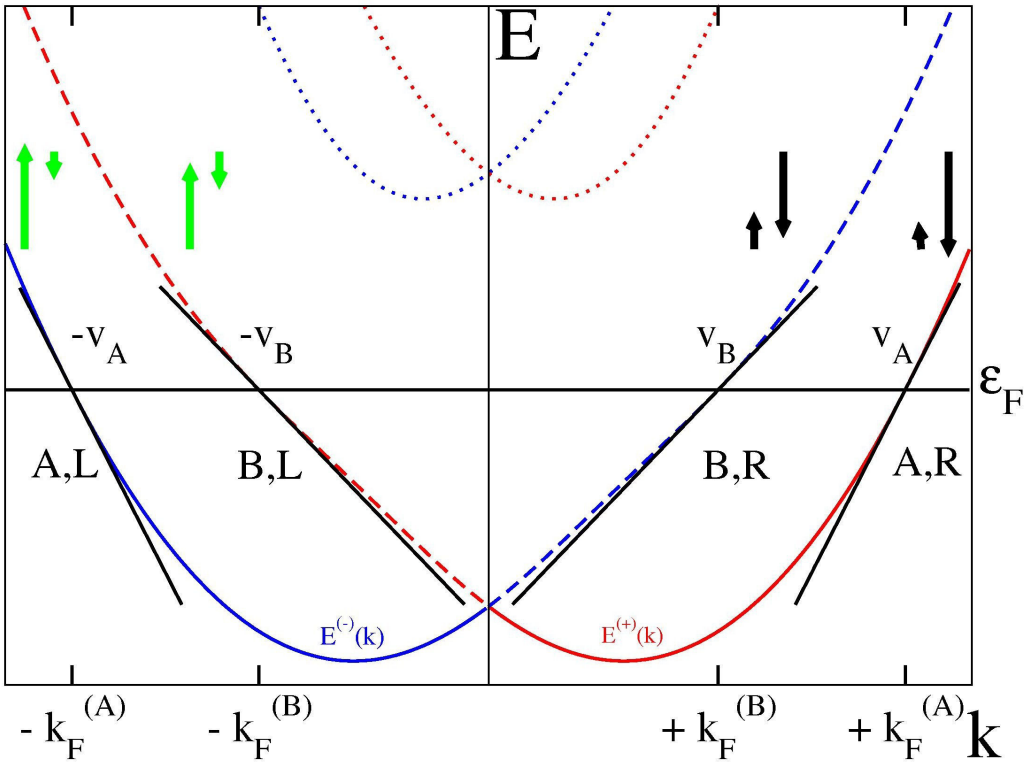

Figure 3.2: Schematic band structure (3.5) of a typical 1D Rashba quantum wire. The red/blue curves show the $s = \pm$ bands, and the dotted curves indicate the next subband (the Fermi energy ε_F is assumed below that band). For the low-energy description, we linearize the dispersion. It is notationally convenient to introduce bands A (solid lines) and B (dashed lines). Green and black arrows indicate the respective spin amplitudes (exaggerated). The resulting Fermi momenta are $\pm k_F^{(A,B)}$, with Fermi velocities $v_{A,B}$.

We mention that $\delta \leq 0.1$ has been estimated for typical geometries in Ref. [38]. The transverse spinors $\phi_{ks}(z)$, Eq. (3.6), entering the low-energy description can be taken at $k = \pm k_F^{(A,B)}$, where the spin rotation angle (3.7) only assumes one of the two values

$$\theta_A = \theta_+ \left(k_F^{(A)}\right), \quad \theta_B = \theta_- \left(k_F^{(B)}\right). \tag{3.9}$$

The electron field operator $\Psi(x,z)$ for the linearized two-band model with $\nu = A,B = +,-$ can then be expressed in terms of 1D fermionic field operators $\psi_{\nu,r}(x)$, where $r = R,L = +,-$ labels right- and left-movers,

$$\Psi(x,z) = \sum_{\nu,r=\pm} e^{irk_F^{(\nu)}x}\, \phi_{rk_F^{(\nu)},s=\nu r}(z)\, \psi_{\nu,r}(x), \tag{3.10}$$

with $\phi_{k,s}(z)$ specified in Eq. (3.6). Note that in the left-moving sector, band indices have been interchanged according to the labeling in Fig. 3.2.

In this way, the noninteracting second-quantized Hamiltonian takes the standard form for two inequivalent species of 1D massless Dirac fermions with different velocities,

$$H_0 = -i \sum_{\nu,r=\pm} r v_\nu \int dx\, \psi^\dagger_{\nu,r} \partial_x \psi_{\nu,r}. \tag{3.11}$$

The velocity difference implies the breaking of the spin $SU(2)$ symmetry, a direct consequence of SOI. For $\alpha = 0$, the index ν coincides with the spin quantum number σ for left-movers and with $-\sigma$ for right-movers, and the above formulation reduces to the usual Hamiltonian for a spinful single-channel quantum wire.

3.3. Interaction effects

In this section, we will analyse the different possible scattering processes and derive their bare (i.e. un-renormalized) coupling constants. Unlike the treatment of interaction processes in Sec. 2.3.1, we here take e-e backscattering into account explicitly. We will see that all processes, except for one (The g_f term which corresponds to intraband backscattering with band flip, cf. Eq. (3.20)), can be written as bilinears of electron density operators. Next we shall briefly present the second order RG-equations (see below) and use the bare coupling constants to determine the fixed point of the RG-flow.

3.3.1. Including interactions

Let us now include e-e interactions into a single-channel Rashba quantum wire. With the expansion (3.10) and $\mathbf{r} = (x,z)$, the second-quantized two-body Hamiltonian

$$H_I = \frac{1}{2} \int d\mathbf{r}_1 d\mathbf{r}_2\, \Psi^\dagger(\mathbf{r}_1) \Psi^\dagger(\mathbf{r}_2)\, V(\mathbf{r}_1 - \mathbf{r}_2)\, \Psi(\mathbf{r}_2) \Psi(\mathbf{r}_1) \tag{3.12}$$

leads to 1D interaction processes. We here assume that the e-e interaction potential $V(\mathbf{r}_1 - \mathbf{r}_2)$ is externally screened, allowing to describe the 1D interactions as effectively local. Following standard arguments, for weak e-e interactions, going beyond this approximation leads at most to irrelevant corrections [1]. We then obtain the local 1D interaction Hamiltonian [55]

$$H_I = \frac{1}{2} \sum_{\{\nu_i, r_i\}} V_{\{\nu_i, r_i\}} \int dx \; \psi^\dagger_{\nu_1, r_1} \psi^\dagger_{\nu_2, r_2} \psi_{\nu_3, r_3} \psi_{\nu_4, r_4}, \tag{3.13}$$

where the summation runs over all quantum numbers $\nu_1, \ldots, \nu_4$ and $r_1, \ldots, r_4$ subject to momentum conservation,

$$r_1 k_F^{(\nu_1)} + r_2 k_F^{(\nu_2)} = r_3 k_F^{(\nu_3)} + r_4 k_F^{(\nu_4)}. \tag{3.14}$$

With the momentum transfer $q = r_1 k_F^{(\nu_1)} - r_4 k_F^{(\nu_4)}$ and the partial Fourier transform

$$\tilde{V}(q; z) = \int dx \, e^{-iqx} V(x, z) \tag{3.15}$$

of the interaction potential, the interaction matrix elements in Eq. (3.13) are given by

$$\begin{aligned} V_{\{\nu_i, r_i\}} &= \int dz_1 dz_2 \, \tilde{V}(q; z_1 - z_2) \\ &\times \left[\phi^\dagger_{r_1 k_F^{(\nu_1)}, \nu_1 r_1} \cdot \phi_{r_4 k_F^{(\nu_4)}, \nu_4 r_4} \right](z_1) \\ &\times \left[\phi^\dagger_{r_2 k_F^{(\nu_2)}, \nu_2 r_2} \cdot \phi_{r_3 k_F^{(\nu_3)}, \nu_3 r_3} \right](z_2). \end{aligned} \tag{3.16}$$

Since the Rashba SOI produces a splitting of the Fermi momenta for the two bands, $\left| k_F^{(A)} - k_F^{(B)} \right| \simeq 2\alpha m$, the condition (3.14) eliminates one important interaction process available for $\alpha = 0$, namely interband backscattering (see below). This is a distinct SOI effect besides the broken spin $SU(2)$ invariance. Obtaining the complete "g-ology" classification [1] of all possible interaction processes allowed for $\alpha \neq 0$ is then a straightforward exercise. The corresponding values of the interaction matrix elements are generally difficult to evaluate explicitly, but in the most important case of a thin wire,

$$d \gg \frac{1}{\sqrt{m\omega}}, \tag{3.17}$$

where d is the screening length (representing, e.g., the distance to a backgate), analytical expressions can be obtained . To simplify the analysis and allow for analytical progress,

[1] Technically, one expresses the fermion operators as functions of centre-of-mass $X = \frac{x_1 + x_2}{2}$ and relative coordinates $x = x_1 - x_2$ and performs a gradient expansion in the relative coordinate $\psi_{\nu,r}\left(x_{1/2} = X \pm \frac{x}{2}\right) = \psi_{\nu,r}(X) + \mathcal{O}(x)$. In this procedure, it is crucial to understand the products of fermionic operators in the sense of operator product expansions. Corrections to the leading terms are then irrelevant in the RG sense (see, e.g. [**?**]).

we therefore employ the thin-wire approximation Eq. (3.17) in what follows. In that case, we can neglect the z dependence in Eq. (3.15). Going beyond this approximation would only imply slightly modified values for the e-e interaction couplings used below. Using the identity

$$\begin{aligned}&\int dz \left[\phi^{\dagger}_{rk_F^{(\nu)},\nu r}\cdot\phi_{r'k_F^{(\nu')},\nu' r'}\right](z) = \\ &= \delta_{\nu\nu'}\delta_{rr'}+\cos(\theta_A-\theta_B)\delta_{\nu,-\nu'}\delta_{r,-r'},\end{aligned} \tag{3.18}$$

where the angles $\theta_{A,B}$ were specified in Eq. (3.9), only two different values W_0 and W_1 for the matrix elements in Eq. (3.16) emerge. These nonzero matrix elements are

$$\begin{aligned}&V_{\nu r,\nu' r',\nu' r',\nu r}\equiv W_0=\tilde{V}(q=0),\\ &V_{\nu r,\nu' r',-\nu'-r',-\nu-r}\equiv W_1\\ &=\cos^2(\theta_A-\theta_B)\,\tilde{V}\left(q=k_F^{(A)}+k_F^{(B)}\right).\end{aligned} \tag{3.19}$$

We then introduce 1D chiral fermion densities $\rho_{\nu r}(x) = :\psi^{\dagger}_{\nu r}\psi_{\nu r}:$, where the colons indicate normal-ordering. The interacting 1D Hamiltonian is $H = H_0 + H_I$ with Eq. (3.11) and

$$\begin{aligned}H_I &= \frac{1}{2}\sum_{\nu\nu',rr'}\int dx\Big([g_{2\|\nu}\delta_{\nu,\nu'}+g_{2\perp}\delta_{\nu,-\nu'}]\delta_{r,-r'}\\ &+ [g_{4\|\nu}\delta_{\nu,\nu'}+g_{4\perp}\delta_{\nu,-\nu'}]\delta_{r,r'}\Big)\,\rho_{\nu r}\rho_{\nu' r'}\\ &+ \frac{g_f}{2}\sum_{\nu r}\int dx\;\psi^{\dagger}_{\nu r}\psi^{\dagger}_{\nu,-r}\psi_{-\nu r}\psi_{-\nu,-r}.\end{aligned} \tag{3.20}$$

The e-e interaction couplings are denoted in analogy to the standard g-ology, whereby the g_4 (g_2) processes describe forward scattering of 1D fermions with equal (opposite) chirality $r = R,L = +,-$, and the labels $\|$, $\perp$, and f denote intraband, interband, and band flip processes, respectively. Since the bands $\nu = A,B = +,-$ are inequivalent, we keep track of the band index in the intraband couplings. The g_f term corresponds to intraband backscattering with band flip. The interband backscattering without band flip is strongly suppressed since it does not conserve total momentum [2] and is neglected in the following. For $\alpha = 0$, the $g_{4,\|/\perp}$ couplings coincide with the usual ones [1] for spinful electrons, while g_f reduces to $g_{1\perp}$ and $g_{2,\|/\perp}\to g_{2,\perp/\|}$ due to our exchange of band indices in the left-moving sector. According to Eq. (3.19), the bare values of these coupling constants are

$$\begin{aligned}&g_{4\|\nu}=g_{4\perp}=g_{2\|\nu}=W_0,\\ &g_{2\perp}=W_0-W_1,\quad g_f=W_1.\end{aligned} \tag{3.21}$$

[2] It is in principle possible that such a process becomes important if a collective density readjustment between subbands takes place in the wire. However, this can only happen for almost equivalent subbands, see Ref. [55] for a detailed discussion. Here we assume that the SOI is strong enough to guarantee that such a readjustment does not occur.

The equality of the intraband coupling constants for the two bands is a consequence of the thin-wire approximation, which also eliminates certain exchange matrix elements.

3.3.2. RG-flow

The bosonization method allows one to map the non-interacting Hamiltonian H_0 as well as interaction terms which can be expressed in terms of bilinears of electron densities $\rho_{n,r}(x)$ to a quadratic and massless bosonic theory which is exactly solvable. This was illustrated in section 2.4. There are however interaction terms which cannot be expressed as bilinears of $\rho_{n,r}(x)$ and thus cannot be incorporated into the exactly solvable model. In the present situation, the only term of this form is the one $\propto g_F$. The system can only be treated in the Luttinger-liquid framework if its coupling constant g_F decreases when going to lower and lower energies, or technically speaking, if g_F is an irrelevant coupling in the RG sense (see, e.g. [56]).

The Hamiltonian $H_0 + H_I$ (see above) corresponds to a specific realization of a general asymmetric two band-model, where the one-loop RG equations are known [55,57]. (Note that a detailed derivation of the RG equations using the operator product expansion (OPE) technique can also be found in Ref. [23]). Using RG invariants, we arrive after some algebra at the two-dimensional Kosterlitz-Thouless RG flow equations,

$$\frac{d\bar{g}_2}{dl} = -\bar{g}_f^2, \quad \frac{d\bar{g}_f}{dl} = -\bar{g}_f \bar{g}_2, \tag{3.22}$$

for the rescaled couplings

$$\begin{aligned} \bar{g}_2 &= \frac{g_{2\|A}}{2\pi v_A} + \frac{g_{2\|B}}{2\pi v_B} - \frac{g_{2\perp}}{\pi v_F}, \\ \bar{g}_f &= \sqrt{\frac{1+\gamma}{2}} \frac{g_f}{\pi v_F}, \end{aligned} \tag{3.23}$$

where we use the dimensionless constant

$$\gamma = \frac{v_F^2}{v_A v_B} = \frac{1}{1-\delta^2} \geq 1. \tag{3.24}$$

As usual, the g_4 couplings do not contribute to the one-loop RG equations. The initial values of the couplings can be read off from Eq. (3.21),

$$\begin{aligned} \bar{g}_2(l=0) &= \frac{(\gamma-1)W_0 + W_1}{\pi v_F}, \\ \bar{g}_f(l=0) &= \sqrt{\frac{1+\gamma}{2}} \frac{W_1}{\pi v_F}. \end{aligned} \tag{3.25}$$

The solution of Eq. (3.22) is textbook material [1], and $\bar{g}_f$ is known to be marginally irrelevant for all initial conditions with $|\bar{g}_f(0)| \leq \bar{g}_2(0)$. Using Eqs. (3.19) and (3.25), this implies with $\gamma \simeq 1+\delta^2$ the condition

$$\tilde{V}(0) \geq \frac{1}{4} \cos^2(\theta_A - \theta_B)\, \tilde{V}\left(k_F^{(A)} + k_F^{(B)}\right), \tag{3.26}$$

which is satisfied for all physically relevant repulsive e-e interaction potentials. As a consequence, intraband backscattering processes with band flip, described by the coupling $\bar{g}_f$, are *always marginally irrelevant*, i.e., they flow to zero as the energy scale is reduced, $\bar{g}_f^* = \bar{g}_f(l \to \infty) = 0$. Therefore *no gap arises*, and a modified LL model is the appropriate low-energy theory. We mention in passing that even if we neglect the velocity difference in Eq. (3.1), no spin gap is expected in a Rashba wire, i.e., the broken $SU(2)$ invariance in our model is not required to establish the absence of a gap.

The above RG procedure also allows us to extract *renormalized couplings* entering the low-energy LL description. The fixed-point value $\bar{g}_2^* = \bar{g}_2(l \to \infty)$ now depends on the Rashba SOI through γ in Eq. (3.24). With the interaction matrix elements $W_{0,1}$ in Eq. (3.19), it is given by

$$\bar{g}_2^* = \frac{\sqrt{[(\gamma-1)W_0 + W_1]^2 - (\gamma+1)W_1^2/2}}{\pi v_F}. \tag{3.27}$$

For $\alpha = 0$, we have $\gamma = 1$ and therefore $\bar{g}_2^* = 0$. The Rashba SOI produces the nonzero fixed-point value (3.27), reflecting the broken $SU(2)$ symmetry.

3.4. Luttinger liquid description

In this section, we describe the resulting effective low-energy Luttinger liquid (LL) theory of an interacting single-channel Rashba wire. A detailed description of the application of the bosonization procedure to a similar system was already presented in section 2.4, thus we shall merely summarize the results here.

Employing Abelian bosonization [1], we introduce a boson field and its conjugate momentum for each band $\nu = A, B = +, -$. It is useful to switch to symmetric ("charge"), $\phi_c(x)$ and $\Pi_c(x) = -\partial_x \theta_c(x)$, and antisymmetric ("spin" for $\alpha = 0$), $\phi_s(x)$ and $\Pi_s(x) = -\partial_x \theta_s$, linear combinations of these fields and their momenta. The dual fields ϕ and θ then allow to express the electron operator from Eq. (3.10) as,

$$\Psi(x,z) \;=\; \sum_{\nu,r} \phi_{r k_F^{(\nu)},\nu r}(z)\; e^{i r k_F^{(\nu)} x} \psi_{\nu,r}(x) \tag{3.28}$$

with

$$\psi_{\nu,r} \equiv \frac{\eta_{\nu r}}{\sqrt{2\pi a}} e^{i\sqrt{4\pi}\frac{r}{\sqrt{8}}[(\phi_c + r\theta_c) + \nu(\phi_s + r\theta_s)]} \tag{3.29}$$

where a is a cutoff length and $\eta_{\nu r}$ are the standard Klein factors[3] [1, 53].[4] The low-energy Hamiltonian is then taken with the fixed-point values for the interaction constants,

[3] Where we adopt the convention $.\eta_{\nu R}\eta_{\nu L}\eta_{-\nu,R}\eta_{-\nu,L} = 1$

[4] To recover the conventional expression for $\alpha = 0$, due to our convention for the band indices in the left-moving sector, one should replace $\phi_s, \theta_s \to -\theta_s, -\phi_s$.

ex.	c	s	λ
v_i	$v_c = v_F\sqrt{(1+\bar{g}_4)^2 - y_+^2}$	$v_s = v_F\sqrt{1-y_-^2}$	$v_\lambda = v_F\sqrt{\delta^2 - y_\delta^2}$
K_i	$K_c = \sqrt{\frac{1+\bar{g}_4-y_+}{1+\bar{g}_4+y_+}}$	$K_s = \sqrt{\frac{1-y_-}{1+y_-}}$	$K_\lambda = \sqrt{\frac{\delta-y_\delta}{\delta+y_\delta}}$
app.			
$\tilde{v}_i$	$\tilde{v}_c = v_F\sqrt{\left(1+\frac{W_0}{\pi v_F}\right)^2 - \left(\frac{2W_0-W_1}{2\pi v_F}\right)^2}$	$\tilde{v}_s = v_F$	$\tilde{v}_\lambda = v_F\delta\sqrt{1-\left(\frac{W_1}{4\pi v_F}\right)^2}$
$\tilde{K}_i$	$\tilde{K}_c = \sqrt{\frac{2\pi v_F+W_1}{2\pi v_F+4W_0-W_1}}$,	$\tilde{K}_s = 1 - \frac{\sqrt{W_0W_1}}{\sqrt{2}\,\pi v_F}\lvert\delta\rvert$	$\tilde{K}_\lambda = \sqrt{\frac{4\pi v_F+W_1}{4\pi v_F-W_1}}$,

Table 3.1: Luttinger-liquid parameters: velocities v_i and spring-constants K_i. Exact values in top half, approximations $\tilde{v}_i, \tilde{K}_i$ to first order in δ (i.e.$v_i, K_i = \tilde{v}_i, \tilde{K}_i + \mathscr{O}\left(\delta^2\right)$) in lower half of the table.

i.e., backscattering processes only appear via the renormalized value of $\bar{g}_2^*$ in Eq. (3.27). Following standard steps (cf. section 2.4), the kinetic term H_0 and the forward scattering processes then lead to the exactly solvable Gaussian field theory of a modified (extended) Luttinger liquid

$$\begin{aligned} H &= \sum_{j=c,s} \frac{v_j}{2} \int dx \left(K_j \Pi_j^2 + \frac{1}{K_j} (\partial_x \phi_j)^2 \right) \\ &+ v_\lambda \int dx \left(K_\lambda \Pi_c \Pi_s + \frac{1}{K_\lambda} (\partial_x \phi_c)(\partial_x \phi_s) \right). \end{aligned} \tag{3.30}$$

Using the notations $\bar{g}_4 = W_0/\pi v_F$ and

$$\begin{aligned} y_\delta &= \frac{g_{2\|A}^* - g_{2\|B}^*}{4\pi v_F}, \\ y_\pm &= \frac{g_{2\|A}^* + g_{2\|B}^* \pm 2g_{2\perp}^*}{4\pi v_F}, \end{aligned}$$

where explicit (but lengthy) expressions for the fixed-point values $g_{2\|A/B}^*$ and $g_{2\perp}^*$ can be straightforwardly obtained from Eqs. (3.23) and (3.27), the renormalized velocities and LL-interaction-parameters appearing in Eq. (3.30) are given in the table 3.1. In the respective second equalities ($\tilde{v}/\tilde{K}$), we have specified the leading terms in $|\delta| \ll 1$, since the SOI-induced relative velocity asymmetry δ is small even for rather large α, see Eq. (3.1). The corrections to those expressions are of $\mathscr{O}(\delta^2)$ and are negligible in practice.

It is noteworthy that the "spin" velocity v_s is *not* renormalized for a Rashba wire, although it is well-known that v_s will be renormalized due to W_1 for $\alpha = 0$ [1]. This difference can be traced back to our thin-wire approximation (3.17). When releasing this approximation, there will be a renormalization in general. When the $2k_F$ component of the interaction potential $W_1 = 0$, see Eq. (3.19), we obtain $K_s = K_\lambda = 1$, and thus recover the theory of Ref. [36]. Furthermore the Hamiltonian is formally equivalent to the interacting

sector of the low-energy-Hamiltonian Eq. (2.29) for $W_1 = 0$, and to the noninteracting sector if setting both $W_0, W_1 \to 0$. The broken spin $SU(2)$ symmetry is reflected in $K_s < 1$ when both $\delta \neq 0$ and $W_1 \neq 0$.

3.5. Correlation functions

Since we arrived at a Gaussian field theory, Eq. (3.30), all low-energy correlation functions can now be computed analytically without further approximation. Analogous to the previous chapter, we shall first re-write the Hamiltonian in normal form (see below) and use the general formalism detailed in App.A.4 to derive a generic correlation function for vertex operators that allow to compute all observables of interest. We shall apply this to compute density-density correlation functions which will form the building blocks to study the RKKY-interaction in a an interacting Rashba-wire.

3.5.1. Diagonalization

Due to the structural similarity of the bosonic Hamiltonian in Eq. (3.30) with the interacting sector of the Hamiltonian in Eq.(2.29), it is not surprising that the former is diagonalized by the same symplectic transformation Eq.(2.31), albeit with modified parameters:

$$\begin{aligned} \tan(2\eta) &= 2\frac{v_\lambda}{K_\lambda}\frac{\sqrt{\left(v_c K_\lambda^2 + K_c K_s v_s\right)\left(v_s K_\lambda^2 + K_c K_s v_c\right)}}{\sqrt{K_c K_s}\left(v_c^2 - v_s^2\right)}, \\ y^2 &= \frac{K_s}{K_c}\frac{v_c K_\lambda^2 + K_c K_s \tilde{v}_s}{v_s K_\lambda^2 + K_c K_s v_c}. \end{aligned} \tag{3.31}$$

Re-writing the Hamiltonian in terms of the new field vectors $\hat{\Phi} = (\hat{\phi}_+, \hat{\theta}_+, \hat{\phi}_-, \hat{\theta}_-)^T$ with mutually dual boson fields $\hat{\phi}_j$ and $\hat{\theta}_j$, the diagonalized Hamiltonian is seen to describe an unconventional two-channel Luttinger liquid,

$$H = \sum_{j=1/2=\pm} \frac{\hbar v_j}{2} \int dx \left(\frac{1}{K_j} \left(\partial_x \hat{\phi}_j\right)^2 + K_j \left(\partial_x \hat{\theta}_j\right)^2 \right). \tag{3.32}$$

The Luttinger-liquid parameters K_j (where $j = 1/2 = +/-$) and plasmon velocities v_j are given by

$$\begin{aligned} v_j^2 &= \frac{1}{2}\left[\eta_c^2 + \eta_s^2 + 2\eta_\lambda^2 + j\left(\eta_c^2 - \eta_s^2\right)\triangle\right] \\ K_j^2 &= y^{-2j} K_\lambda^2 \frac{\eta_c^2 + \eta_s^2 + 2\eta_c\eta_s \frac{K_c K_s}{K_\lambda^2} + j\triangle}{\eta_c^2 + \eta_s^2 + 2\eta_c\eta_s \frac{K_\lambda^2}{K_c K_s} + j\triangle} \end{aligned} \tag{3.33}$$

where $\triangle \equiv \left(\eta_c^2 - \eta_s^2\right)\sqrt{1 + \tan(2\eta)}$. Note that $K_\pm = \tilde{K}_{c/s} + \mathscr{O}\left(\delta^2\right)$ and that the above expressions recover the LL theory for $\delta = 0$, where $v_j = v_F/K_j$ with $K_- = 1$.

3.5.2. Vertex-operator correlation functions

As before, we obtain an expression for the two-point-correlation function of a formal vertex operator $e^{ir\sqrt{4\pi}\vec{n}\cdot\vec{\phi}}$, specified by an index-vector $\vec{n} = \begin{pmatrix} n_{\phi_c} & n_{\theta_c} & n_{\phi_s} & n_{\theta_s} \end{pmatrix}$, by using the functional-integral formalism detailed in App. A (cf. Eq.(A.20-A.21))

$$\begin{aligned} &\left\langle T_t\, e^{i\sqrt{4\pi}\vec{n}\cdot\vec{\Phi}(x,\tau)} e^{i\sqrt{4\pi}\vec{m}\cdot\vec{\Phi}(0,0)} \right\rangle \\ &= \delta_{\vec{n},-\vec{m}} \prod_{j,\mu=\pm} \left[\frac{v_j\beta}{-ia\pi} \sinh\left(\frac{\pi}{v_j\beta} \left(\mu x - i\left(v_j\tau + a \right) \right) \right) \right]^{-\Gamma_{j;\mu}} \end{aligned} \tag{3.34}$$

Since we use the same transformation as in section 2.4.2, the exponents $\Gamma_{j;\mu}(\vec{n})$ are obtained by inserting the expressions for y and K_j given in Eqs. (3.31) and (3.33) in Eq.(2.37-2.38) and neglecting the ρ labels. We obtain

$$\Gamma_{+;\mu}(\vec{n}) = \left[\cos(\eta) \left(\sqrt{K_+} n_{\phi_c} - \mu \frac{1}{\sqrt{K_+}} n_{\theta_c} \right) + \sin(\eta) \left(y\sqrt{K_+} n_{\phi_s} - \mu \frac{1}{y\sqrt{K_+}} n_{\theta_s} \right) \right]^2, \tag{3.35}$$

$$\Gamma_{-;\mu}(\vec{n}) = \left[\cos(\eta) \left(\sqrt{K_-} n_{\phi_s} - \mu \frac{1}{\sqrt{K_-}} n_{\theta_s} \right) - \sin(\eta) \left(\frac{\sqrt{K_-}}{y} n_{\phi_c} - \mu \frac{y}{\sqrt{K_-}} n_{\theta_c} \right) \right]^2. \tag{3.36}$$

With the general expressions Eqs. (3.34-3.36), we can calculate all correlation function straightforwardly.

3.5.3. Density-Density correlations

The 1D charge-and spin densities $S^a(x)$ (with $a = x, y, z$) are defined as:

$$\rho(x) = \int dz \Psi^\dagger \Psi, \quad \boldsymbol{S}(x) = \int dz \Psi^\dagger \frac{\boldsymbol{\sigma}}{2} \Psi, \tag{3.37}$$

Using the identity Eq. (3.18) together with Eqs. (3.28-3.29), we can now express charge-density in bosonized form:

$$\begin{aligned} \rho(x) &= \sqrt{\frac{2}{\pi}}\, \partial_x \phi_c - \frac{2i}{\pi a} \eta_{AR}\eta_{AL} \cos(\theta_A - \theta_B) \\ &\times \sin\left[\left(k_F^{(A)} + k_F^{(B)} \right) x + \sqrt{2\pi}\phi_c \right] \cos(\sqrt{2\pi}\theta_s). \end{aligned}$$

Similarly, using the identity

$$\int dz \left[\phi^{\dagger}_{rk_F^{(\nu)},\nu r}\boldsymbol{\sigma}\,\phi_{r'k_F^{(\nu')},\nu' r'}\right](z) = \delta_{r,r'}\begin{pmatrix}\cos(\theta_A-\theta_B)\,\delta_{\nu,-\nu'}\\ -i\nu r\cos(\theta_A+\theta_B)\,\delta_{\nu,-\nu'}\\ \nu r\cos(2\theta_\nu)\,\delta_{\nu,\nu'}\end{pmatrix} + \delta_{r,-r'}\begin{pmatrix}\delta_{\nu,\nu'}\\ -i\nu r\cos(2\theta_\nu)\,\delta_{\nu,\nu'}\\ \nu r\cos(\theta_A+\theta_B)\,\delta_{\nu,-\nu'}\end{pmatrix},$$

the 1D spin density vector has the components[5]

$$\begin{aligned}
S^x(x) &= -i\frac{\eta_{AR}\eta_{BR}}{\pi a}\cos(\theta_A-\theta_B)\cos\left[\left(k_F^{(A)}-k_F^{(B)}\right)x+\sqrt{2\pi}\phi_s\right]\sin(\sqrt{2\pi}\theta_s)\\
&\quad -i\frac{\eta_{AR}\eta_{AL}}{\pi a}\cos\left[\left(k_F^{(A)}+k_F^{(B)}\right)x+\sqrt{2\pi}\phi_c\right]\sin\left[\left(k_F^{(A)}-k_F^{(B)}\right)x+\sqrt{2\pi}\phi_s\right],\\
S^y(x) &= i\frac{\eta_{AR}\eta_{BR}}{\pi a}\cos(\theta_A+\theta_B)\sin\left[\left(k_F^{(A)}-k_F^{(B)}\right)x+\sqrt{2\pi}\phi_s\right]\sin(\sqrt{2\pi}\theta_s)\\
&\quad -i\sum_{\nu=A,B=+,-}\nu\frac{\eta_{\nu R}\eta_{\nu L}}{2\pi a}\cos(2\theta_\nu)\cos\left[2k_F^{(\nu)}x+\sqrt{2\pi}\left(\phi_c+\nu\phi_s\right)\right],\\
S^z(x) &= \frac{1}{\sqrt{8\pi}}\left[\left(\cos 2\theta_A+\cos 2\theta_B\right)\partial_x\theta_s+\left(\cos 2\theta_A-\cos 2\theta_B\right)\partial_x\theta_c\right]\\
&\quad -i\frac{\eta_{AR}\eta_{BL}}{\pi a}\cos(\theta_A+\theta_B)\cos\left[\left(k_F^{(A)}+k_F^{(B)}\right)x+\sqrt{2\pi}\phi_c\right]\sin\left(\sqrt{2\pi}\theta_s\right).
\end{aligned}$$

Note that while $\partial_x\phi_c$ is proportional to the (slow part of the) charge density, the (slow) spin density is determined by both c and s sectors (where we refer to oscillations with large (small) momentum as fast (slow)).

Next we specify the nonzero components of the imaginary-time spin-spin correlation function

$$\chi^{ab}(x,\tau)=\langle S^a(x,\tau)S^b(0,0)\rangle. \tag{3.38}$$

Using the above bosonized expressions, some algebra yields

$$\chi^{a,b}(x,\tau)=\frac{1}{2(2\pi a)^2}\sum_{\nu}\begin{pmatrix}\cos\left(2k_F^{(\nu)}x\right) & \nu\cos(2\theta_\nu)\sin\left(2k_F^{(\nu)}x\right)\\ \nu\cos(2\theta_\nu)\sin\left(2k_F^{(\nu)}x\right) & \cos^2(2\theta_\nu)\cos\left(2k_F^{(\nu)}x\right)\end{pmatrix}\tilde{F}_\nu^{(1)}(x,\tau), \tag{3.39}$$

for $a,b=x$, y and

$$\chi^{zz}(x,\tau)=\frac{\cos^2(\theta_A+\theta_B)}{2(2\pi a)^2}\sum_{\nu r}\cos\left[\left(k_F^{(A)}+k_F^{(B)}\right)x\right]\tilde{F}_{\nu r}^{(2)}(x,\tau), \tag{3.40}$$

[5]From $\left\{\eta_{\nu,r},\eta_{\nu',r'}\right\}=2\delta_{\nu,\nu'}\delta_{r,r'}$ follows $\eta_{\nu r}\eta_{\nu r}=1$ and together with our convention $\eta_{\nu R}\eta_{\nu L}\eta_{-\nu,R}\eta_{-\nu,L}=1$ one obtains $\eta_{\nu L}\eta_{-\nu R}=-\eta_{\nu R}\eta_{-\nu,L}$.

where we kept only the long-ranged $2k_F^{(A/B)}$ oscillatory terms, since the "slow" terms that have wavelength $k_F^{(A)} - k_F^{(B)}$ or zero turn out to decay much faster. The functions $\tilde{F}^{(1,2)}_{\nu=A,B=+,-}(x,\tau)$ are obtained using Eq. (3.34) and Eqs. (3.35-3.36) to compute the thermal expectation values of operators $e^{i\sqrt{4\pi}\left(\frac{-r}{\sqrt{2}}\right)(\phi_+ + \nu\,\phi_-)(x,\tau)}$ and $e^{i\sqrt{4\pi}\left(\frac{-r}{\sqrt{2}}\right)(\phi_+ + \nu r\,\theta_-)}$ yielding $\tilde{F}^{(1)}_{\nu}$ and $\tilde{F}^{(2)}_{\nu}$, respectively , and are given by

$$\begin{aligned}
\tilde{F}^{(1/2)}_{\nu r}(x,\tau) &= \prod_{j,\mu=\pm}\left[\frac{v_j\beta}{-ia\pi}\sinh\left(\frac{\pi}{v_j\beta}\left(\mu x - i\left(v_j\tau + a\right)\right)\right)\right]^{-\Gamma^{(1/2)}_{j;\mu\nu r}} \\
&= \prod_{j,=\pm}\left|\frac{v_j\beta}{a\pi}\sin\left(\frac{\pi\left(-ix+\left(v_j\tau+a\right)\right)}{v_j\beta}\right)\right|^{-2\left(\Gamma^{(1/2)}_{j;-,\nu r}+\Gamma^{(1/2)}_{j;+,\nu r}\right)} \\
&\quad\times\left[\frac{\sin\left(\frac{\pi\left(+ix+\left(v_j\tau+a\right)\right)}{v_j\beta}\right)}{\sin\left(\frac{\pi\left(-ix+\left(v_j\tau+a\right)\right)}{v_j\beta}\right)}\right]^{-\frac{1}{2}\left(\Gamma^{(1/2)}_{j;-,\nu r}-\Gamma^{(1/2)}_{j;+,\nu r}\right)}
\end{aligned} \tag{3.41}$$

where the exponents are given by:

$$\begin{aligned}
\Gamma^{(1)}_{j;\mu,\nu,r}(\vec{n}) &= \frac{K_j}{2}\left[\cos(\eta) + j\nu y^j\sin(\eta)\right]^2, \\
\Gamma^{(2)}_{j;\mu,\nu,r}(\vec{n}) &= \frac{1}{2}\left[\cos(\eta)K_j^{\frac{j}{2}} - j\nu\mu r\frac{\sin(\eta)}{y}K_j^{-\frac{j}{2}}\right]^2.
\end{aligned} \tag{3.42}$$

Note that the Klein-factors do not contribute to the thermal expectation values and are omitted in the computation. Note also that the $2k_F$ part of the charge-density operator contains the same fields as the z-component of the spin-density. Hence, its correlation functions scale with the same exponents. Furthermore, it is worth pointing out that the real-time retarded correlation functions can be obtained from the above expressions by a mere Wick-rotation and hence one can set up a "phase-diagram" determining the dominant susceptibility, i.e. the one with the slowest decay.

3.6. RKKY interaction

Following our discussion in Sec. 3.1, we now investigate the combined effects of the Rashba SOI and the e-e interaction on the RKKY range function.

We consider a one-dimensional electron liquid with imaginary time action $S\left[\vec{\Phi}\right] = \int d\tau H\left[\vec{\Phi}\right] + \int dx d\tau \sum_k (-i\partial_\tau\phi_k)(-\partial_x\theta_k)$, where the Hamiltonian H is given in Eqs. (3.30, 3.32). We want to calculate the effective interaction between two magnetic impurities embedded in the system. We include the exchange coupling, $H_{imp} = J\sum_{i=1,2}\mathbf{\Sigma}_i\cdot\boldsymbol{S}(x_i)$, of

the 1D conduction electron spin density $\boldsymbol{S}(x)$ to localized spin-1/2 magnetic impurities, separated by $x = x_1 - x_2$, i.e., we include into the action the term

$$S_{imp} = J \sum_{i=1,2} \int_0^\beta d\tau \boldsymbol{\Sigma}_i \cdot \boldsymbol{S}(x_i)$$

describing the local coupling of two spin-1/2 impurities 1,2 at positions $x_{1,2}$ with the electron spin density. The effective action for the impurities is then given by

$$\begin{aligned} e^{-S_{eff}} = \int \mathscr{D}\left[\vec{\Phi}\right] e^{-S\left[\vec{\Phi}\right] - S_{imp}\left[\vec{\Phi}\right]} &= \left\langle e^{-S_{imp}\left[\vec{\Phi}\right]} \right\rangle \\ &= 1 - \left\langle S_{imp}\left[\vec{\Phi}\right] \right\rangle + \frac{1}{2}\left\langle S_{imp}^2\left[\vec{\Phi}\right] \right\rangle + \mathscr{O}\left(J^3\right) \end{aligned}$$

Assuming that the electron liquid is not magnetized, i.e. $\langle \boldsymbol{S}(x,\tau)\rangle = 0 \Leftrightarrow \left\langle S_{imp}\left[\vec{\Phi}\right]\right\rangle = 0$, we obtain the effective action to lowest order in J as:

$$\begin{aligned} S_{eff} = -\ln\left[\left\langle e^{-S_{imp}\left[\vec{\Phi}\right]}\right\rangle\right] &= -\frac{1}{2}\left\langle S_{imp}^2\left[\vec{\Phi}\right]\right\rangle + \mathscr{O}\left(J^3\right) \\ &\simeq -\beta J^2 \sum_{a,b} \Sigma_1^a \Sigma_2^b \int_0^\beta d\tau \, \langle S_a(x_{12},\tau) S_b(0,0)\rangle \end{aligned}$$

Thus we obtain the RKKY interaction

$$H_{\mathrm{RKKY}} = -J^2 \sum_{a,b} F^{ab}(x) \Sigma_1^a \Sigma_2^b, \tag{3.43}$$

describing spin-spin interactions between the two magnetic impurities, by perturbation theory to second order in J [49]. In the simplest 1D case (no SOI, no interactions), it is given by Eq. (3.2). In the present, more general case, the range function appears as a tensor ($\beta = 1/k_B T$ for temperature T)

$$F^{ab}(x) = \int_0^\beta d\tau \, \chi^{ab}(x,\tau). \tag{3.44}$$

Here, the imaginary-time (τ) spin-spin correlation function $\chi^{ab}(x,\tau)$ (see Eq. (3.38)) appears, which we derived in the previous subsection using the unperturbed ($J = 0$) LL model (cf. Eq. (3.30, 3.32)).

The range function thus effectively coincides with the static space-dependent spin susceptibility *tensor*, which is anisotropic (in the xy-plane), cf. Eq. (3.38-3.40).

In order to relate those results to more familiar forms, we shall now decompose the susceptibility tensor into three terms: a scalar, a vector, and a tensor-part, analogous to the decomposition of two spin-1/2 particles into a scalar (singlet) and a vector (triplet).

When spin $SU(2)$ symmetry is realized, $\chi^{ab}(x) = \delta^{ab} F_{\mathrm{ex}}(x)$, and one recovers Eq. (3.2), but in general this tensor is not diagonal. For a LL without Rashba SOI, $F_{\mathrm{ex}}(x)$ is as in

Eq. (3.2) but with a slower power-law decay $|x|^{-\eta}$ with an exponent $\eta < 1$ depending on the interaction [53]. If spin $SU(2)$ symmetry is broken, general arguments imply that Eq. (3.43) can be decomposed into three terms, namely (i) an isotropic exchange scalar coupling, (ii) a Dzyaloshinsky-Moriya (DM) vector term, and (iii) an Ising-like interaction,

$$\begin{aligned} H_{\mathrm{RKKY}}/J^2 &= -F_{\mathrm{ex}}(x)\boldsymbol{\Sigma}_1\cdot\boldsymbol{\Sigma}_2 - \boldsymbol{F}_{\mathrm{DM}}(x)\cdot(\boldsymbol{\Sigma}_1\times\boldsymbol{\Sigma}_2) \\ &\quad -\sum_{a,b} F^{ab}_{\mathrm{Ising}}(x)\Sigma_1^a\Sigma_2^b, \end{aligned} \tag{3.45}$$

where $F_{\mathrm{ex}}(x) = \frac{1}{3}\sum_a F^{aa}(x)$. The DM vector has the components

$$F^c_{\mathrm{DM}}(x) = \frac{1}{2}\sum_{a,b}\varepsilon^{cab}F^{ab}(x),$$

and the Ising-like tensor

$$F^{ab}_{\mathrm{Ising}}(x) = \frac{1}{2}\left(F^{ab}+F^{ba}-\frac{2}{3}\sum_c F^{cc}\delta^{ab}\right)(x)$$

is symmetric and traceless. For a 1D noninteracting quantum wire with Rashba SOI, the "twisted" RKKY Hamiltonian (3.45) has recently been discussed [50–52], and all range functions appearing in Eq. (3.45) were shown to decay $\propto |x|^{-1}$, as expected for a *noninteracting* system. Moreover, it has been emphasized [51] that there are different spatial oscillation periods, reflecting the presence of different Fermi momenta $k_F^{(A,B)}$ in a Rashba quantum wire.

Let us then consider the extended LL model (3.30), which includes the effects of both the e-e interaction and the Rashba SOI. The correlation functions (3.38) obey $\chi^{ba}(x,\tau) = \chi^{ab}(-x,-\tau)$, and since we find $\chi^{xz} = \chi^{yz} = 0$, the anisotropy acts only in the xy-plane. The four nonzero correlators are specified in Eqs. (3.39, 3.40), where only the long-ranged $2k_F^{(A,B)}$ oscillatory terms are kept. These are the relevant correlations determining the RKKY interaction in the interacting quantum wire. We note that in the noninteracting case, there is also a "slow" oscillatory component, corresponding to a contribution to the RKKY range function $\propto \cos\left[\left(k_F^{(A)}-k_F^{(B)}\right)x\right]/|x|$. Remarkably, we find that this $1/x$ decay law is not changed by interactions. However, we will show below that interactions cause a slower decay (i.e. with exponents smaller than unity) of certain "fast" oscillatory terms, e.g., the contribution $\propto \cos\left(2k_F^{(B)}x\right)$. We therefore do not further discuss the "slow" oscillatory terms in what follows.

Collecting everything, we find the various range functions in Eq. (3.45) for the inter-

acting case,

$$\begin{aligned} F_{\rm ex}(x) &= \frac{1}{6}\sum_{\nu}\Big[\left(1+\cos^2(2\theta_\nu)\right)\cos\left(2k_F^{(\nu)}x\right)F_\nu^{(1)}(x) \\ &\quad +\cos^2(\theta_A+\theta_B)\cos\left[(k_F^{(A)}+k_F^{(B)})x\right]F_\nu^{(2)}(x)\Big], \\ \boldsymbol{F}_{\rm DM}(x) &= \hat{e}_z\sum_{\nu}\frac{\nu}{2}\cos(2\theta_\nu)\sin\left(2k_F^{(\nu)}x\right)F_\nu^{(1)}(x), \\ F^{ab}_{\rm Ising}(x) &= \left[\frac{1}{2}\sum_{\nu}G^a_\nu(x)-F_{ex}(x)\right]\delta^{ab}, \end{aligned} \tag{3.46}$$

with the auxiliary vector

$$\boldsymbol{G}_\nu = \begin{pmatrix} \cos\left(2k_F^{(\nu)}x\right)F_\nu^{(1)}(x) \\ \cos^2(2\theta_\nu)\cos\left(2k_F^{(\nu)}x\right)F_\nu^{(1)}(x) \\ \cos^2(\theta_A+\theta_B)\cos\left[(k_F^{(A)}+k_F^{(B)})x\right]F_\nu^{(2)}(x) \end{pmatrix}.$$

The functions $F_\nu^{(1,2)}(x)$ follow by integration over τ from $\tilde{F}_\nu^{(1,2)}(x,\tau)$, see Eq. (3.41) in Sec. 3.37. This implies the respective decay laws for $a \ll |x| \ll v_F/k_BT$,

$$F_\nu^{(1/2)}(x) \;\propto\; |a/x|^{-1+2\left(\Gamma^{(1/2)}_{j;-}+\Gamma^{(1/2)}_{j;+}\right)}, \tag{3.47}$$

From Eq.(3.42), we obtain the exponents of the decay laws (Recall $\eta = \mathcal{O}(\delta)$and $\tilde{K}_- = 1 - const\,|\delta| < 1$)

$$\begin{aligned} 2\left(\Gamma^{(1)}_{j;-,\nu,r}+\Gamma^{(1)}_{j;+,\nu,r}\right) &= \cos^2(\eta)\,(K_++K_-)+\sin^2(\eta)\,\left(y^2K_++y^{-2}K_-\right) \\ &\quad +\nu\sin(2\eta)\,\left(yK_+-y^{-1}K_-\right) \\ &\simeq K_++K_-+\nu\sin(2\eta)\,\left(\tilde{y}\tilde{K}_c-\frac{1}{\tilde{y}}\right)+\mathcal{O}\left(\delta^2\right) \end{aligned}$$

$$\begin{aligned} 2\left(\Gamma^{(2)}_{j;-,\nu,r}+\Gamma^{(2)}_{j;+,\nu,r}\right) &= \cos^2(\eta)\left(K_++\frac{1}{K_-}\right)+\frac{\sin^2(\eta)}{y^2}\left(\frac{1}{K_+}+K_-\right) \\ &\simeq K_++\frac{1}{K_-}+\mathcal{O}\left(\delta^2\right) \end{aligned}$$

All those exponents approach unity in the noninteracting limit, in accordance with previous results [50, 51]. Moreover, in the absence of SOI ($\alpha = \delta = 0$), Eq. (3.47) reproduces the known $|x|^{-K_c}$ decay law for the RKKY interaction in a conventional LL [53].

Since $K_- \simeq \tilde{K}_s + \mathcal{O}\left(\delta^2\right) < 1$ for an interacting Rashba wire with $\delta \neq 0$, see Eq. (3.1), we conclude that $F_\nu^{(1)}$ with $\nu = B$, corresponding to the slower velocity $v_B = v_F(1-\delta)$,

leads to the slowest decay of the RKKY interaction. For large distance x, the RKKY interaction is therefore dominated by the $2k_F^{(B)}$ oscillatory part, and all range functions decay $\propto |x|^{-\eta_B}$ with the exponent

$$\begin{aligned}\eta_B &= -1+\cos^2(\eta)\,(K_+ + K_-) + \sin^2(\eta)\,\left(y^2 K_+ + y^{-2} K_-\right) - \sin(2\eta)\,\left(yK_+ - y^{-1}K_-\right) \\ &\simeq -1 + \tilde{K}_c + \tilde{K}_s + \nu 2\,\frac{\tilde{v}_\lambda}{\tilde{K}_\lambda}\,\frac{\left(\tilde{K}_\lambda^2 - \tilde{K}_c\right)}{(\tilde{v}_c + \tilde{v}_s)}. \end{aligned} \tag{3.48}$$

This exponent depends both on the e-e interaction potential and on the Rashba coupling α. The latter dependence also implies that electric fields are able to change the power-law decay of the RKKY interaction in a Rashba wire. The DM vector coupling also illustrates that the SOI is able to effectively induce off-diagonal couplings in spin space, reminiscent of spin precession effects. Also these RKKY couplings are $2k_F^{(B)}$ oscillatory and show a power-law decay with the exponent (3.48).

3.7. Conclusion

In this chapter, we have derived the low-energy theory of a homogeneous 1D quantum wire with (not too weak) Rashba spin-orbit interactions. We have studied the simplest case (no magnetic field, no disorder, single-channel limit), and in particular analyzed the possibility for a spin gap to occur because of electron-electron backscattering processes. The initial values for the coupling constants entering the one-loop RG equations were determined, and for rather general conditions, they are such that backscattering is marginally irrelevant and no spin gap opens. The resulting low-energy theory is a modified Luttinger liquid, Eq. (3.30), i.e. a Gaussian field theory formulated in terms of the boson fields $\phi_c(x)$ and $\phi_s(x)$ (and their dual fields). In this state, spin-charge separation is broken due to the Rashba coupling, but the theory still admits exact results for essentially all low-energy correlation functions.

Based on our bosonized expressions for the 1D charge and spin density and their correlation functions, the frequency dependence of various susceptibilities of interest, e.g., charge- or spin-density wave correlations, can then be computed in essentially the same way as presented above . One can then infer a "phase diagram" from the study of the dominant susceptibilities. According to our calculations, due to a conspiracy of the Rashba SOI and the e-e interaction, spin-density-wave correlations in the xy plane are always dominant for repulsive interactions.

Our low-energy theory allowed us to study the RKKY interaction between two magnetic impurities in such an interacting 1D Rashba quantum wire. On general grounds, the RKKY interaction can be decomposed into an exchange term, a DM vector term, and a traceless symmetric tensor interaction. For a noninteracting wire, the corresponding three range functions have several spatial oscillation periods with a common overall decay $\propto |x|^{-1}$. We have shown that interactions modify this picture. The dominant contribution (characterized by the slowest power-law decay) to the RKKY range function is now $2k_F^{(B)}$

oscillatory for all three terms, with the same exponent $\eta_B < 1$, see Eq. (3.48). This exponent depends both on the interaction strength and on the Rashba coupling. This raises the intriguing possibility to tune the power-law exponent η_B governing the RKKY interaction by an electric field, since α is tunable via a backgate voltage. We stress again that interactions imply that a single spatial oscillation period (wavelength $\pi/k_F^{(B)}$) becomes dominant, in contrast to the noninteracting situation where several competing wavelengths are expected.

4. Critical Josephson current through a bistable single-molecule junction

4.1. Introduction

In the following two chapters we will focus on molecular Josephson junctions, in which the contacting molecule has a conformational degree of freedom. The molecule bridges the gap between two superconductors and electrons can tunnel through the junction via the electronic level of the molecule. Such a setup is called a Josephson junction. Additionally, we consider the case where the molecule can flip to a different conformation (geometrical configuration) in which the energy of the electronic level available for tunneling is also different. This change of the conformational state can be caused by, e.g. vibrational states excited by the electrons tunneling through the junction [58].

The device setup of a quantum dot Josephson junction (QDJJ) is represented schematically in Fig. 4.1: A quantum dot , realized e.g. by a single molecule, is coupled to two superconducting leads (we denote the strength of the coupling to the electrodes by Γ, cf. Eq. (4.13)). Due to size quantization there are only discrete levels available for tunneling into and out of the insulating region. We consider the situation in which there is only one level available for resonant tunneling processes (represented by two red arrows in the figure), assuming that the level spacing is larger than the superconducting gap $\triangle$.

Let us first focus on the QDJJ without a conformational degree of freedom. This case, considered e.g. by Glazman and Matveev (1989) [59] is somewhat different from the one originally considered by Brian Josephson in 1962. Josephson considered an SIS-junction (where the "I" stands for an insulating region that can only be tunneled through) in which electrons tunnel directly from one lead to the other. However, the current-phase relation for weakly coupled electrodes is the same for the QDJJ and the SIS-junction

$$I(\varphi) = I_c \sin(\varphi), \tag{4.1}$$

with the *critical current* I_c and φ is the difference of the phases of the order parameters in the superconducting leads. Remarkably, this (equilibrium) current flows without any applied bias voltage. It has been measured by employing a superconducting quantum interference device [60–62, 80]. A QDJJ is different in that a (resonant) level is situated in the insulator between two superconductors. This resonant level can be due to, e.g. impurities in the tunnel barrier. Electrons in, say, the left superconductor can tunnel

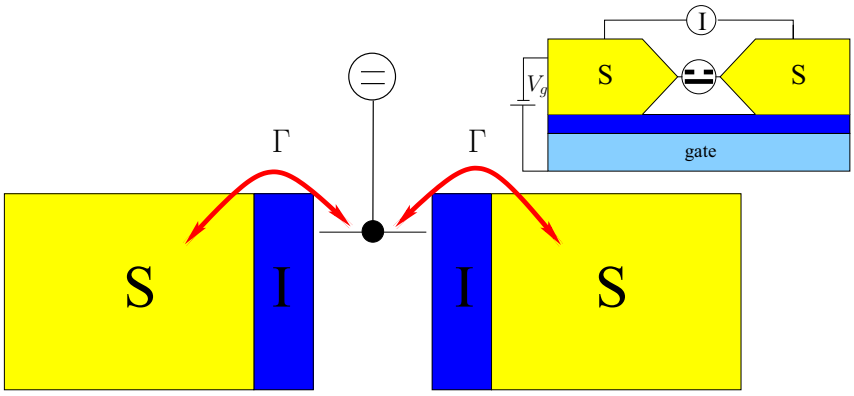

Figure 4.1: Molecular Josephson junction with TLS-coupling (top circle). Tunneling on/off the resonant level is symbolised by red arrows. The inset shows the device setup: a molecular junction between two superconducting banks. The device is current-biased and the resonant level can be shifted by tuning the gate voltage.

through the insulating region onto the level in the middle and from there tunnel through to the right superconductor.

Since tunneling can only occur through the single level, electron-electron interaction plays an important role in the QDJJ [59, 63–67]. Due to Coulomb repulsion, an electron has to pay a charging U in order to hop onto an already occupied dot. In the limit of weak coupling to the electrodes $\Gamma \ll \triangle$, a so-called π-phase can be realized, with $I_c < 0$ in Eq. (4.1) for sufficiently large U. In this π-regime, $\varphi = \pi$ corresponds to the ground state of the system (or to a minimum of the free energy for finite temperature, since $I = 2\partial_\varphi F$), in contrast to the usual 0-state with $I_c > 0$, where $\varphi = 0$ in the ground state.

This behaviour was theoretically predicted by Glazman and Matveev [59] (assuming a (formally) infinite charging energy U of the dot), who found that the critical current I_c changes its sign when the dot is singly occupied. The behaviour for finite U, where double occupation is possiple, is similar in that the critical current is positive if the dot is not occupied or doubly occupied, and negative, if the dot is occupied by a single electron (we assume here that the energy ε_d of the resonant level with respect to the chemical potential of the leads can be tuned by means of a backgate $\varepsilon_d = \varepsilon_d(V_g)$). The critical current $I_c(\varepsilon_d)$ for this model is depicted in Fig. 4.2. Experimental observations of the π-phase were recently reported for InAs nanowire dots [60] and for nanotubes [61, 68], but a π-junction is also encountered in superconductor-ferromagnet-superconductor structures [69, 70].

Since the influence of a TLS coupled to the dot on this π-phase is one of the main results of this chapter, we give a brief explanation for this behaviour before focussing on the model including the TLS considered here. Cooper pairs in single-level interacting quantum dots can be transported via fourth order (co-) tunneling events. Examples of such events are shown in Fig. 4.3, where top and bottom diagrams represent initial and final states, respectively and the diagrams in the middle illustrate the intermediate virtual states. The sequence of the four tunnel processes in both diagrams is indicated by numbers. Fig. 4.3a illustrates the transfer of a Cooper pair through the dot whose level is occupied

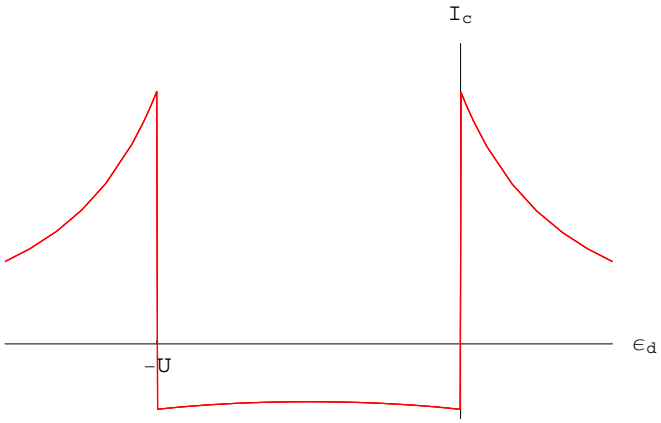

Figure 4.2: Critical current $I_c(\varepsilon_d)$ of the quantum-dot Josephson junction without coupling to a TLS as function of the dot-level energy ε_d. Note the two discontinuities at $\varepsilon_d = 0$ and $\varepsilon_d = -U$, which correspond to a change of the dot-occupation number N. For $N = 0$ and $N = 2$ (i.e. $\varepsilon_d > 0$ and $\varepsilon_d < U$, respectively), the critical current is positive and negative for $N = 1$ (cf. Sec.4.1).

by a *single* electron (with spin up, $|\uparrow\rangle$). The sequence of the tunnel processes is necessarily permutated compared to the ordinary transport of Cooper pairs and consequently, the spin-ordering of the Cooper pair is reversed, i.e. the Cooper pair on the right is created in the order $|\uparrow\rangle, |\downarrow\rangle$ while the pair on the left is annihilated in the order $|\downarrow\rangle, |\uparrow\rangle$. The result of the reversal of the spin-ordering is a sign change of the Cooper pair singlet state (e.g., from $\frac{1}{\sqrt{2}}(|\uparrow\downarrow\rangle - |\downarrow\uparrow\rangle)$ to $e^{i\pi}\frac{1}{\sqrt{2}}(|\uparrow\downarrow\rangle - |\downarrow\uparrow\rangle)$), which leads to a π-shift in the current-phase relation Eq. (4.1) and a negative Josephson-current. If the dot is empty or occupied by two electrons, the sequence of tunneling events detailed above is prohibited (due to the Pauli principle in the case of double occupation), while other sequences are allowed that do not reverse spin-ordering and hence lead to a positive current (cf. Fig. 4.3b for an example of the sequence of processes in the case of double occupation). Hence, in single level quantum-dot that is occupied by an odd (even) number of electrons, the Josephson current is negative (positive).

In the remainder of this chapter, we shall consider a QDJJ wherein a *two-level system* (TLS) is coupled to the dot's charge. The TLS here serves as a simple model for the bistable conformational degree of freedom of a single molecule (see also Sec. 4.2). We calculate the critical current perturbatively to lowest order in the tunneling couplings, allowing for arbitrary e-e interaction strength U and TLS parameters, and show that it can significantly change due to the two-level system. In particular, we will see that the π-junction behavior, generally present for strong interactions, can be completely suppressed.

This chapter is structured as follows: In Sec. 4.2 we discuss the model and present the general perturbative result for the critical current. In the case where the tunnel matrix element W_0 between the two TLS states is zero, the result allows for an elementary interpretation in terms of the uncoupled QDJJ, which we provide in Sec. 4.3. The general case (i.e. $W_0 \neq 0$) is discussed in Sec. 4.4, and we shall give some conclusions in Sec. 4.5.

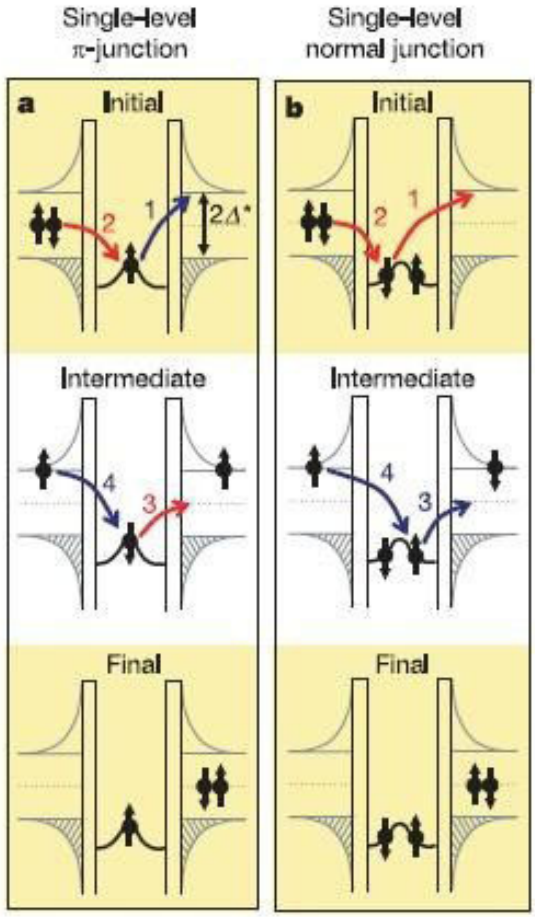

Figure 4.3: Examples of allowed tunneling processes through a single-level quantum dot coupled to superconducting leads. Picture taken from [60].

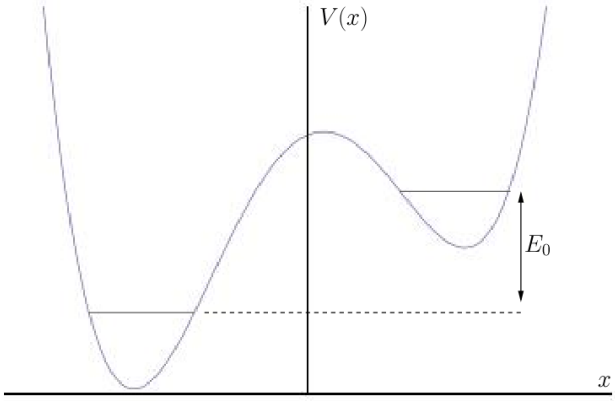

Figure 4.4: Bistable potential energy $V(x)$.

4.2. Model and perturbation theory

We study a spin-degenerate molecular dot level with single-particle energy ε_d and on-site Coulomb repulsion $U > 0$, coupled to the TLS and to two standard s-wave BCS superconducting banks (leads). The TLS is characterized by the (bare) energy difference E_0 of the two states, and by the tunnel matrix element W_0. The model Hamiltonian reads

$$H = H_0 + H_{\rm tun} + H_{\rm leads}, \tag{4.2}$$

where the coupled dot-plus-TLS part is

$$H_0 = -\frac{E_0}{2}\sigma_z - \frac{W_0}{2}\sigma_x + \left(\varepsilon_d + \frac{\lambda}{2}\sigma_z\right)(n_\uparrow + n_\downarrow) + U n_\uparrow n_\downarrow \tag{4.3}$$

with the occupation number $n_s = d_s^\dagger d_s$ for dot fermion d_s with spin $s = \uparrow, \downarrow$. Note that the TLS couples with strength λ to the charge on the dot, which can be rationalized in simple terms by assuming a one-dimensional effective reaction coordinate X describing conformations of the molecule. The dominant (dipole-) coupling to the electronic degrees of freedom is then (as for phonons) of the form $\propto X\left(n_\uparrow + n_\downarrow\right)$ [58, 71–73]. In the limit of interest, the potential energy $V(X)$ is bistable with two local minima (c.f. Fig. 4.4) and the low-energy dynamics of X can be restricted to the lowest quantum state in each well which leads to Eq. (4.3). The TLS parameters and the dipole coupling energy λ can be defined in complete analogy to Refs. [58, 77], and typical values for λ in the *meV* range are expected, comparable to typical charging energies U.

Moreover, the electron operators $c_{\boldsymbol{k}\alpha s}$, corresponding to spin-$s$ and momentum-$\boldsymbol{k}$ states in lead $\alpha = L/R$, are governed by a standard BCS Hamiltonian with complex order parameter $\Delta_{L/R} e^{\pm i\varphi/2}$ (with $\Delta_{L/R} > 0$), respectively,

$$\begin{aligned} H_{\rm leads} = \sum_{\alpha=L,R} H^\alpha_{\rm leads} \;&=\; \sum_\alpha \sum_{\boldsymbol{k}s} \varepsilon_{\boldsymbol{k}\alpha} c^\dagger_{\boldsymbol{k}\alpha s} c_{\boldsymbol{k}\alpha s} \\ &\quad - \sum_\alpha \sum_{\boldsymbol{k}} \left(e^{i\alpha\varphi/2} \Delta_\alpha c^\dagger_{\boldsymbol{k}\alpha\uparrow} c^\dagger_{-\boldsymbol{k},\alpha\downarrow} + \text{h.c.} \right), \end{aligned} \tag{4.4}$$

where $\varepsilon_{\boldsymbol{k}\alpha}$ is the (normal-state) dispersion relation. Finally, the tunneling Hamiltonian is

$$H_{\rm tun} = \sum_{\alpha s} \left(H^{(-)}_{T\alpha s} + H^{(+)}_{T\alpha s} \right), \quad H^{(-)}_{T\alpha s} = \sum_{\boldsymbol{k}} t_{\boldsymbol{k}\alpha} c^\dagger_{\boldsymbol{k}\alpha s} d_s, \tag{4.5}$$

where $H^{(-)}_{T\alpha s}$ describes tunneling of an electron with spin s from the dot to lead α with tunnel amplitude $t_{\boldsymbol{k}\alpha}$, and the reverse process is generated by $H^{(+)}_{T\alpha s} = H^{(-)\dagger}_{T\alpha s}$.

4.2.1. Josephson current and perturbation theory

The operator for the current through contact $\alpha = L, R$ is $\dot{N}_\alpha$ where $N_\alpha = \Sigma_{\boldsymbol{k},s} c^\dagger_{\boldsymbol{k}\alpha s} c_{\boldsymbol{k}\alpha s}$, is the number operator of electrons in lead α and hence, we obtain the current as $I_\alpha =$

$i\langle[H,N_\alpha]\rangle = i\sum_s \left\langle H^{(+)}_{T\alpha s} - H^{(-)}_{T\alpha s}\right\rangle = 2Im\sum_s \left\langle H^{(-)}_{T\alpha s}\right\rangle$. The Josephson current $I(\varphi)$ at temperature $T=\beta^{-1}$ follows from the equilibrium (imaginary-time) average (see, e.g. [78]),

$$I_\alpha = 2\ \mathrm{Im}\sum_s \left\langle \mathscr{T}_\tau e^{-\int_0^\beta d\tau\ H_{\mathrm{tun}}(\tau)} H^{(-)}_{T\alpha s}\right\rangle, \tag{4.6}$$

where the lead $\alpha = L/R$ and spin-index $s=\uparrow,\downarrow$ can be chosen arbitrarily by virtue of current conservation and spin-$SU(2)$ invariance, and $\mathscr{T}_\tau$ is the (imaginary) time-ordering operator.

Equation (4.6) is then evaluated by lowest-order perturbation theory in H_{tun} in a similar manner as in Ref. [67]. The leading contribution is of fourth order in the tunnel matrix elements, since we exclude normal current and only look at Cooper-pair tunneling

$$\begin{aligned} I_\alpha &= -2Im\sum_s \frac{1}{3!}\int_0^\beta d\tau_1\int_0^\beta d\tau_2\int_0^\beta d\tau_3 \left\langle \mathscr{T}_\tau\left[H_{\mathrm{tun}}(\tau_1)\,H_{\mathrm{tun}}(\tau_2)\,H_{\mathrm{tun}}(\tau_3)\,H^{(-)}_{T\alpha s}(0)\right]\right\rangle, \\ &= -4Im\int_0^\beta d\tau_1\int_0^\beta d\tau_2\int_0^\beta d\tau_3 \left\langle T_\tau\left[H^{(+)}_{T\overline{\alpha}\downarrow}(\tau_1)H^{(+)}_{T\overline{\alpha}\uparrow}(\tau_2)H^{(-)}_{T\alpha\downarrow}(\tau_3)H^{(-)}_{T\alpha\uparrow}(0)\right]\right\rangle_0, \end{aligned}$$

where we used that in order to have tunneling of Cooper pairs, we need two operators $H^{(+)}_{T\overline{\alpha}s}$ (describing tunneling of an electron with spin s from lead $-\alpha$ onto the dot) and two operators $H^{(-)}_{T\alpha s}$ (describing tunneling of an electron with spin s from the dot onto lead α). To lowest non-vanishing order in perturbation theory the current is:

$$I_\alpha = -4Im\sum_{\boldsymbol{k}\boldsymbol{k}';\boldsymbol{p}\boldsymbol{p}'} t^*_{\boldsymbol{k}\overline{\alpha}}t^*_{\boldsymbol{k}'\overline{\alpha}}t_{\boldsymbol{p}\alpha}t_{\boldsymbol{p}'\alpha}\int_0^\beta d\tau_1\int_0^\beta d\tau_2\int_0^\beta d\tau_3\, G_{leads}\,G_{D-TLS} \tag{4.7}$$

where the total Green's function factorizes into the lead- and dot+TLS-Green's functions, since the respective parts of the Hamiltonian commute,

$$G_{leads} = \left\langle T_\tau c_{\boldsymbol{k}\overline{\alpha}\downarrow}(\tau_1)\,c_{\boldsymbol{k}'\overline{\alpha}\uparrow}(\tau_2)\,c^\dagger_{\boldsymbol{p}\alpha\downarrow}(\tau_3)\,c^\dagger_{\boldsymbol{p}'\alpha\uparrow}(0)\right\rangle, \tag{4.8}$$

$$G_{D-TLS} = \frac{1}{Z}\sum_{\sigma_z n_\uparrow n_\downarrow}\left\langle \sigma_z n_\uparrow n_\downarrow\left| T_\tau e^{-\beta H_0} d^\dagger_\downarrow(\tau_1)\,d^\dagger_\uparrow(\tau_2)\,d_\downarrow(\tau_3)\,d_\uparrow(0)\right|\sigma_z n_\uparrow n_\downarrow\right\rangle, \tag{4.9}$$

and the partition function is given by $Z=\sum_{n_\uparrow n_\downarrow\sigma_z}\langle n_\uparrow n_\downarrow,\sigma_z|\exp(-\beta H_0)|n_\uparrow n_\downarrow,\sigma_z\rangle$.

Superconducting leads

The (imaginary) time evolution of the lead-operator depends only on H_{leads}, since $[H_0, c_{k\alpha\sigma}]=0$, i.e. $c_{k\alpha\sigma}(\tau) = e^{H_{leads}\tau}c_{k\alpha\sigma}e^{-H_{leads}\tau}$. Furthermore, H_{leads} is quadratic in the lead operators and hence, one can apply Wick's theorem, i.e. by taking contractions

of the lead-electron operators in Eq. (4.8), the leads Green's function can be expressed as a product

$$G_{leads} = F^{*}_{\overline{\alpha}}(\boldsymbol{k}, \tau_1 - \tau_2)\, F_{\alpha}(\boldsymbol{p}, \tau_3)\; \delta_{\boldsymbol{k}',-\boldsymbol{k}}\, \delta_{\boldsymbol{p}',-\boldsymbol{p}}\,, \tag{4.10}$$

where $F_{\alpha}(k,\tau) = -\left\langle T_{\tau} c^{\dagger}_{-\boldsymbol{k}\alpha\downarrow}(\tau)\, c^{\dagger}_{\boldsymbol{k}\alpha\uparrow}(0)\right\rangle$ are the so-called *anomalous* correlation functions[1]. In Fourier-space, the anomalous correlation function can be straightforwardly obtained using the equation of motion technique (see, e.g. [78]). Performing the Matsubara-sums, one obtains

$$F_{\alpha}(\boldsymbol{k}, ik_n) = \frac{-\triangle^{*}_{\boldsymbol{k}}}{(ik_n)^2 - E^2_{\boldsymbol{k}\alpha}} \;\longleftrightarrow\; F_{\alpha}(\boldsymbol{k},\,\tau) = \frac{\triangle^{*}_{\boldsymbol{k}}}{2E_{\boldsymbol{k}\alpha}} f_{\alpha}(E_{\boldsymbol{k}\alpha}, \tau)\,,$$

where $ik_n = i\pi(2n+1)/\beta$ is the Matsubara frequency for fermions and

$$f_{\alpha}(E,\tau) = n_F(-E,\tau)\, e^{-E|\tau|} - n_F(+E,\tau)\, e^{+E|\tau|}. \tag{4.11}$$

The Energy-momentum relation is given by $E_{\boldsymbol{k}\alpha} = \sqrt{\varepsilon^2_{\boldsymbol{k}\alpha} + |\triangle_{\alpha}|^2}$.

Imaginary time evolution of the dot-operators

The dot operators in Eq. (4.9) evolve as $d_{\sigma}(\tau) = e^{H_0\tau} d_{\sigma} e^{-H_0\tau}$. The Hamiltonian H_0, however, is not diagonal in the TLS-degree of freedom. In order to make analytical progress, the exponential can be decomposed as,

$$e^{\tau H_0} = e^{\tau H_{dot}} \sum_{\sigma=\pm} e^{\sigma\,\tau\frac{1}{2}\hat{\Phi}} \hat{A}^{\sigma},$$

where we define the operators $\hat{A}^{\sigma}|N\rangle = A^{\sigma}_{N}|N\rangle$ and $\hat{\phi}\,|N\rangle = A^{\sigma}_{N}|N\rangle$ (with $N = n_{\uparrow} + n_{\downarrow}$) and their eigenvalues are given by the 2×2 matrices (in TLS space)

$$A^{\pm}_{N} = \frac{1}{2}\left(1 \mp \frac{(E_0 - N\lambda)\sigma_z + W_0\sigma_x}{\Phi_N}\right),$$

and the scale

$$\Phi_N = \sqrt{(E_0 - N\lambda)^2 + W_0^2}. \tag{4.12}$$

Using this decomposition, one can now evaluate Eq. (4.9) explicitely. The rather lengthy expression is only an intermediate result that gives no further physical insight and shall be omitted here.

[1] Note that since correlation functions of lead operators that act on different leads are zero, normal Green's functions like $\left\langle T_{\tau} c^{\dagger}_{k\alpha s}(\tau)\, c_{k'\alpha' s'}(0)\right\rangle \propto \delta_{k,k'}\delta_{\alpha,\alpha'}\delta_{s,s'}$ do not appear.

Critical current

We define the hybridizations by

$$\Gamma_\alpha(E) = 2\pi \sum_{\boldsymbol{k}} |t_{\boldsymbol{k}\alpha}|^2 \, \delta(E - \varepsilon_{\boldsymbol{k}\alpha}). \tag{4.13}$$

Since we assume a small central region where the coupling is point-like, we can approximate the tunnel matrix elements by a constant $t_{\boldsymbol{k}\alpha} \approx t_\alpha$ and take the usual wide-band approximation $\Gamma_\alpha \simeq \pi\rho_F |t_\alpha|^2$ where ρ_F is the (normal-state) density of states in the leads. Furthermore, we only consider temperatures well below both BCS gaps, $T \ll \Delta_{L,R}$. Putting $\alpha = L$ and $s = \uparrow$, after some algebra, the Josephson current takes the form of Eq. (4.1) introduced in Sec. 4.1 with the critical current

$$I_c = \frac{2}{\pi^2} \int_{|\Delta_L|}^{\infty} \frac{\Gamma_L \Delta_L dE}{\sqrt{E^2 - \Delta_L^2}} \int_{|\Delta_R|}^{\infty} \frac{\Gamma_R \Delta_R dE'}{\sqrt{E'^2 - \Delta_R^2}} C(E, E'), \tag{4.14}$$

where we used Eqs. (4.9-4.11) and Eq. (4.13). The function C in Eq. (4.14) can be decomposed according to

$$C(E, E') = \sum_{N=0}^{2} C_N(E, E'), \tag{4.15}$$

with contributions C_N for fixed dot occupation number $N = n_\uparrow + n_\downarrow = \{0, 1, 2\}$. For given N, the two eigenenergies (labeled by $\sigma = \pm$) of the dot-plus-TLS Hamiltonian H_0 in Eq. (4.3) are

$$E_N^{\sigma=\pm} = N\varepsilon_d + U\delta_{N,2} + \frac{\sigma}{2}\Phi_N, \tag{4.16}$$

where the scale Φ_N is given in Eq. (4.12). The occupation probability for the state (N, σ) is

$$p_N^\sigma = \frac{1}{Z} e^{-\beta E_N^\sigma} (1 + \delta_{N,1}), \tag{4.17}$$

where Z ensures normalization, $\sum_{N\sigma} p_N^\sigma = 1$. With the propagator

$$G_\xi(E) = \frac{1}{E - \xi}, \tag{4.18}$$

we then find the contributions C_N in Eq. (4.15),

$$C_0(E,E') = \sum_{\sigma_1\cdots\sigma_4} \Big[p_0^{\sigma_2}\, T_{1010}^{\sigma_1\sigma_2\sigma_3\sigma_4}\, G_{E_0^{\sigma_2}-E_1^{\sigma_3}}(E)\, G_{E_0^{\sigma_2}-E_1^{\sigma_1}}(E')\, G_{E_0^{\sigma_2}-E_0^{\sigma_4}}(E+E') + 2p_0^{\sigma_4}\, T_{1210}^{\sigma_1\sigma_2\sigma_3\sigma_4}\, G_{E_0^{\sigma_4}-E_1^{\sigma_1}}(E)\, G_{E_0^{\sigma_4}-E_1^{\sigma_3}}(E')\, G_{E_0^{\sigma_4}-E_2^{\sigma_2}}(0) \Big], \tag{4.19}$$

$$\begin{aligned} C_1(E,E') = -\sum_{\sigma_1\cdots\sigma_4} \Big[& T_{1210}^{\sigma_1\sigma_2\sigma_3\sigma_4} \Big(p_1^{\sigma_1}\, G_{E_1^{\sigma_1}-E_0^{\sigma_4}}(E)\, G_{E_1^{\sigma_1}-E_2^{\sigma_2}}(E)\, G_{E_1^{\sigma_1}-E_1^{\sigma_3}}(E+E') \\ & + p_1^{\sigma_3}\, G_{E_1^{\sigma_3}-E_0^{\sigma_4}}(E')\, G_{E_1^{\sigma_3}-E_2^{\sigma_2}}(E')\, G_{E_1^{\sigma_3}-E_1^{\sigma_1}}(E+E') \Big) \\ & + \frac{p_1^{\sigma_1}}{2}\, T_{1010}^{\sigma_1\sigma_2\sigma_3\sigma_4}\, G_{E_1^{\sigma_1}-E_0^{\sigma_4}}(E)\, G_{E_1^{\sigma_1}-E_0^{\sigma_2}}(E')\, G_{E_1^{\sigma_1}-E_1^{\sigma_3}}(E+E') \\ & + \frac{p_1^{\sigma_2}}{2}\, T_{2121}^{\sigma_1\sigma_2\sigma_3\sigma_4}\, G_{E_1^{\sigma_2}-E_2^{\sigma_3}}(E)\, G_{E_1^{\sigma_2}-E_2^{\sigma_1}}(E')\, G_{E_1^{\sigma_2}-E_1^{\sigma_4}}(E+E') \Big], \end{aligned} \tag{4.20}$$

$$C_2(E,E') = \sum_{\sigma_1\cdots\sigma_4} \Big[p_2^{\sigma_1}\, T_{2121}^{\sigma_1\sigma_2\sigma_3\sigma_4}\, G_{E_2^{\sigma_1}-E_1^{\sigma_4}}(E)\, G_{E_2^{\sigma_1}-E_1^{\sigma_2}}(E')\, G_{E_2^{\sigma_1}-E_2^{\sigma_3}}(E+E') + 2p_2^{\sigma_2}\, T_{1210}^{\sigma_1\sigma_2\sigma_3\sigma_4}\, G_{E_2^{\sigma_2}-E_1^{\sigma_1}}(E)\, G_{E_2^{\sigma_2}-E_1^{\sigma_3}}(E')\, G_{E_2^{\sigma_2}-E_0^{\sigma_4}}(0). \tag{4.21}$$

Here, we have used the matrix elements

$$T_{N_1N_2N_3N_4}^{\sigma_1\sigma_2\sigma_3\sigma_4} = \mathrm{Tr}\left(A_{N_1}^{\sigma_1} A_{N_2}^{\sigma_2} A_{N_3}^{\sigma_3} A_{N_4}^{\sigma_4} \right). \tag{4.22}$$

Note that the critical current can be written as sum of three contributions representing processes with zero, single and double occupation. The respective occupation probabilities p_N^σ govern which processes (belonging to $N = 0, 1, 2$, respectively) contribute (the ones belonging to different occupation numbers are strongly suppressed). For $T = 0$, it can be shown that C_0 and C_2 are always positive, while C_1 yields a negative contribution to the critical current. When C_1 outweighs the two other terms, we arrive at the π-phase with $I_c < 0$ (see also the discussion in Sec. 4.1).

Below, we consider identical superconductors, $\Delta_L = \Delta_R = \Delta$, and assume $\lambda > 0$. It is useful to define the reference current scale

$$I_0 = \frac{\Gamma_L \Gamma_R}{\Delta^2} \frac{2e\Delta}{\pi^2 \hbar}. \tag{4.23}$$

Within lowest-order perturbation theory, the hybridizations Γ_L and Γ_R only enter via Eq. (4.23) and thus can be different. Eq. (4.14) provides a general but rather complicated expression for the critical current, even when considering the symmetric case $\Delta_L = \Delta_R$. In the next section, we will therefore first analyze the limiting case $W_0 = 0$.

4.3. No TLS tunneling

When there is no tunneling between the two TLS states, $W_0 = 0$, the Hilbert space of the system can be decomposed into two orthogonal subspaces $\mathscr{H}_+ \oplus \mathscr{H}_-$, with the fixed conformational state $\sigma = \pm$ in each subspace. Eq. (4.16) then simplifies to

$$E_N^\sigma = \left(\varepsilon_d + \frac{\sigma\lambda}{2}\right) N + U\delta_{N,2} - \frac{\sigma E_0}{2}. \tag{4.24}$$

One thus arrives at two decoupled copies of the usual interacting dot problem (without TLS), but with a shifted dot level $\varepsilon_\sigma = \varepsilon_d + \sigma\lambda/2$ and the "zero-point" energy shift $-\sigma E_0/2$. As a result, the critical current I_c in Eq. (4.14) can be written as a weighted sum of the partial critical currents $I_c(\varepsilon_\sigma)$ through an interacting dot level (without TLS) at energy ε_σ,

$$I_c = \sum_{\sigma=\pm} p^\sigma I_c(\varepsilon_\sigma), \tag{4.25}$$

where $p^\sigma = \sum_N p_N^\sigma$ with Eq. (4.17) and Eq. (4.24) denotes the probability for realizing the conformational state σ. The current $I_c(\varepsilon)$ has already been calculated in Ref. [67] (in the absence of phonons), and has been reproduced here. In the absence of TLS tunneling, the matrix elements (4.22) simplify to $T^{\sigma_1\sigma_2\sigma_3\sigma_4}_{N_1N_2N_3N_4} = \prod_{i=1}^4 \delta_{\tilde\sigma_i,1} + \prod_{i=1}^4 \delta_{\tilde\sigma_i,-1}$ where $\tilde\sigma_i = \sigma_i \mathrm{sgn}(N_i\lambda - E_0)$. We now rename $\tilde\sigma \to \sigma$ to denote the conformational state (eigenstate of σ_z). The partial current $I_c(\varepsilon_\sigma)$ corresponding to fixed conformational state $\sigma = \pm$ is then given by Eq. (4.14) where the expressions Eqs. (4.19-4.21) reduce to

$$C_N^\sigma(E,E') \;=\; \tilde p_N^\sigma c_N^\sigma(E,E'), \tag{4.26}$$

where $\tilde p_N^\sigma = \frac{1}{Z_\sigma} e^{-\beta E_N^\sigma}(1+\delta_{N,1})$ with Z_σ such that $\sum_N \tilde p_N^\sigma = 1$. Moreover, the c_N^σ are given by

$$c_0^\sigma(E,E') = \frac{1}{(E+\varepsilon_\sigma)(E'+\varepsilon_\sigma)}\left[\frac{1}{E+E'} + \frac{2}{2\varepsilon_\sigma+U}\right],$$

$$\begin{aligned} c_1^\sigma(E,E') = -\frac{1}{E+E'}\Bigg[&\frac{1}{(E-\varepsilon_\sigma)(E+\varepsilon_\sigma+U)} \\ &+ \frac{1}{(E'-\varepsilon_\sigma)(E'+\varepsilon_\sigma+U)} + \frac{1/2}{(E-\varepsilon_\sigma)(E'-\varepsilon_\sigma)} \\ &+ \frac{1/2}{(E+\varepsilon_\sigma+U)(E'+\varepsilon_\sigma+U)}\Bigg], \end{aligned}$$

$$c_2^\sigma(E,E') \;=\; \frac{1}{(E-\varepsilon_\sigma-U)(E'-\varepsilon_\sigma-U)}\left[\frac{1}{E+E'} - \frac{2}{2\varepsilon_\sigma+U}\right].$$

In order to establish the relevant energy scales determining the phase diagram, we now take the $T = 0$ limit. Then the probabilities Eq. (4.17) simplify to $\tilde p_N^\sigma = \delta_{N\bar N}\delta_{\sigma\bar\sigma}$, where

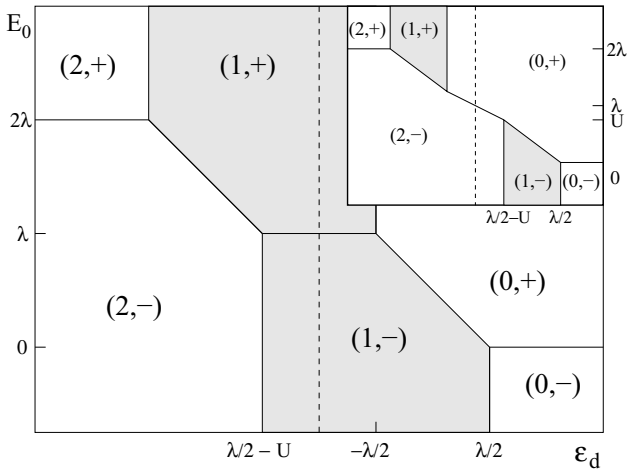

Figure 4.5: Ground-state phase diagram in the $E_0 - \varepsilon_d$ plane for $W_0 = 0$. Different regions $(\bar{N}, \bar{\sigma})$ are labelled according to the ground-state dot occupation number $\bar{N} = 0, 1, 2$ and the conformational state $\bar{\sigma} = \pm$. Dark areas correspond to π-junction behavior. The charge-degeneracy line $\varepsilon_d = -U/2$ is indicated as dashed line. Main panel: $\lambda < U$. Inset: $\lambda > U$, where no π-junction behavior is possible for $U < E_0 < 2\lambda - U$.

$E_{\bar{N}}^{\bar{\sigma}} = \min_{(N,\sigma)} \left(E_N^{\sigma}\right)$ is the ground-state energy of H_0 for $W_0 = 0$. Depending on the system parameters, the ground state then realizes the dot occupation number $\bar{N}$ and the TLS state $\bar{\sigma}$. The different regions $(\bar{N}, \bar{\sigma})$ in the $E_0 - \varepsilon_d$ plane are shown in the phase diagram in Fig. 4.5. The corresponding critical current in each of these regions is then simply given by $I_c = I_c(\varepsilon_{\bar{\sigma}})$.

By analyzing the dependence of the ground-state energy on the system parameters, one can always (even for $W_0 \neq 0$) write the function $C(E, E')$ in Eq. (4.14) as

$$\begin{aligned} C(E,E') &= \Theta(\xi_- - \varepsilon_d)\, C_2 \\ &+ \Theta(\varepsilon_d - \xi_-)\, \Theta(\xi_+ - \varepsilon_d)\, C_1 + \Theta(\varepsilon_d - \xi_+)\, C_0, \end{aligned} \tag{4.27}$$

where Θ is the Heaviside function and the energies $\xi_\pm = \xi_\pm(U, \lambda, E_0)$ are the boundaries enclosing the π-phase region with $\bar{N} = 1$, i.e., ξ_+ (ξ_-) denotes the boundary between the $\bar{N} = 0$ and $\bar{N} = 1$ (the $\bar{N} = 1$ and $\bar{N} = 2$) regions, see Fig. 4.5. Explicit results for $\xi_\pm$ follow from Eq. (4.24) for $W_0 = 0$. For $E_0 < 0$ ($E_0 > 2\lambda$) and arbitrary $\bar{N}$, the ground state is realized when $\bar{\sigma} = -$ ($\bar{\sigma} = +$), leading to $\xi_+ = \lambda/2$ ($\xi_+ = -\lambda/2$). In both cases, the other boundary energy follows as $\xi_- = \xi_+ - U$. In the intermediate cases, with $\xi_0 = \frac{1}{2}(\lambda - U - E_0)$, we find for $0 < E_0 < \lambda$,

$$\xi_+ = \max(\lambda/2 - E_0, \xi_0), \quad \xi_- = \min(\lambda/2 - U, \xi_0), \tag{4.28}$$

while for $\lambda < E_0 < 2\lambda$, we obtain

$$\xi_+ = \max(-\lambda/2, \xi_0), \quad \xi_- = \min(\xi_0, \lambda/2 + 2\xi_0). \tag{4.29}$$

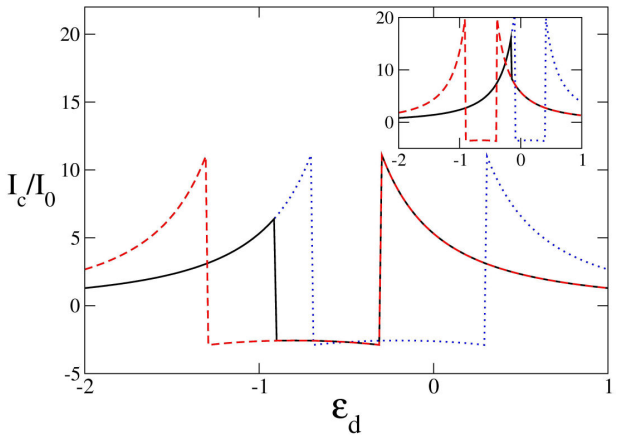

Figure 4.6: Ground-state critical current I_c as a function of ε_d for $W_0 = 0$. I_c is given in units of I_0, see Eq. (4.23). In all figures, the energy scale is set by $\Delta = 1$. Dashed (red), dotted (blue) and solid (black) curves represent the partial critical currents $I_c(\varepsilon_+)$, $I_c(\varepsilon_-)$, and the realized critical current I_c, respectively. Main panel: $E_0 = 0.8, \lambda = 0.6$, $U = 1$, such that $\xi_+ > \xi_-$. This corresponds to the π-phase region with $\lambda < E_0 < 2\lambda$ in the main panel of Fig. 4.5. Inset: $E_0 = 0.6, \lambda = 0.8, U = 0.5$, where $\xi_+ < \xi_-$ and no π-junction behavior is possible. This corresponds to $U < E_0 < 2\lambda - U$, see inset of Fig. 4.5.

These results for $\xi_\pm$ are summarized in Fig. 4.5. Remarkably, in the $E_0 - \varepsilon_d$ plane, the phase diagram is inversion-symmetric with respect to the point $(E_0 = \lambda, \varepsilon_d = -U/2)$. Furthermore, we observe that for many choices of E_0, one can switch the TLS between the $\bar{\sigma} = \pm$ states by varying ε_d, see Fig. 4.5.

We now notice that Eq. (4.27) implies the same decomposition for the critical current (4.14). We can therefore immediately conclude that the π-junction regime (where $\bar{N} = 1$) can exist only when $\xi_+ > \xi_-$. This condition is always met away from the window $0 < E_0 < 2\lambda$. However, inside that window, Eqs. (4.28) and (4.29) imply that for sufficiently strong dot-TLS coupling, $\lambda > U$, the π-phase may disappear completely. Indeed, for $U < E_0 < 2\lambda - U$, no π-phase is possible for any value of ε_d once λ exceeds U. The resulting ground-state critical current is shown as a function of the dot level ε_d for two typical parameter sets in Fig. 4.6. The inset shows a case where the π-phase has been removed by a strong coupling of the interacting dot to the TLS. The above discussion shows that the π-junction regime is very sensitive to the presence of a strongly coupled TLS.

4.4. Finite TLS tunneling

Next we address the case of finite TLS tunneling, $W_0 \neq 0$. Due to the σ_x term in H_0, the critical current cannot be written anymore as a weighted sum, see Eq. (4.25), and no abrupt switching of the TLS happens when changing the system parameters. Nev-

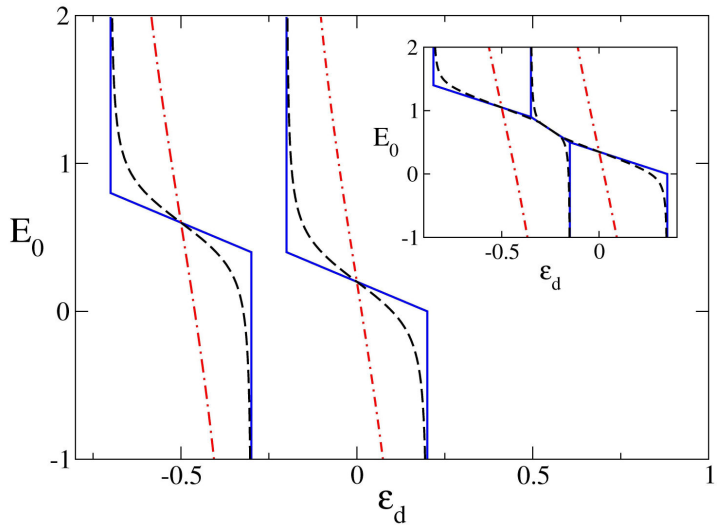

Figure 4.7: Phase diagram and boundary energies $\xi_\pm$ enclosing the π-phase for finite W_0. Main figure: $\lambda = 0.4$ and $U = 0.5$, where a π-phase is present; $W_0 = 0, 0.2$ and 5, for solid (blue), dashed (black) and dash-dotted (red) curves, respectively. Inset: $\lambda = 0.7$ and $U = 0.5$, where the π-phase vanishes; $W_0 = 0, 0.3$ and 3, for solid (blue), dashed (black) and dash-dotted (red) curves, respectively.

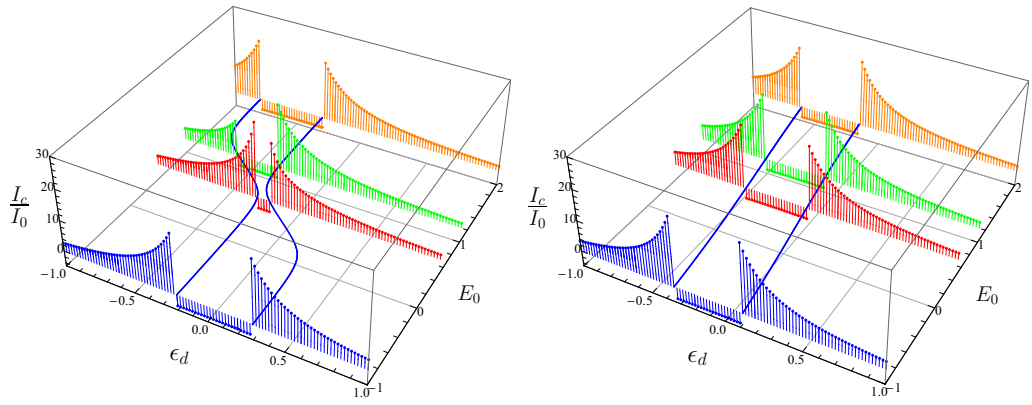

Figure 4.8: Listline plots of the $W_0 \neq 0$ ground-state critical current I_c (in units of I_0) in the $E_0 - \varepsilon_d$ plane, with $\lambda = 0.6$ and $U = 0.5$. The boundaries $\xi_\pm$ enclosing the π-phase, see also Fig. 4.7, are indicated as solid (blue) curves. Left panel: Small tunnel amplitude, $W_0 = 0.2$. Right panel: Large tunnel amplitude, $W_0 = 3$.

ertheless, we now show that the size and even the existence of the π-phase region still sensitively depend on the TLS coupling strength (and on the other system parameters). In particular, the π-phase can be completely suppressed for strong λ again.

For finite W_0, the ground-state critical current is obtained from Eq. (4.27), where the

C_N are given by Eqs. (4.19)–(4.21) and the π-phase border energies $\xi_\pm$ are replaced by

$$\xi_+ = \frac{1}{2}(\Phi_1 - \Phi_0), \quad \xi_- = \frac{1}{2}(\Phi_2 - \Phi_1 - 2U). \tag{4.30}$$

The Φ_N are defined in Eq. (4.12). Compared to the $W_0 = 0$ case in Fig. 4.5, the phase diagram boundaries now have a smooth (smeared) shape due to the TLS tunneling. Nevertheless, the critical current changes sign abruptly when the system parameters are tuned across such a boundary. The energies (4.30) are shown in Fig. 4.7 for various values of W_0 in the $E_0 - \varepsilon_d$ plane. In between the ξ_+ and ξ_- curves, the π-phase is realized. From the inset of Fig. 4.7, we indeed confirm that the π-phase can again be absent within a suitable parameter window. Just as for $W_0 = 0$, the π-phase vanishes for $\xi_+ < \xi_-$, and the transition between left and right 0-phase occurs at $\bar{\xi} = (\xi_+ + \xi_-)/2$. For $|E_0| \gg \max(\lambda, W_0)$, we effectively recover the phase diagram for $W_0 = 0$, since the TLS predominantly occupies a fixed conformational state.

The corresponding critical current I_c is shown in Fig. 4.8 for both a small and a very large TLS tunnel matrix element W_0. In the limit of large $W_0 \gg \max(\lambda, |E_0|)$, see right panel in Fig. 4.8, the dot and the TLS are effectively decoupled, since $\langle\sigma_z\rangle \simeq 0$ and $\langle\sigma_x\rangle \simeq \mathrm{sgn}(W_0)$. While this limit is unrealistic for molecular junctions, it may be realized in a side-coupled double-dot system [135]. Finally we note that, unlike for $W_0 = 0$, the perturbative result for the critical current *diverges* at the point where the π-phase vanishes, i.e., for $\varepsilon_d = \bar{\xi}$. This divergence is an artefact of perturbation theory and is caused by the appearance of the factor $G_{E_0^- - E_2^-}(0) = (\varepsilon_d - \bar{\xi})^{-1}$ in Eqs. (4.19) and (4.21).

4.5. Conclusion

In this chapter, we have presented a perturbative calculation of the critical Josephson current, I_c, through an interacting single-level quantum dot Josephson junction coupled to a two-level system (TLS). Such a TLS serves as a simple model for a bistable conformational degree of freedom of the connecting single molecule, and has previously been introduced in the literature [58, 77]. We have focused on the weak-coupling limit and computed the critical current I_c to lowest non-vanishing order. The ground-state critical current can then be computed exactly for otherwise arbitrary interaction strength and TLS-parameters. Our main result is that the π-phase with $I_c < 0$ is quite sensitive to the presence of the TLS. In particular, for strong coupling λ of the molecular level to the TLS as compared to the Coulomb energy U on the level, the π-phase can disappear altogether. Our predictions can be tested experimentally in molecular break junctions using a superconducting version of existing setups [58, 73, 74].

5. Josephson-current induced conformational switching of a molecular quantum dot

5.1. Introduction

In the previous chapter, we focussed on the effects of the TLS on the Josephson current in the weak-coupling limit $\Gamma \ll \triangle$, more specifically on the π-junction behavior of the QDJJ+TLS system, taking arbitrary values of interaction strength U and TLS-parameters into account.

In this chapter, we address a completely different parameter regime in which the Josephson current is carried by Andreev states (thereby neglecting contributions from continuum states outside the region $[-\triangle, \triangle]$) and focus both on the effects of the TLS on the current-phase relation and the influence of the Josephson current on the expectation value $S = \langle \sigma_z \rangle$ of the conformational state. While we cannot examine the π -junction behavior within this approach, it allows us to obtain exact solutions in several different parameter regimes .

Our results indicate that over a wide range of parameters, the TLS state can be significantly affected by varying the phase φ, including a complete reversal of the conformational configuration. This remarkable effect allows for the dissipationless control (including switching) of the conformational degree of freedom (σ_z) in terms of the phase difference φ, which can be tuned experimentally by embedding the device in a SQUID geometry [60]. Conversely, changing the conformational state will affect the Josephson current in a distinct manner, leading to non-standard current-phase relations.

This chapter is organized as follows: In section 5.2, we will derive an effective action for the dot+TLS system by integrating out the electronic degrees of freedom of the leads using the functional integral approach. The result is the starting point for the effective models presented throughout this chapter. Next, we will derive an exact solution for the case of vanishing charging energy U and tunnel splitting W_0 in section 5.3. We derive necessary conditions for switching the TLS state S via the phase difference φ and the non-standard current-phase relation in this limit, which deviates from the purely sinusoidal weak link current-phase relation (cf. (4.1)). Next we study the effects of finite U and/or tunneling W_0, addressing both limits $\Gamma \gg \Delta$ and $\Delta \gg \Gamma$.

In section 5.4, we treat the case in which Δ is the largest relevant energy scale, while keeping U and W_0 finite. The junction dynamics is then confined to the subgap regime

(Andreev states) while contributions from the continuum states may be neglected. This is a good approximation to the 0-junction state, even for small interaction strength U. We find that interaction has no effect within this regime up to a critical value U_c. The toy model derived in this section can be thought of as describing a regime which is complementary to the one addressed within the perturbative treatment presented in the previous section. We derive an exactly solvable effective Hamiltonian for the Andreev levels coupled to the TLS that allows us to compute the Josephson current and $S(\varphi)$. We observe again a non-standard current-phase relation and switching of the conformational state via the phase φ, both in good agreement (within suitable choice of parameters) with the exact calculation of section 5.3.

Next, we consider briefly the opposite limit of strong coupling to the electrodes $\Gamma \gg \Delta$, setting $U = 0$ in section 5.4.2. We give some conclusions in sec. 2.6.

5.2. Integrating out the leads

In our following treatment, it is convenient to work with Nambu spinors $d^T(\tau) = \left(d_\uparrow d_\downarrow^\dagger\right)$ and $\Psi_{\alpha\boldsymbol{k}}^T(\tau) = \left(c_{\boldsymbol{k}\alpha\uparrow}\, c_{-\boldsymbol{k}\alpha\downarrow}^\dagger\right)$ in imaginary time τ. Furthermore, we perform the $U(1)$-gauge transformation of the lead operators $c_\alpha \to e^{-\alpha i\phi/4} c_\alpha$, such that the phase-factor of the superconducting order-parameters is absorbed in the tunneling-amplitudes. Then the expression H_{leads}^α for the left/right lead in Eq. (4.4) and the tunneling Hamiltonian Eq. (4.5) become

$$H_{\text{leads}}^\alpha = \sum_{\boldsymbol{k}} \Psi_{\alpha\boldsymbol{k}}^\dagger \left(\varepsilon_{\boldsymbol{k}\alpha}\tau_z + \Delta_\alpha \tau_x\right) \Psi_{\alpha\boldsymbol{k}}, \tag{5.1}$$

and

$$H_{\text{tun}} = \sum_{\alpha\boldsymbol{k}} \Psi_{\alpha\boldsymbol{k}}^\dagger T_{\boldsymbol{k}\alpha} d + h.c., \tag{5.2}$$

respectively, where $\tau_{x,y,z}$ denote the Pauli-matrices in spin-space and we introduced $T_{\boldsymbol{k}\alpha} = e^{+\alpha i\phi/4\tau_z} t_{\boldsymbol{k}\alpha}\tau_z$. For convenience, we split H_0 (cf. Eq. (4.3)) into a TLS and a dot-part $H_0 = H_{dot-TLS} + H_{TLS}$, where

$$\begin{aligned} H_{dot-TLS} &= \left(\varepsilon_d + \sigma_z \lambda/2\right)\left(n_\uparrow + n_\downarrow\right) + U n_\uparrow n_\downarrow, \\ H_{TLS} &= -\frac{E_0}{2}\sigma_z - \frac{W_0}{2}\sigma_x. \end{aligned}$$

We compute the partition function using the functional integral approach

$$Z = Tr_\sigma \left[\int \mathscr{D}\left[\overline{\Psi}_{\alpha\boldsymbol{k}}, \Psi_{\alpha\boldsymbol{k}}\right] \mathscr{D}\left[\overline{d}, d\right] e^{-S\left[\overline{\Psi}, \Psi; \overline{d}, d\right]}\right],$$

where Z is written as functional integral over Grassman fields $\left(\overline{\Psi}_{\alpha \boldsymbol{k}}, \Psi_{\alpha \boldsymbol{k}}\right)$ and $\left(\overline{d}, d\right)$ that correspond to the respective operators in the Hamiltonian and $Tr_\sigma[...] = \sum_{\sigma=\pm} \langle \sigma |...| \sigma \rangle$ denotes the (partial) trace over the TLS-degrees of freedom. A detailed review of the fermionic functional integral over Grassman fields is beyond the scope of this thesis, it can be found in e.g. [79]. The euclidean action reads

$$S = S_0 + \int_0^\beta d\tau \sum_{\alpha \boldsymbol{k}} \left[\overline{\Psi}_{\alpha \boldsymbol{k}}(\tau) \left(\partial_\tau + \varepsilon_{\boldsymbol{k}\alpha}\tau_z + \Delta_\alpha \tau_x\right) \Psi_{\alpha \boldsymbol{k}}(\tau) \right.$$
$$\left. + \ \overline{\Psi}_{\alpha \boldsymbol{k}}(\tau) T_{\boldsymbol{k}\alpha} d(\tau) + \overline{d}(\tau) T_\alpha^\dagger \Psi_{\alpha \boldsymbol{k}}(\tau) \right].$$

The Action for the dot-TLS system reads $S_0 = \beta H_{TLS} + \int_0^\beta d\tau \overline{d}\, \partial_\tau d + H_{dot-TLS}\left[\overline{d}, d\right]$. After integrating out the leads (i.e. using Gaussian integration, which is formally analogous to the bosonic case detailed in the Appendix, cf. [79]), the partition function has the form $Z = Tr_\sigma \left[\int \mathscr{D}\left[\overline{d}, d\right] e^{-S_{eff}} \right]$ with an effective action

$$S_{eff} = S_0 - \int_0^\beta d\tau d\tau' \overline{d}(\tau)\, \Sigma\left(\tau - \tau'\right) d\left(\tau'\right). \tag{5.3}$$

The effect of the BCS leads is now contained in the 2×2 Nambu self-energy matrix $\Sigma(\tau) = \sum_\alpha T_\alpha^\dagger G_{leads}(\tau) T_\alpha$ where $G_{leads}(\tau) = \sum_{\boldsymbol{k}} \left(\partial_\tau + \varepsilon_{\boldsymbol{k}\alpha}\tau_z + \Delta_\alpha \tau_x\right)^{-1} \delta(\tau)$ is the leads Green's function. The Fourier transform of Σ is readily calculated

$$\Sigma(\omega;\varphi) = \frac{\Gamma}{\sqrt{\omega^2 + \Delta^2}} \begin{pmatrix} -i\omega & \Delta\cos(\varphi/2) \\ \Delta\cos(\varphi/2) & -i\omega \end{pmatrix}, \tag{5.4}$$

where we assume again $t_{\boldsymbol{k}\alpha} \simeq t_\alpha = const$, i.e. $T_{\boldsymbol{k}\alpha} \simeq T_\alpha$. Furthermore, we assume symmetric leads, i.e. $\varepsilon_{\boldsymbol{k}\alpha} = \varepsilon_{\boldsymbol{k}}$ and $\triangle_\alpha = \triangle$ and symmetric coupling to the dot, $\Gamma_{L/R} = \Gamma/2$ from now on. The tunneling width Γ of the dot level is given by $\Gamma = \pi \rho_F t^2$ (in the wideband limit), where ρ_F is the normal-electrode density of states at the Fermi level.

We mostly consider zero temperature, where both the Josephson current $I(\varphi)$ through the dot and the expectation value $S = \langle \sigma_z \rangle$ of the conformational state follow from the ground-state energy $E_g(\varphi, E_0)$ according to

$$I(\varphi) = 2\frac{\partial E_g}{\partial \varphi}, \quad S(\varphi) = -2\frac{\partial E_g}{\partial E_0}. \tag{5.5}$$

5.3. Exact results for $U, W_0 \to 0$

Let us first illustrate our central findings when both the charging energy U and the tunnel splitting W_0 are very small. In this limit, we can also trace out the dot-degrees of freedom in the functional integral, since the remaining effective action

$$S_{eff} = \frac{\beta}{2}(\lambda - E_0)\sigma_z + \frac{1}{\beta}\sum_{k_n} \overline{d}_{k_n} G_{dot}^{-1}(k_n, \sigma_z)\, d_{k_n},$$

where $G_{dot}^{-1}(\omega,\sigma_z) = (i\omega - \tau_z(\varepsilon_d + \sigma_z\lambda/2) - \Sigma(\omega;\varphi))$, is gaussian.
Later on we show that for sufficiently small $U < U_c$, finite U has no effect. The partition function Z can then be written as a sum of two terms $Z = Tr_\sigma\left[\int \mathscr{D}\left[\overline{d},d\right] e^{-S_{eff}}\right] = Z_+ + Z_-$, where $Z_\pm$ correspond to fixed configurations $\sigma_z \to \sigma = \pm$ of the TLS

$$Z_\sigma = \int \mathscr{D}\left[\overline{d},d\right] e^{-S_{eff}^\sigma} = e^{-\frac{\beta}{2}(\lambda - E_0)\sigma} \prod_{k_n} \det\left[G_{dot}^{-1}(k_n,\sigma)\right].$$

The partial free energies $F_\sigma(\varphi) = -\frac{1}{\beta}\ln(Z_\sigma)$ are given by

$$F_\sigma(\varphi) = \sigma\frac{\lambda - E_0}{2} - \frac{1}{\beta}\sum_{k_n} \ln\left(\det\left[G_{dot}^{-1}(k_n,\sigma)\right]\right) \tag{5.6}$$

The ground-state energy $E_g = \min(E_+,E_-)$, necessary to compute the current-phase relation and S, then follows from the energies $E_\sigma = \sigma(\lambda - E_0)/2 - \varepsilon_\sigma^A(\varphi)$ for fixed conformational state $\sigma = \pm$ with dot level $\varepsilon_\sigma = \varepsilon + \sigma\lambda/2$. The so-called *Andreev state* energy for arbitrary Δ/Γ follows from Eq. (5.6),

$$\varepsilon_\sigma^A(\varphi) = \varepsilon_\sigma^A(0) + \int \frac{d\omega}{2\pi} \ln \frac{\det\left[i\omega - \tau_z\varepsilon_\sigma - \Sigma(\omega;\varphi)\right]}{\det\left[i\omega - \tau_z\varepsilon_\sigma - \Sigma(\omega;0)\right]}. \tag{5.7}$$

In this approach, we assumed that other quasiparticle contributions to the free energy, namely those of the continuum states outside the gap $[-\triangle,\triangle]$, are negligible. In the limits $\Gamma \gg \Delta$ and $\Delta \gg \Gamma$, one can obtain exact results[1] [80]

$$\begin{aligned} \varepsilon_\sigma^A(\varphi) &= \Delta_\sigma\sqrt{1 - \mathscr{T}_\sigma \sin^2(\varphi/2)}, \\ \Delta_\sigma &= \begin{cases} \frac{\Delta}{1+\Delta/\Gamma}, & \Gamma \gg \Delta, \\ \frac{\Gamma}{\sqrt{\mathscr{T}_\sigma}}, & \Delta \gg \Gamma, \end{cases} \end{aligned} \tag{5.8}$$

with the normal transmission probability $\mathscr{T}_\sigma = [1 + \varepsilon_\sigma^2/\Gamma^2]^{-1}$.

Let us now focus on conditions for switching the TLS-state S via the phase difference φ: As long as $E_+ < E_-$ ($E_- < E_+$), we have $S(\varphi) = +1(-1)$, i.e. the conformational state $\sigma = +(-)$ is realized, with ideal (perfect) switching when the bands $E_+(\varphi)$ and $E_-(\varphi)$ cross at some phase $\varphi^* \in [0,\pi]$. Hence a necessary condition for switching is that both relations $E_+(\varphi = 0) \lessgtr E_-(\varphi = 0)$ and $E_+(\varphi = \pi) \gtrless E_-(\varphi = \pi)$ are satisfied. This means that one of the two inequality chains (with $\mathscr{R}_\sigma = 1 - \mathscr{T}_\sigma$)

$$\Delta_+\sqrt{\mathscr{R}_+} - \Delta_-\sqrt{\mathscr{R}_-} \lessgtr \lambda - E_0 \lessgtr \Delta_+ - \Delta_- \tag{5.9}$$

must be obeyed. If the dot level is close to a resonance, $\varepsilon_\pm \approx 0 \Leftrightarrow \varepsilon_\mp \approx \mp\lambda$, the reflection probabilities $\mathscr{R}_+$ and $\mathscr{R}_-$ are significantly different, and Eq. (5.9) holds over a wide

[1] Using $\int dx \ln(x^2+a^2) = -2x + 2a\arctan\left(\frac{x}{a}\right) + x\ln(x^2+a^2)$,i.e. $\int_0^\infty dx \ln\left(\frac{x^2+a^2}{x^2+b^2}\right) = \pi\left[\sqrt{a^2} - \sqrt{b^2}\right]$.

parameter range. Then Eq. (5.5) yields the current-phase relation

$$I(\varphi) = \frac{e\Delta_{S(\varphi)}}{2\hbar} \frac{\mathscr{T}_{S(\varphi)} \sin(\varphi)}{\sqrt{1 - \mathscr{T}_{S(\varphi)} \sin^2(\varphi/2)}}. \tag{5.10}$$

In the regime (5.9), the transmission amplitude switches between $\mathscr{T}_+$ and $\mathscr{T}_-$ when $\varphi = \varphi^*$. This implies non-standard current-phase relations, as shown in the upper inset of Fig. 5.1. Having established the basic phenomenon in the exactly solvable limit $U, W_0 = 0$, we now focus on the effects of finite U and/or tunneling W_0. We will address both limits $\Gamma \gg \Delta$ and $\Delta \gg \Gamma$.

5.4. Limit of large △

Let us start with the case when Δ is the largest energy scale of relevance. Consider the effective dot-action Eq. (5.3). Since we regard finite (but sufficiently small, see below) interaction strength U, we cannot trace out the dot-degrees of freedom exactly as before, because the interaction term is quartic in the dot-operators. If $\triangle$ is the largest energy scale, the dynamics is always confined to the subgap regime (Andreev states), and quasiparticle tunneling processes from the leads (continuum states) are negligible. This is expected to be a good approximation to the 0-junction state, where the continuum contribution to the Josephson current is negligible. However, the π-junction behavior (for large U/Γ) cannot be described within this approximation. Technically, this approximation means that the self-energy Eq. (5.4) can be replaced by the expression $\Sigma(\tau) = \Gamma\cos(\varphi/2)\delta(\tau)\,\tau_x$ (formally taking the limit $\triangle \to \infty$), which is now diagonal in τ . From Eq. (5.3) it is then straightforward to see that the problem is now equivalently described by the effective Hamiltonian (since $H\left[d^\dagger, d\right] \to S = \int d\tau\, \overline{d}\, \partial_\tau d + H\left[\overline{d}, d\right]$)

$$\begin{aligned} H_{\text{eff}} &= H_0 + \Gamma\cos(\varphi/2)\left(d_\downarrow d_\uparrow + h.c.\right) \\ &= -\frac{E_0}{2}\sigma_z - \frac{W_0}{2}\sigma_x + \left(\varepsilon + \frac{\lambda}{2}\sigma_z\right)\left(n_\uparrow + n_\downarrow\right) + \Gamma\cos(\varphi/2)\left(d_\downarrow d_\uparrow + h.c.\right) \\ &\quad - \frac{U}{2}\left(n_\uparrow - n_\downarrow\right)^2 \end{aligned} \tag{5.11}$$

where we introduced the renormalized dot level $\varepsilon = \varepsilon_d + U/2$. The resulting Hilbert space can be decomposed into orthogonal subspaces, $\mathscr{H} = \mathscr{H}_A \otimes \mathscr{H}_S$, where the Andreev sector $\mathscr{H}_A$ is spanned by the zero- and two-electron dot states $|0\rangle$ and $|2\rangle = d_\uparrow^\dagger d_\downarrow^\dagger |0\rangle$ (and, of course, by the conformational TLS states), while $\mathscr{H}_S$ is spanned by the one-electron states $|s\rangle \equiv d_s^\dagger |0\rangle$. Notice that in Eq. (5.11) the last term (the 'residual' Coulomb interaction) is identically zero in the Andreev-state subspace $\mathscr{H}_A$, while it gives a contribution $-\frac{U}{2}$ in the one-particle sector H_S. For convenience shifting $H_{\text{eff}} \to H_{\text{eff}} - \varepsilon$, the single-particle sector has a pair of doubly-degenerate eigenenergies $-\frac{U}{2} \pm \varepsilon_S$ with $\varepsilon_S = \frac{1}{2}\sqrt{(E_0 - \lambda)^2 + W_0^2}$,

whereas the Andreev sector is described by

$$H^A_{\rm eff} = \begin{pmatrix} \frac{(\lambda-E_0)\sigma_z - W_0\sigma_x}{2} + \left(\varepsilon\,\sigma_0 + \frac{\lambda}{2}\sigma_z\right) & \Gamma\cos(\varphi/2)\,\sigma_0 \\ \Gamma\cos(\varphi/2)\,\sigma_0 & \frac{(\lambda-E_0)\sigma_z - W_0\sigma_x}{2} - \left(\varepsilon\,\sigma_0 + \frac{\lambda}{2}\sigma_z\right) \end{pmatrix}$$
$$= \frac{\lambda - E_0}{2}\sigma_z - \frac{W_0}{2}\sigma_x + \frac{\lambda}{2}\tau_z\sigma_z + \varepsilon\,\tau_z + \Gamma\cos(\varphi/2)\,\tau_x \tag{5.12}$$

with Pauli matrices $\tau_{x,z}$ acting in the $\{|2\rangle, |0\rangle\}$ (Andreev sector) subspace. If the ground state of $H_{\rm eff}$ lies in the Andreev sector, the Josephson current can be non-zero, while otherwise $I = 0$ due to the φ-independence of the single-particle sector (Note that the vanishing of the Josephson current is an artifact of taking the limit $\triangle \to \infty$). For sufficiently strong interactions, $U > U_c(\varphi)$, the ground state of $H_{\rm eff}$ is in the single-particle sector $\mathscr{H}_S$. This is indicative of a quantum phase transition to the magnetic π-junction regime [81]. While this regime is outside the scope of Eq. (5.12) (since continuum states are not included), this scenario is confirmed by the perturbative calculation expanding in $\Gamma/\triangle$ for the full model in the previous chapter, where we observed a suppression of the π-phase even for finite U. For $\lambda \to 0$, we find $U_c = 2\sqrt{\varepsilon^2 + \Gamma^2\cos^2(\varphi/2)}$, see Eq. (5.8) for $\Delta \gg \Gamma$. Note that ε and hence U_c can in principle be tuned by a gate voltage. For $\lambda \gg \max(|E_0|, |\varepsilon|, \Gamma)$, we instead find $U_c = \lambda$.

Because $H^A_{\rm eff}$ is independent of U (up to the shift $\varepsilon = \varepsilon_d + U/2$), a weak interaction $U < U_c$ has no effect, and in what follows we set $U = 0$. Since a coupling of the TLS to the dot's *spin* involves only the φ-independent subspace $\mathscr{H}_S$, such couplings are also of little relevance for switching, in accordance with the small polar displacements predicted for spins in a Josephson junction [82].

Physical observables can then be computed from $H^A_{\rm eff}$ in Eq. (5.12). The eigenenergies are roots to the exactly solvable quartic equation

$$E^4 - 2\Lambda_2 E^2 + \Lambda_1 E + \Lambda_0 = 0, \tag{5.13}$$

with coefficients $\Lambda_2 = \varepsilon_A^2 + \varepsilon_S^2 + \lambda^2/4, \Lambda_1 = 2\lambda\varepsilon(E_0 - \lambda)$ and $\Lambda_0 = \left(\varepsilon_A^2 - \varepsilon_S^2 + \lambda^2/4\right)^2 - \lambda^2(\varepsilon^2 - W_0^2/4)$. The lowest-lying of the four roots yields the exact but lengthy result for the ground-state energy E_g. Convenient expressions for $S(\varphi)$ and $I(\varphi)$ in Eq. (5.5) follow by taking the respective derivatives directly in Eq. (5.13). For instance, with $\Lambda_i' = \partial\Lambda_i/\partial E_0$, the conformational variable reads

$$S(\varphi) = -\frac{2\Lambda_2' E_g^2 - \Lambda_1' E_g - \Lambda_0'}{2E_g(E_g^2 - \Lambda_2) + \Lambda_1/2}. \tag{5.14}$$

Typical results for $S(\varphi)$ and $I(\varphi)$ are shown in Fig. 5.1.

5.4.1. Weak coupling regime

The most efficient way to induce conformational changes, including a complete (symmetric) reversal $S \to -S$, is achieved in the weak-coupling regime $\lambda \ll \varepsilon_A$, where the four

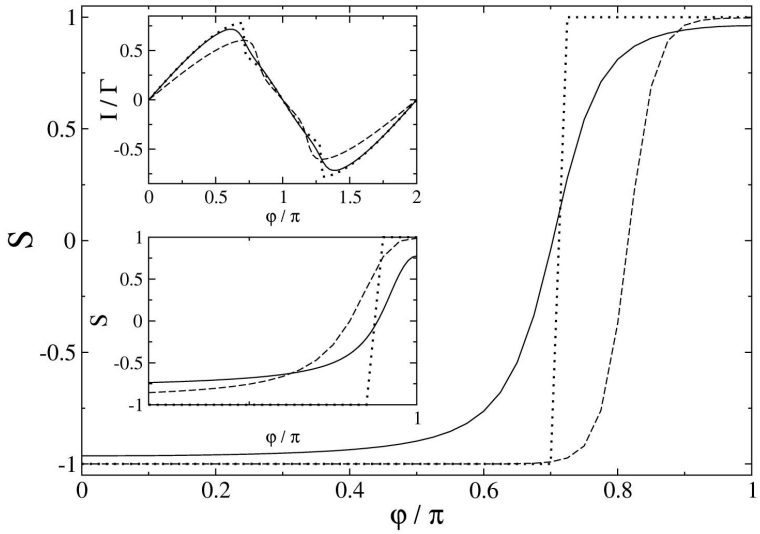

Figure 5.1: Conformational state $S(\varphi) = S(-\varphi)$ vs superconductor's phase difference φ. Results from Eq. (5.14) for $\Delta \gg \Gamma$ are shown for tunnel amplitudes $W_0 = 0$ (dotted) and $W_0 = 0.04\Gamma$ (solid), with $\lambda = \varepsilon = \Gamma/2$ and $E_0 = 0.14\Gamma$. The dashed curve gives the exact result for $W_0 = 0$ and $\Delta = 5\Gamma$, see Eq. (5.7), extended to finite temperature $T = 0.01\Gamma$. The upper inset shows the corresponding Josephson current-phase relations. Lower inset: Same as main figure but for $\Gamma = 4\Delta$ with $\lambda = 2\varepsilon = \Delta/2$ and $E_0 = 0.45\Delta$. The dotted (solid) curve is obtained from the $\Gamma \gg \Delta$ effective Hamiltonian (5.17) with $W_0 = 0$ ($W_0 = 0.04\Delta$). The exact result for $W_0 = 0$ is shown as dashed curve for $T = 0.01\Delta$.

roots to Eq. (5.13) can be simplified to

$$E_{\pm,\pm} = \pm\varepsilon_A(\varphi) \pm \frac{1}{2}\sqrt{W_0^2 + [\lambda(1-\varepsilon/\varepsilon_A(\varphi)) - E_0]^2}, \tag{5.15}$$

with ground-state energy $E_g = E_{--}$. Remarkably, Eq. (5.15) remains accurate even for $\lambda \approx \varepsilon_A$.

A complete reversal is achieved when tuning E_0 or ε such that $E_0 = \lambda[1-\mathrm{sgn}(\varepsilon)] - \mathscr{F}$ with $\mathscr{F} = -\frac{\lambda}{2}\mathrm{sgn}(\varepsilon)[1-|\varepsilon|/\varepsilon_A(0)]$. In that case, $S(0) = -S(\pi) = \mathscr{F}/\sqrt{W_0^2+\mathscr{F}^2}$. When comparing to the $W_0 = 0$ result, we observe that a finite tunnel amplitude W_0 only leads to a rounding of the transition and a decrease in the switching amplitude, but it does not destroy the effect. Finally, with Eq. (5.15), the Josephson current in the weak-coupling limit is

$$I(\varphi) = \frac{\Gamma^2 \sin\varphi}{2\varepsilon_A(\varphi)}\left(1 + \frac{\lambda\varepsilon}{2\varepsilon_A^2(\varphi)}S(\varphi)\right). \tag{5.16}$$

5.4.2. Strong coupling to the electrodes $\Gamma \gg \Delta$

Next we briefly discuss the opposite limit within a similar truncation scheme, setting $U = 0$. For $\Gamma \gg \Delta$ and $\varphi \neq 2\pi n$ (integer n), the relevant subgap dynamics is again captured by an effective two-level Hamiltonian describing the Andreev states [83], coupled to the conformational TLS. With Pauli matrices $\tau_{x,y,z}$ in Andreev level subspace and the notation (see Eq. (5.8))

$$H_\sigma = \Delta_\sigma e^{-i\tau_y\sqrt{\mathscr{R}_\sigma}\varphi/2}\left(\sqrt{\mathscr{R}_\sigma}\,\sin(\varphi/2)\tau_z + \cos(\varphi/2)\tau_x\right),$$

the effective Hamiltonian follows in TLS space as

$$H_{\rm eff} = \begin{pmatrix} \frac{\lambda - E_0}{2} + H_+ & -\frac{W_0}{2} \\ -\frac{W_0}{2} & -\frac{\lambda - E_0}{2} + H_- \end{pmatrix}. \tag{5.17}$$

Physical observables are then easily obtained, see the lower inset of Fig. 5.1. Again the qualitative features of the $W_0 = 0$ solution persist.

5.5. Conclusion

In this chapter, we have studied the influence of the Josephson current on the conformational degree of freedom (represented by a TLS) in a superconducting molecular dot or break junction. Our theory predicts that the variation of the phase difference φ across the dot/junction can induce conformational changes, including a complete reversal of the TLS state. This allows for the dissipationless control (including switching) of the TLS. We have first computed the dependence of $S(\varphi)$ on the phase as well as the current-phase relation, neglecting Coulomb interaction and tunnel splitting W_0. Next, we have focussed on the case where $\triangle$ is the largest relevant energy allowing for finite W_0 and a small charging energy U. Within our approximations this has no effect up to a critical value of U. We have derived expressions for $S(\varphi)$ and $I(\varphi)$ and found qualitative agreement with the exact results for $U, W_0 = 0$ for suitable choice of parameters. We have also presented results for the case $\Gamma \gg \triangle$ with finite W_0 and $U = 0$ and seen that qualitatively, S shows similar behaviour as in the case with $W_0 = 0$.

6. Summary

Within this thesis we have presented studies of the electronic properties of three low dimensional nanoscale systems. In the first part, we have focussed on the influence of spin-orbit coupling in interacting one dimensional systems. Our second focus was on superconducting transport in quantum dot Josephson junctions coupled to a two-level system, which represents e.g. the conformational degree of freedom of a molecule.

In chapters 2 and 3, we have carefully derived low energy theories for carbon nanotubes as well as quantum wires in the presence of SOI. Using the bosonization technique, we have obtained analytic expressions for the correlation functions that allow us to compute basically all observables of interest.

In chapter 2 we have shown that a four channel Luttinger liquid theory can still be applied when the combined effects of SOI and Coulomb interaction are taken into account. However, compared to previous formulations, the low-energy Hamiltonian is characterized by different Luttinger parameters and plasmon velocities. In particular, the total (relative) charge mode is coupled to the relative (total) spin mode. The changes reflect the broken $SU(2)$ invariance due to SOI. Our theory allowed us to obtain an asymptotically exact expression for the spectral function $A(\omega, q)$ of a metallic carbon nanotube. We find modifications to the previously predicted structure of A, most notably an additional peak, due to the coupling of spin and charge modes. We also found that A is finite within a large region in which the spectral function vanishes in the standard case. Our predictions could in principle be tested by photoemission spectroscopy experiments.

In chapter 3, we focussed on an interacting Rashba wire. First we have derived a two component Luttinger liquid Hamiltonian in the presence of RSOI, taking into account all e-e interaction processes allowed by the conservation of total momentum. We presented the effective low energy Hamiltonian, which includes an additional perturbation due to intraband backscattering processes with band flip. Within a one-loop RG scheme, this perturbation is marginally irrelevant. While the fixed point model is then still a two channel Luttinger liquid, the modifications to the RG flow due to SOI lead to a non standard form. As in the theory presented in chapter 2, the charge and spin mode are coupled.

We used our low energy theory to address the problem of the RKKY interaction in the Rashba wire. The broken $SU(2)$ invariance due to spin-orbit effects implies, among other notable changes, that the power-law decay exponent of the RKKY Hamiltonian in the wire explicitly depends on both RSOC and interaction strength. Furthermore, the inclusion of RSOC into the interacting model leads to an anisotropic range function.

In chapter 4, we have calculated perturbatively the critical current I_c through an interacting single-level quantum dot Josephson junction coupled to a two-level system to lowest non-vanishing order in the tunneling couplings. Such a TLS serves as a simple model

for a bistable conformational degree of freedom of the connecting single molecule. Our perturbative calculation in the weak coupling limit ($\Gamma \ll \triangle$) allows for arbitrary charging energy U and TLS parameters.

We found that the π-phase, in which $I_c < 0$, is strongly affected and can even be completely suppressed for sufficiently strong coupling of the dot level to the TLS. Our results can be tested experimentally in superconducting break junctions.

In chapter 5, we have studied the influence of the Josephson current on the state of the TLS in the regime of weak or vanishing charging energy. Within a wide range of parameters, our calculations predict that the TLS is quite sensitive to a variation of the phase difference φ across the junction. Conformational changes, up to a a complete reversal, can be induced by sweeping φ . This allows for the dissipationless control (including switching) of the TLS. Additionally we have found modifications to the current-phase relation due to the coupling to the two state system.

To conclude, let us mention a few directions in which the work presented in this thesis could be extended. The formalism developed here could be used to address other aspects of the low energy physics of CNTs and Rashba wires subject to SOI, for example transport in the presence of single or multiple impurities or the RKKY interaction in carbon nanotubes. Another interesting problem would be the study of SOI effects in a double-wall nanotube with an applied bias voltage between inner and outer tube. In principle, the spin-orbit coupling strength might be tuned as in the Rashba wire. We leave those interesting problems for the future.

A. Gaussian integration

A.1. Gaussian integration for symmetric, positive definite matrices

The following identity for multi-dimensional integrals over real variables holds for any symmetric matrix S with a positive hermitian part:

$$I\left(\underline{\underline{S}},\vec{J}\right) \equiv \int \frac{dx_1 \dots dx_n}{(2\pi)^{\frac{n}{2}}} e^{-\frac{1}{2}\sum_{i,j} x_i S_{ij} x_j + \sum_i x_i J_i} = [\det S]^{-\frac{1}{2}} e^{\frac{1}{2}\sum_{i,j} J_i S^{-1}_{ij} J_j}. \quad \text{(A.1)}$$

For real, symmetric matrices this identity can be checked in the following way: One changes the integration variables to reduce S to diagonal form and then makes use of the relation for the one-dimensional case:

$$\int_{-\infty}^{\infty} dx\, e^{-\alpha x^2} = \sqrt{\frac{\pi}{\alpha}},$$

which is valid for $\alpha > 0$. More explicitly: using the transformations $y_i = x_i - \sum_j S^{-1}_{ij} J_j$ and $z_k = \sum_i T^{-1}_{ki} y_i$ in Eq. A.1, where T is the orthogonal transformation that diagonalizes S, yields:

$$\begin{aligned}
\int \frac{dx_1 \dots dx_n}{(2\pi)^{\frac{n}{2}}} e^{-\frac{1}{2}\sum_{i,j} x_i S_{ij} x_j + \sum_i x_i J_i} &= e^{\frac{1}{2}\sum_{ij} J_i S^{-1}_{ij} J_j} \int \frac{dy_1 \dots dy_n}{(2\pi)^{\frac{n}{2}}} e^{-\frac{1}{2}\sum_{i,j} y_i S_{ij} y_j} \\
&= \frac{e^{\frac{1}{2}\sum_{ij} J_i S^{-1}_{ij} J_j}}{(2\pi)^{\frac{n}{2}}} \int dz_1 \dots dz_n\, e^{-\frac{1}{2}\sum_k \lambda_k z_k^2} \\
&= \frac{e^{\frac{1}{2}\sum_{ij} J_i S^{-1}_{ij} J_j}}{(2\pi)^{\frac{n}{2}}} \frac{1}{\sqrt{\prod_k \lambda_k}} \left(\sqrt{2\pi}\right)^n \\
&= \frac{e^{\frac{1}{2}\sum_{ij} J_i S^{-1}_{ij} J_j}}{\sqrt{\det[S]}}.
\end{aligned}$$

Note that, analogous to the one-dimensional case, all λ_k must be positive for the integrals to converge, thus positivity of S is essential.

A.2. Generalization to multiple fields

One can generalize the above Gaussian integration also to fields (see for example [1], [147]). For brevity, we will frequently use the notation $\vec{k} \equiv (k, \omega)$, $\vec{x} \equiv (x, \tau)$, such that

$\vec{k}\cdot\vec{x} = (kx + \omega\tau)$, where $\tau = it$ is the imaginary time and ω is the zero-temperature Matsubara frequency. We start with the Euclidean action:

$$S_E \equiv \frac{1}{2}\int d\vec{x}\vec{\Phi}^T \underline{\underline{S}}(\partial_x, \partial_\tau)\,\vec{\Phi}, \tag{A.2}$$

which becomes

$$S_E = \frac{1}{2}\int \frac{d\vec{k}}{(2\pi)^2}\vec{\Phi}^T\left(-\vec{k}\right)\underline{\underline{S}}\left(\vec{k}\right)\vec{\Phi}\left(\vec{k}\right) \tag{A.3}$$

in momentum space. Note that we directly used vectors of fields $\vec{\Phi} = (\phi_1, \theta_1, ..., \phi_n, \theta_n)$, so the discrete index i in Eq. (A.1) now becomes a mixture of continuous variables $\vec{x}$ or $\vec{q}$ and discrete labels. The matrix $\left(S_{ij}\right)$ then becomes an integral kernel containing differential operators. The *generating functional* is defined by

$$Z[\vec{\eta}] \equiv \int \mathscr{D}\vec{\Phi} e^{-S_E + \int d\vec{x}\vec{\eta}(\vec{x})\vec{\Phi}(\vec{x})}, \tag{A.4}$$

in coordinate space, or equivalently:

$$Z[\vec{\eta}] \equiv \int \mathscr{D}\vec{\Phi} e^{-S_E + \frac{1}{2}\int \frac{d\vec{k}}{(2\pi)^2}\left\{\vec{\eta}^\dagger\left(\vec{k}\right)\vec{\Phi}\left(\vec{k}\right) + \vec{\eta}\left(\vec{k}\right)\vec{\Phi}^\dagger\left(\vec{k}\right)\right\}}, \tag{A.5}$$

in momentum space. Note that by defining a field

$$\vec{\Phi}_0(\vec{x}) = \vec{\Phi}(\vec{x}) - \int d\vec{y}\,\underline{\underline{S}}^{-1}(\vec{x}-\vec{y})\,\vec{\eta}(\vec{y}),$$

where the *source fields* $\vec{\eta}$, just as $\vec{\Phi}$ are real fields (thus $\vec{\Phi}^*(\vec{q}) = \vec{\Phi}(-\vec{q})$ and same property for $\vec{\eta}$), one can formally complete the square in the argument of the exponential:

$$\begin{aligned} S'_E &\equiv -\frac{1}{2}\int d\vec{x}\vec{\Phi}_0^T(\vec{x})\,\underline{\underline{S}}(\partial_x, \partial_\tau)\,\vec{\Phi}_0(\vec{x}) \\ &= -S_E + \vec{\eta}(\vec{x})\cdot\vec{\Phi}(\vec{x}) - \frac{1}{2}\int d\vec{x}\int d\vec{y}\,\vec{\eta}^T(\vec{y})\,\underline{\underline{S}}^{-1}(\vec{x}-\vec{y})\,\vec{\eta}(\vec{x}), \end{aligned}$$

and obtain the equivalent to the r.h.s. of Eq. (A.1):

$$Z[\vec{\eta}] = Z[0]\, e^{\frac{1}{2}\int d\vec{x}\int d\vec{y}\,\vec{\eta}^T(\vec{y})\underline{\underline{S}}^{-1}(\vec{x}-\vec{y})\vec{\eta}(\vec{x})} \tag{A.6}$$

$$= Z[0]\, e^{\frac{1}{2}\int \frac{d\vec{q}}{(2\pi)^2}\vec{\eta}^T(-\vec{q})\underline{\underline{S}}^{-1}(\vec{q})\vec{\eta}(\vec{q})}, \tag{A.7}$$

where $Z[0]$ is the partition function. The inverse kernel is defined by:

$$\underline{\underline{S}}(\partial_x, \partial_\tau)\,\underline{\underline{S}}^{-1}(\vec{x}) \equiv \delta(\vec{x}),$$

and can conveniently be computed in momentum space $\underline{\underline{S}}^{-1}(\vec{x}) = \int \frac{d\vec{q}}{(2\pi)^2}\left(\underline{\underline{S}}^{-1}\right)(\vec{q})\, e^{i\vec{q}\cdot\vec{x}}$.

A.3. Bosonic correlation functions

Correlation functions of bosonic fields $\vec{\Phi}(\vec{q}) := (\phi_1, \theta_1, \ldots, \phi_n, \theta_n))$ can be computed by using the functional integral formalism:

$$\left\langle \Phi_\alpha(\vec{q}_1)\, \Phi^*_\beta(\vec{q}_2) \right\rangle \equiv \frac{1}{Z[0]} \int \mathscr{D}\left[\vec{\Phi}\right] \Phi_\alpha(\vec{q}_1)\, \Phi^*_\beta(\vec{q}_2)\, e^{-S_E[\vec{\Phi}]}.$$

The euclidean action is defined as the integral of the Lagrangian density $\mathscr{L}(\{\phi_n, \theta_n\})$, which is obtained from the Hamiltonian density by Legendre transform. We focus on quadratic Hamiltonian densities like the ones introduced in Chapters 2 and 3 and obtain (using $\Pi_k = -\partial_x \theta_k$)

$$\mathscr{H}(\{\phi_n, \theta_n\}) = \left(\partial_x \vec{\Phi}\right)^T \underline{\underline{H}} \left(\partial_x \vec{\Phi}\right) \longrightarrow \mathscr{L}(\{\phi_n, \theta_n\}) = \mathscr{H} + \sum_k (-i\partial_\tau \phi_k)(-\partial_x \theta_k).$$

The euclidean action can then be written as:

$$S_E\left[\vec{\Phi}\right] \equiv \int dx d\tau\, \mathscr{L}(\{\phi_n, \theta_n\}) = \int dx d\tau \sum_{\alpha,\beta} \Phi_\alpha(x,\tau)\, S_{\alpha,\beta}(\partial_x, \partial_\tau)\, \Phi_\beta(x,\tau),$$

where the Kernel $\underline{\underline{S}}(\partial_x, \partial_\tau) = \left\{\left(-\partial_x^2\right) \underline{\underline{H}} + (-i\partial_\tau \partial_x)\, \underline{\underline{B}}\right\}$[1] is bilinear in differential operators. One applies the usual recipe of going to momentum space to obtain algebraic expressions $S_{\alpha,\beta}(\partial_x \to ik, \partial_\tau \to i\omega)$ in order to write the euclidean action as an integral of an algebraic bilinear form

$$S_E\left[\vec{\Phi}\right] = \frac{1}{2} \int \frac{d\vec{k}}{(2\pi)^2}\, \vec{\Phi}^\dagger\left(\vec{k}\right) \underline{\underline{S}}\left(\vec{k}\right) \vec{\Phi}\left(\vec{k}\right). \tag{A.8}$$

The bosonic correlation functions in momentum space can be computed by functional differentiation of the generating functional in Eq. (A.5) with respect to the *source fields* $\vec{\eta}\left(\vec{k}\right) := (\eta_1, \eta_2, \ldots, \eta_n)$

$$\left\langle \Phi_\alpha(\vec{q}_1)\, \Phi^*_\beta(\vec{q}_2) \right\rangle \equiv \frac{(2\pi)^4}{Z[0]} \left. \frac{\delta^2 Z[\vec{\eta}]}{\delta \eta^*_\alpha(\vec{q}_1)\, \delta \eta_\beta(\vec{q}_2)} \right|_{\vec{\eta}=0}. \tag{A.9}$$

The generating functional can be written in Gaussian form $Z[\vec{\eta}] = Z[0]\, e^{\frac{1}{2}\int \frac{d\vec{q}}{(2\pi)^2}\, \vec{\eta}^\dagger \underline{\underline{S}}^{-1}(\vec{q})\, \vec{\eta}}$, thus the functional derivatives can be easily computed, yielding

$$\left\langle \Phi_\alpha(\vec{q})\, \Phi^*_\beta\left(\vec{q}'\right) \right\rangle = \left(\underline{\underline{S}}^{-1}\right)_{\alpha\beta}(\vec{q})\, (2\pi)^2\, \delta\left(k - k'\right) \delta\left(\omega - \omega'\right). \tag{A.10}$$

[1] where $\underline{\underline{B}} \equiv \begin{pmatrix} 0 & 1 \\ 1 & 0 \end{pmatrix} \otimes 1_n$

In our model, the fields $\Phi_\alpha(\vec{x})$ are real fields, thus $\Phi^*_\alpha\left(\vec{k}\right) = \Phi_\alpha\left(-\vec{k}\right)$, yielding:

$$\left\langle \Phi_\alpha(\omega,k)\,\Phi_\beta\left(\omega',k'\right)\right\rangle = \left(\underline{\underline{S}}^{-1}\right)_{\alpha\beta}(\omega,k)\,(2\pi)^2\,\delta\left(k+k'\right)\delta\left(\omega+\omega'\right) \quad \text{(A.11)}$$

Note that the correlators are diagonal in momentum space.

A.3.1. Diagonalization transformation

In the systems that we consider, there is a coupling between phase fields (and of course their respective conjugate momentum fields). While it is possible to directly invert the matrix $\underline{\underline{S}}$ in the euclidean action (Eq.(A.8)) to obtain the prefactors of the bosonic correlators, we prefer to take a different approach. In the two systems that we consider, it is possible to transform to fields in which the Hamiltonian is diagonal. This has the advantage that both the following derivation is simpler (since the matrix $\underline{\underline{S}}$ is then block-diagonal) and also the obtained expressions are simpler. We start from a Hamiltonian density $\mathscr{H}\left(\vec{\Phi}\right) = \left(\partial_x\vec{\Phi}\right)^T \underline{\underline{H}}\left(\partial_x\vec{\Phi}\right)$ with $\vec{\Phi} \equiv \left(\begin{array}{ccccccc}\phi_1 & ,..., & \phi_n & \theta_1 & ,..., & \theta_n\end{array}\right)$ and the symmetric (and positive) matrix $\underline{\underline{H}}$. We assume the existence of a *canonical* transformation:

$$\underline{\underline{U}}^T\,\underline{\underline{H}}\,\underline{\underline{U}} = diag\left(\frac{v_1}{K_1},...,\frac{v_n}{K_n};\,v_1K_1,...,v_nK_n\right) \equiv \underline{\underline{\hat{H}}}, \quad \text{(A.12)}$$

where $\underline{\underline{U}}$ additionally has to satisfy

$$\underline{\underline{J}} = \underline{\underline{U}}\,\underline{\underline{J}}\,\underline{\underline{U}}^T, \quad \text{(A.13)}$$

with $\underline{\underline{J}} = \begin{pmatrix} 0 & 1_n \\ -1_n & 0 \end{pmatrix}$, since the transformation has to preserve the *bosonic* commutation relations $\left[\Phi_\mu(\vec{x}),\,\Phi_\nu(\vec{x})\right]_- = J_{\mu,\nu}\frac{1}{2}sign(\vec{x}-\vec{y})$ (Transformations that satisfy this additional constraint are called *symplectic*). It can be shown that such a transformation always exists for real, symmetric and positive $2n\times 2n$ matrices.

A.3.2. Bosonic correlation functions in coordinate space

We work in the basis of fields $\hat{\vec{\phi}} = \underline{\underline{V}}\,\vec{\phi}$, where $\vec{\Phi} \equiv \left(\begin{array}{ccccccc}\phi_1, \theta_1 & ,..., & \phi_n, \theta_n\end{array}\right)$, in which the Hamiltonian is diagonal $\underline{\underline{\hat{h}}} = \underline{\underline{V}}^T\,\underline{\underline{h}}\,\underline{\underline{V}} = diag\left(\frac{v_1}{K_1},...,\frac{v_n}{K_n};\,v_1K_1,...,v_nK_n\right)$.

The correlations in coordinate-space are obtained by Fourier-transform[2] of Eq. (A.11):

$$\begin{aligned}\left\langle \Phi_\alpha(x,\tau)\,\Phi_\beta\left(x',\tau'\right)\right\rangle &= \int d\vec{q}\left(\underline{\underline{s}}^{-1}\right)_{\alpha\beta}(\vec{q})\,e^{i\vec{q}\cdot(\vec{x}-\vec{x}')} \\ &= \left(\underline{\underline{s}}^{-1}\right)_{\alpha\beta}\left(\vec{x}-\vec{x}'\right) \\ &= \left(\underline{\underline{V}}\,\underline{\underline{\hat{s}}}^{-1}\left(\vec{x}-\vec{x}'\right)\,\underline{\underline{V}}^T\right)_{,\alpha\beta}\end{aligned}$$

[2]Where $\int d\vec{q}... = \int\frac{dk}{2\pi}\,\frac{1}{\beta}\sum_{i\omega_n}...$ with $\omega_n = \frac{2\pi}{\beta}n$ for finite temperature and $\int d\vec{q}... = \int\frac{dq}{2\pi}\int\frac{d\omega}{2\pi}...$ for $T=0$.

where $\underline{\underline{\hat{s}}} = \underline{\underline{V}}^T \underline{\underline{s}} \underline{\underline{V}} = i\omega k \underline{\underline{b}} + \underline{\underline{\hat{h}}}$ has a block-diagonal form

$$\left(\underline{\underline{\hat{s}}}\right)^{-1} = \begin{pmatrix} (\hat{s}_1)^{-1} & 0\ldots 0 & 0 \\ \vdots & \ddots & \vdots \\ 0 & 0\ldots 0 & (\hat{s}_N)^{-1} \end{pmatrix}, \tag{A.14}$$

and each block is of the form $\hat{s}_j = \begin{pmatrix} \frac{v_j}{K_j} & i\frac{\omega}{k} \\ i\frac{\omega}{k} & v_j K_j \end{pmatrix}$. In coordinate space, this becomes:

$$\begin{aligned} \hat{s}_j^{-1}(\vec{x}) &= \int d\vec{q} \frac{e^{i\vec{q}\cdot\vec{x}}}{\omega^2 + v_j^2 k^2} \begin{pmatrix} v_j K_j & -i\frac{\omega}{k} \\ -i\frac{\omega}{k} & \frac{v_j}{K_j} \end{pmatrix} \\ &= I_1(x,\tau,v_j) \begin{pmatrix} K_j & 0 \\ 0 & \frac{1}{K_j} \end{pmatrix} + \begin{pmatrix} 0 & 1 \\ 1 & 0 \end{pmatrix} I_2(x,\tau,v_j), \end{aligned} \tag{A.15}$$

where the two integrals I_j are given by:

$$I_j(x,\tau,v) \equiv \int \frac{dk}{2\pi} e^{ikx} \frac{1}{\beta} \sum_{i\omega_n} \frac{e^{i\omega_n \tau}}{\omega_n^2 + (v|k|)^2} P_j(\omega,k),$$

with $P_1 = v$ and $P_2 = i\frac{\omega_n}{k}$.
Consider a function $g_0(z) = h(z) \prod_{n=1}^{N} \frac{1}{z - z_j}$, (where $z \in \mathbb{C}$ and h is entire and diverging slower than e^z at $|z| \to \infty$) a function with a finite number of simple poles. Performing the Matsubara-Summation, i.e. employing the residue calculus, yields

$$\frac{1}{\beta} \sum_{i\omega_n} g_0(z) = -\sum_n n_B(z_n) h(z_n) \prod_{m \neq n} \frac{1}{z_n - z_m}, \tag{A.16}$$

where $n_B(z) = \frac{1}{e^{\beta z} - 1}$ is the Bose-distribution function which has poles $i\omega_n = i\frac{2\pi}{\beta} n$ along the imaginary axis. Using this result, we obtain:

$$I_{1/2}(x,\tau,v) = \frac{1}{4\pi} \int_0^\infty dk' \frac{1}{k'} \left\{ \frac{e^{-k'(1-(\tau'+ix'))} + e^{-k'(\tau+ix')}}{1 - e^{-k'}} \pm x \to -x \right\},$$

where we defined $x' = \frac{x}{v\beta}$, $k' = vk\beta$ and $\tau' = \frac{\tau}{\beta}$. Note that this expression diverges for $x, \tau = 0$. To regularize the IR-divergence, one subtracts the divergent part, i.e. computes $I_{1/2}(x,\tau,v) - I_{1/2}(0,0,v)$, which is just the quantity we need, as we shall see in a moment. The resulting integral can be written as

$$\begin{aligned} I_{1/2}(x,\tau) - I_{1/2}(0,0) = -\frac{1}{4\pi} \int_0^\infty dk' \frac{e^{-\alpha' k'}}{k'} \Bigg\{ & \frac{\left(1 - e^{-k'(1-(ix'+\tau'))}\right)\left(1 - e^{-k'(ix'+\tau')}\right)}{1 - e^{-k'}} \\ & \pm x \to -x \Bigg\}. \end{aligned}$$

Note we introduced a UV-cutoff (where $\alpha = 0^+$ and $\alpha' = \frac{\alpha}{v\beta}$) to regularize the divergence at large momenta. This integral can be solved analytically (c.f. [148] 3.413 [3]) and after a bit of algebra, we obtain:

$$I_{1/2}(x,\tau) - I_{1/2}(0,0) = -\frac{1}{4\pi}\left[\ln\left[C(x,\tau,v)\right] \pm \ln\left[C(-x,\tau,v)\right]\right],$$

where $C(x,\tau,v) \equiv \frac{v\beta}{i\alpha\pi}\sinh\left[\frac{\pi}{v\beta}(x - i(v\tau+\alpha))\right]$. The bosonic correlation function in coordinate space for each block can then be readily derived from Eq. (A.14,A.15),

$$\hat{g}_l(x,t) \equiv \hat{s}_l^{-1}(x,t) - \hat{s}_l^{-1}(0,0) = -\frac{1}{4\pi}\sum_{\mu=\pm}\hat{f}_{l,\mu}\ln\left[C(x,t,v_l)\right], \tag{A.17}$$

where

$$\hat{f}_{l,\mu} = \begin{pmatrix} K_l & -\mu \\ -\mu & \frac{1}{K_l} \end{pmatrix}, \tag{A.18}$$

and we did the Wick rotation $\tau = it$, i.e. $C(x,t,v) \equiv \frac{v\beta}{-i\alpha\pi}\sinh\left(\frac{\pi}{v\beta}(x+\mu(vt - i\alpha sign(t)))\right)$. The total Green'sfunction is then a block-diagonal matrix composed of the $\underline{\underline{\hat{g}_l}}$

$$\underline{\underline{\hat{G}}}(x,t) = \underline{\underline{\hat{S}}}(x,t) - \underline{\underline{\hat{S}}}(0,0) = \begin{pmatrix} \hat{g}_1 & 0\ldots0 & 0 \\ \vdots & \ddots & \vdots \\ 0 & 0\ldots0 & \hat{g}_N \end{pmatrix}, \tag{A.19}$$

and $\underline{\underline{G}} \equiv \underline{\underline{V}}\,\underline{\underline{\hat{G}}}\,\underline{\underline{V}}^T$.

A.4. Correlation functions of vertex operators

Now that we have the bosonic building blocks, we can compute arbitrary correlation functions of exponentials of the boson fields (so-called vertex operators). An n-point correlation function of such an operator can be obtained by inserting the special source $\vec{\eta}(\vec{x}) = \sum_{j=1}^m \vec{n}^{(j)}\delta\left(\vec{x} - \vec{x}_j\right)$ into the generating functional in Eq. (A.4)[4]:

$$\begin{aligned} \frac{Z[i\vec{\eta}]}{Z[0]} &= \frac{1}{Z[0]}\int \mathscr{D}\vec{\Phi}\prod_{j=1}^n e^{i\vec{n}^{(j)}\cdot\vec{\Phi}(\vec{x}_1)}\, e^{-S_E} \\ &= \left\langle \prod_{j=1}^n e^{i\vec{n}^{(j)}\cdot\vec{\Phi}(\vec{x}_1)} \right\rangle. \end{aligned}$$

[3] $\int_0^\infty dx\, \frac{e^{-\mu x}}{x}\,\frac{\left(1-e^{-\beta x}\right)\left(1-e^{-\gamma x}\right)}{1-e^{-x}} = \ln\left[\frac{\Gamma(\mu)\Gamma(\beta+\gamma+\mu)}{\Gamma(\mu+\beta)\Gamma(\mu+\gamma)}\right]$
valid for $Re[\mu] > 0, Re[\mu] > -Re[\beta], Re[\mu] > -Re[\gamma], Re[\mu] > -Re[\beta+\gamma]$

[4] In the functional integral formalism, the operators are replaced by ordinary functions, thus $\left\langle \prod_{j=1}^n e^{i\vec{n}^{(j)}\cdot\vec{\Phi}(\vec{x}_1)} \right\rangle = \left\langle e^{i\sum_j \vec{n}^{(j)}\cdot\vec{\Phi}(\vec{x}_1)} \right\rangle$

Using the Gaussian integration formula Eq. (A.6), $\frac{Z[i\vec{\eta}]}{Z[0]}$ is easily evaluated:

$$\left\langle \prod_{j=1}^{n} e^{i\vec{n}^{(j)}\cdot\vec{\Phi}(\vec{x}_1)} \right\rangle = e^{-\frac{1}{2}\sum_{i,j}\left(\vec{n}^{(i)}\right)^T \underline{\underline{S}}^{-1}\left(\vec{x}_{ij}\right)\vec{n}^{(j)}}.$$

Defining a regularized correlation matrix $\underline{\underline{G}}(\vec{x}) \equiv \underline{\underline{S}}^{-1}(\vec{x}) - \underline{\underline{S}}^{-1}(0,0)$, this can be written as:

$$\begin{aligned}\left\langle \prod_{j=1}^{n} e^{i\vec{n}^{(j)}\cdot\vec{\Phi}(\vec{x}_1)} \right\rangle &= e^{-\frac{1}{2}\sum_{i,j}\left(\vec{n}^{(i)}\right)^T \left[\underline{\underline{G}}\left(\vec{x}_{ij}\right)+\underline{\underline{S}}^{-1}(0,0)\right]\vec{n}^{(j)}}, \\ &= e^{-\sum_{i<j}\left(\vec{n}^{(i)}\right)^T \left[\underline{\underline{G}}\left(\vec{x}_{ij}\right)\right]\vec{n}^{(j)}} e^{-\frac{1}{2}\left(\sum_i \vec{n}^{(i)}\right)^T \left[\underline{\underline{S}}^{-1}(0,0)\right]\left(\sum_j \vec{n}^{(j)}\right)}.\end{aligned}$$

Note that if the system length is assumed to be infinite, most elements of $\underline{\underline{S}}^{-1}(0,0)$ are divergent (see above), thus one must require that $\sum_i \vec{n}^{(i)} = 0$. This requirement is also called "charge neutrality condition". For two-point correlation functions, this becomes:

$$\left\langle e^{i\vec{n}\cdot\vec{\Phi}(\vec{x}_1)} e^{i\vec{m}\cdot\vec{\Phi}(\vec{x}_2)} \right\rangle = \delta_{\vec{n},-\vec{m}} \exp\left[\vec{n}^T \underline{\underline{G}}(\vec{x}_{12})\,\vec{n}\right].$$

Using the explicit form of $\underline{\underline{G}} = \underline{\underline{V}}\,\underline{\underline{\hat{G}}}\,\underline{\underline{V}}^T$ derived in the previous section (cf. Eq.(A.18-A.19), we can conveniently express $\underline{\underline{G}}$ in its block-diagonal form, while absorbing the change of basis into the vector $\vec{n} \to \hat{\vec{n}} = \underline{\underline{V}}^T\vec{n}$ that specifies the operator under consideration:

$$\begin{aligned}&\left\langle e^{i\sqrt{4\pi}\vec{n}\cdot\vec{\Phi}(\vec{x})} e^{i\sqrt{4\pi}\vec{m}\cdot\vec{\Phi}(0,0)} \right\rangle \\ &= \delta_{\vec{n},-\vec{m}} \exp\left[\sum_{l=1}^{N}\sum_{\mu=\pm} \Gamma_{l,\mu}\, \ln\left[C(\mu x, t, v_l)\right]\right], \\ &= \delta_{\vec{n},-\vec{m}} \prod_{l=1}^{N}\prod_{\mu=\pm}\left[\frac{v_l\beta}{-i\mu\alpha\pi}\sinh\left(\frac{\pi}{v_l\beta}\left(x+\mu\left(v_l t - i\alpha\, sign(t)\right)\right)\right)\right]^{-\Gamma_{l,\mu}}, \qquad \text{(A.20)}\end{aligned}$$

where the exponents $\Gamma_{l,\mu}$ of each mode have the simple form

$$\begin{aligned}\Gamma_{l,\mu} \equiv \hat{\vec{n}}_l^T\, \hat{f}_{l,\mu}\, \hat{\vec{n}}_l &= \begin{pmatrix} \hat{n}_{\phi_l} & \hat{n}_{\theta_l} \end{pmatrix} \begin{pmatrix} K_l & -\mu \\ -\mu & \frac{1}{K_l} \end{pmatrix} \begin{pmatrix} \hat{n}_{\phi_l} \\ \hat{n}_{\theta_l} \end{pmatrix} \\ &= \left(\hat{n}_{\phi_l} K_l^{\frac{1}{2}} - \mu\, \hat{n}_{\theta_l} K_l^{-\frac{1}{2}}\right)^2. \qquad \text{(A.21)}\end{aligned}$$

B. Bosonization formulae

The first goal of this appendix is to show that the bosonization formula

$$\psi_{nr}(x,t) = \frac{\eta_{nr}}{\sqrt{2\pi\alpha}} e^{ir\sqrt{4\pi}\phi_{nr}(x,t)}, \tag{B.1}$$

leads to the correct correlation functions and commutation relations for the free system, as was stated in Sec. 2.4. After that, we derive the identities needed to bosonize the two-channel Hamiltonian

$$H_0 = \sum_{n=A.B} \int dx \left\{ : \psi_{nR}^{\dagger}(-iv_n\partial_x)\psi_{nR} : + : \psi_{nL}^{\dagger}(iv_n\partial_x)\psi_{nL} : \right\}, \tag{B.2}$$

using the point-splitting technique. Those identities will then directly lead to the Hamiltonian Eq. (2.27).

Basic operator identities

One important tool is the following operator identity:

$$e^A e^B = : e^{A+B} : e^{\frac{1}{2}\langle 2AB+A^2+B^2\rangle}, \tag{B.3}$$

where $\langle ...\rangle$ is the bosonic vacuum expectation value, $: ... :$ denotes normal ordering and A and B are linear combinations of bosonic creation and destruction operators:

$$\begin{aligned} A &= \alpha a + \alpha' a^{\dagger}, \\ B &= \beta a + \beta' a^{\dagger}, \end{aligned}$$

This identity is derived (for example in [149]) by using the Campbell-Baker-Hausdorff formula:

$$e^C e^D = e^{C+D} e^{\frac{1}{2}[C,D]}, \tag{B.4}$$

$$\Rightarrow e^C e^D = e^D e^C e^{[C,D]}, \tag{B.5}$$

which also provides another useful relation. From Eq. (B.3), one can conclude that $\left\langle e^A e^B \right\rangle = e^{\frac{1}{2}\langle 2AB+A^2+B^2\rangle}$, because in the normal-ordered exponential all orders except the first contain a bosonic destruction operator that would act on the vacuum, thus $\left\langle : e^A : \right\rangle = 1$.

$$e^A e^B = : e^{A+B} : \left\langle e^A e^B \right\rangle, \tag{B.6}$$

The same relation also holds for time-ordered products of Operators, as long as $\langle ....\rangle$ is replaced by the time-ordered average:

$$T_t\, e^A e^B \;=\; :e^{A+B}: \left\langle T_t\, e^A e^B \right\rangle. \tag{B.7}$$

B.1. Correlation functions

In the fermionic picture, one obtains the following correlation function for right-moving fermions:

$$\begin{aligned}
\left\langle \psi^\dagger_{nR}(x)\,\psi_{nR}(0)\right\rangle &= \int \frac{dk}{2\pi}\, e^{-ikx} e^{-\alpha|k|} \left\langle FS \left| c^\dagger_{nR}(k)\, c_{nR}(k) \right| FS \right\rangle \\
&= \int \frac{dk}{2\pi}\, e^{-ikx}\, e^{-\alpha|k|}\, \theta(-k) \\
&= \int_{-\infty}^{0} \frac{dk}{2\pi}\, e^{-ik(x+i\alpha)} \\
&= \frac{1}{2\pi}\,\frac{i}{x+i\alpha},
\end{aligned}$$

where $|FS\rangle$ denotes the Fermi-sea. The calculation for left-movers is similar, yielding $\left\langle \psi^\dagger_{nL}(x)\,\psi_{nL}(0)\right\rangle = \frac{1}{2\pi}\frac{-i}{x-i\alpha}$. Because of the linear dispersion relation of the Dirac Hamiltonian Eq. (B.2), it is obvious that one obtains the correlation functions $\left\langle \psi^\dagger_{nr}(x,t)\,\psi_{nr}(0)\right\rangle = \frac{1}{2\pi}\frac{ir}{x-rv_nt+ir\alpha}$ from the equal time correlators by replacing x with $x-rv_nt$, and the fermionic time-ordered Green's function for the free system by replacing and α with $\alpha\, sign(t)$ in the above expressions, yielding:

$$G^T_{0,nr}(x,t) \;=\; \frac{ir}{2\pi}\,\frac{1}{x-rv_nt+ir\alpha\, sign(t)}.$$

The same quantity can be computed in the bosonic picture using Eq. (2.35) for $K=1$

$$\begin{aligned}
G^T_{0,nr}(x,t) &= \frac{sign(t)}{2\pi\alpha}\left\langle T_t\, e^{ir\sqrt{4\pi}\phi_{nr}(x,t)} e^{-ir\sqrt{4\pi}\phi_{nr}(0,0)}\right\rangle \\
&= \frac{ir}{2\pi}\,\frac{1}{x-rv_nt+ir\alpha\, sign(t)}.
\end{aligned} \tag{B.8}$$

B.2. Commutation relations

Using Eq. (B.7) and Eq. (B.8), it is straightforward to derive:

$$T_t\, e^{-ir\sqrt{4\pi}\phi_{nr}(x,t)} e^{ir\sqrt{4\pi}\phi_{nr}(0,0)} \;=\; \frac{+ir\alpha\, sign(t)\,:e^{-ir\sqrt{4\pi}[\phi_{nr}(x,t)-\phi_{nr}(0,0)]}:}{x-rv_nt+ir\alpha\, sign(t)}. \tag{B.9}$$

When evaluating equal-time products one has to take care as to choose the right sign, i.e. $A(x,0)B(x,0) = T_t A(x,t=0^+)B(x,0)$ and $B(x,0)A(x,0) = \pm T_t A(x,t=0^-)B(x,0)$ where the upper (lower) sign is for bosonic (fermionic) operators. We can use this expression to evaluate products of fermionic operators ψ_{nr} in bosonized form. We start by computing equal-time commutation relations:

$$\begin{aligned}
\left\{\psi_{nr}^\dagger(x_1),\psi_{nr}(x_2)\right\} &= \lim_{\alpha\to 0}\frac{\eta_{nr}^2}{2\pi\alpha}T_t\left[e^{-ir\sqrt{4\pi}\phi_{nr}\left(x,t=0^+\right)}e^{ir\sqrt{4\pi}\phi_{nr}(0,0)}\right.\\
&\qquad\left.+e^{-ir\sqrt{4\pi}\phi_{nr}\left(x,t=0^-\right)}e^{ir\sqrt{4\pi}\phi_{nr}(0,0)}\right]\\
&= \lim_{\alpha\to 0}\frac{1}{2\pi\alpha}:e^{-ir\sqrt{4\pi}[\phi_{nr}(x_1)-\phi_{nr}(x_2)]}:\left[\frac{ir\alpha}{x_{12}+ir\alpha}+\frac{-ir\alpha}{x_{12}-ir\alpha}\right]\\
&= \lim_{\alpha\to 0}\frac{1}{\pi}:e^{-ir\sqrt{4\pi}[\phi_{nr}(x_1)-\phi_{nr}(x_2)]}:\frac{\alpha}{{x_{12}}^2+\alpha^2}\\
&= \frac{1}{\pi}:e^{-ir\sqrt{4\pi}[\phi_{nr}(x_1)-\phi_{nr}(x_2)]}:\pi\,\delta(x_1-x_2)\\
&= \delta(x_1-x_2).
\end{aligned}\tag{B.10}$$

In line 2, identity (B.9) was used. $\frac{\alpha}{x_{12}^2+\alpha^2}\overset{(\alpha\to 0)}{\longrightarrow}\pi\,\delta(x_1-x_2)$ was used in the third line.

The anticommutation relations $\left\{\psi_{nr}(x_1),\psi_{n',r'}^\dagger(x_2)\right\}=0$ for fermions that have different branch or chirality index are provided by the Klein-factors, since the bosonic field operators and thus also their exponentials (cf. Eq. (B.5)) commute for $n,r\neq n',r'$

$$\begin{aligned}
\left\{\psi_{nr}^\dagger(x_1),\psi_{n'r'}(x_2)\right\} &= \frac{1}{2\pi\alpha}\left[\eta_{nr}\eta_{n'r'}e^{-ir\sqrt{4\pi}\phi_{nr}(x_1)}e^{ir'\sqrt{4\pi}\phi_{n'r'}(x_2)}\right.\\
&\qquad\left.+\eta_{n'r'}\eta_{nr}e^{ir'\sqrt{4\pi}\phi_{n'r'}(x_2)}e^{-ir\sqrt{4\pi}\phi_{nr}(x_1)}\right]\\
&= \frac{1}{2\pi\alpha}\left[\eta_{nr}\eta_{n'r'}+\eta_{n'r'}\eta_{nr}\right]e^{-ir\sqrt{4\pi}\phi_{nr}(x_1)}e^{ir'\sqrt{4\pi}\phi_{n'r'}(x_2)}\\
&= 0.
\end{aligned}$$

B.3. Point Splitting

When bringing together two operators at the same point, there's no guarantee that the product will have finite matrix elements in the vacuum as the points approach each other. For small distances, one can use Taylor-expansion, but only *within* the normal ordering symbol, as only normal ordered operators have finite matrix elements that can also be differentiated. Furthermore, products of bosonic operators inside the normal ordering symbol do commute and thus the ϕ_{nr} can be treated as mere functions:

$$\begin{aligned}
:e^{c[\phi_{nr}(x_1)-\phi_{nr}(x_2)]}: &= 1+x_{12}:c\left(\partial_x\phi_{nr}\right)(x_1):\\
&\quad+\frac{1}{2}x_{12}^2:\left[c^2\left(\partial_x\phi_{nr}\right)^2+c\left(\partial_x^2\phi_{nr}\right)\right](x_1):+\mathscr{O}\left(x_{12}^3\right).
\end{aligned}\tag{B.11}$$

Using the previous formula, we can compute products of fermionic operators at equal points, defined by a limiting procedure called *point splitting*:

$$\psi_{nr}^{\dagger}(x)\left(\partial_x^i\right)\psi_{nr}(x) \equiv \lim_{x_{12}\to 0}\partial_{x_2}^i\left[\psi_{nr}^{\dagger}(x_1)\,\psi_{nr}(x_2)\right],$$

where $i = 0,1,2,\ldots$.

Densities

Using Eq. (B.9) and Eq. (B.11), one arrives at:

$$\begin{aligned}
\lim_{x_1\to x_2}\psi_{nr}^{\dagger}(x_1)\,\psi_{nr}(x_2) &= \lim_{x_1\to x_2}\lim_{\alpha\to 0}\frac{\eta_{nr}^2}{2\pi\alpha}\left[e^{-ir\sqrt{4\pi}\phi_{nr}(x_1)}e^{ir\sqrt{4\pi}\phi_{nr}(x_2)}\right]\\
&= \lim_{x_1\to x_2}\lim_{\alpha\to 0}\frac{1}{2\pi\alpha}\left[:e^{-ir\sqrt{4\pi}[\phi_{nr}(x_1)-\phi_{nr}(x_2)]}:\frac{ir\alpha}{x_{12}+ir\alpha}\right]\\
&= \lim_{x_1\to x_2}\lim_{\alpha\to 0}\frac{1}{2\pi}:e^{-ir\sqrt{4\pi}\left[x_{12}\partial_x\phi_{nr}(x_1)+\mathscr{O}\left(x_{12}^2\right)\right]}:\frac{ir}{x_{12}+ir\alpha}\\
&= \lim_{x_1\to x_2}\lim_{\alpha\to 0}\frac{ir}{2\pi}\frac{:1-ir\sqrt{4\pi}\left[x_{12}\partial_x\phi_{nr}(x_1)\right]+\mathscr{O}\left(x_{12}^2\right):}{x_{12}+ir\alpha}\\
&= \lim_{x_1\to x_2}\lim_{\alpha\to 0}\underbrace{\frac{ir}{2\pi}\frac{1}{x_{12}+ir\alpha}}+\lim_{x_1\to x_2}:\frac{1}{\sqrt{\pi}}\partial_x\phi_{nr}(x_1)+\mathscr{O}(x_{12}):\\
&= \left\langle T_t\,\psi_{n,r}^{\dagger}(x_1)\,\psi_{n,r}(x_2)\right\rangle.
\end{aligned}$$

The terms of higher order in x_{12} *inside* the normal ordering symbol now really are small and can be dropped at $x_{12}\to 0$, as the matrix elements of the field operators inside the normal ordering are finite. Note that because α represents a smallest lengthscale in the system, it must be set to zero *before* performing the $x_{12}\to 0$-limit, the two limits do not commute. While this can safely be done in all terms of the form $\frac{x_{12}^n}{x_{12}+ir\alpha}$ $n\geq 1$, taking both limits in the first term yields a divergent C- number piece. This merely reflects the infinite number of fermions in each branch, which is a consequence of the unbounded spectrum of the Dirac Hamiltonian. Defining a normal ordered density, in which this vacuum average is removed, one finds that it has a nice limit in the continuum:

$$:\psi_{nr}^{\dagger}\psi_{nr}:(x) = \frac{1}{\sqrt{\pi}}\partial_x\phi_{nr}(x). \tag{B.12}$$

Kinetic term

Next we focus on the kinetic term in the Hamiltonian. We use Eq. (B.9) again to obtain:

$$\begin{aligned}
\lim_{x_1\to x_2}\psi_{nr}^{\dagger}(x_1)\left(-ir\partial_{x_2}\right)\psi_{nr}(x_2) &= \lim_{x_1\to x_2}\left(-ir\partial_{x_2}\right)\left[\psi_{nr}^{\dagger}(x_1)\,\psi_{nr}(x_2)\right]\\
&= \lim_{x_1\to x_2}\left(-ir\partial_{x_2}\right)\frac{1}{2\pi\alpha}\frac{ir\alpha:e^{-ir\sqrt{4\pi}[\phi_{nr}(x_1)-\phi_{nr}(x_2)]}:}{x_{12}+ir\alpha}.
\end{aligned}$$

Because of the derivative, one has to first expand to 2nd order in Eq. (B.11), next take the derivative with respect to x_2 and finally send the cutoff to zero before taking the limit $x_1 \to x_2$ in every nonsingular term. In that way, one obtains:

$$\begin{aligned}\lim_{x_1\to x_2}\partial_{x_2}\frac{:e^{c[\phi_{nr}(x_1)-\phi_{nr}(x_2)]}:}{x_{12}+ir\alpha} &= \lim_{x_1\to x_2}\partial_{x_2}\left\{\frac{1}{x_{12}+ir\alpha}+\frac{x_{12}}{x_{12}+ir\alpha}:c\left(\partial_x\phi_{nr}\right)(x_1):\right.\\ &\left.+\frac{1}{2}\frac{x_{12}^2}{x_{12}+ir\alpha}:\left[c^2\left(\partial_x\phi_{nr}\right)^2+c\left(\partial_x^2\phi_{nr}\right)\right](x_1):+\mathscr{O}\left(x_{12}^3\right)\right\}\\ &= \lim_{x_1\to x_2}\frac{1}{\left(x_{12}+ir\alpha\right)^2}-\frac{1}{2}\left[c^2\left(\partial_x\phi_{ir}\right)^2+c\left(\partial_x^2\phi_{ir}\right)\right](x_1),\end{aligned}$$

where $c=-ir\sqrt{4\pi}$. The kinetic term finally reads:

$$\begin{aligned}\lim_{x_1\to x_2}\psi_{nr}^{\dagger}(x_1)\left(-ir\partial_{x_2}\right)\psi_{nr}(x_2) &= \lim_{x_1\to x_2}\frac{1}{2\pi}\frac{1}{\left(x_{12}+ir\alpha\right)^2}\\ &+\left(\partial_x\phi_{ir}\right)^2(x_1)+\frac{ir}{\sqrt{\pi}}\left(\partial_x^2\phi_{ir}\right)(x_1).\end{aligned}$$

The first term is a divergent $\mathbb{C}$- number piece, the vacuum average. The $\left(\partial_x^2\phi_{ir}\right)$ in the third term is a total derivative that does not contribute to the Hamiltonian. Just as before, one defines the normal ordered quantity, in which the vacuum average is removed:

$$:\psi_{nr}^{\dagger}\left(-ir\partial_x\right)\psi_{nr}:(x,\tau) = \left(\partial_x\phi_{ir}\right)^2(x,\tau). \tag{B.13}$$

Bibliography

[1] A.O. Gogolin, A.A. Nersesyan, and A.M. Tsvelik, *Bosonization and Strongly Correlated Systems* (Cambridge University Press, Cambridge, 1998).

[2] R. Egger and A.O. Gogolin, Phys. Rev. Lett. **79**, 5082 (1997); Eur. Phys. J. B **3**, 281 (1998); C. Kane, L. Balents, and M.P.A. Fisher, Phys. Rev. Lett. **79**, 5086 (1997).

[3] M. Bockrath *et al.*, Nature **397**, 598 (1999); Z. Yao, H.W.C. Postma, L. Balents, and C. Dekker, Nature **402**, 273 (1999); B. Gao, A. Komnik, R. Egger, D.C. Glattli, and A. Bachtold, Phys. Rev. Lett. **92**, 216804 (2004).

[4] H. Ishii *et al.*, Nature **426**, 540 (2003).

[5] F. Kuemmeth, S. Ilani, D.C. Ralph, and P.L. McEuen, Nature **452**, 448 (2008).

[6] R. Winkler, *Spin-Orbit Coupling Effects in Two-Dimensional Electron and Hole Systems* (Springer, Berlin, 2003).

[7] D.V. Bulaev, B. Trauzettel, and D. Loss, Phys. Rev. B **77**, 235301 (2008); B. Wunsch, Phys. Rev. B **79**, 235408 (2009); A. Secchi and M. Rontani, Phys. Rev. B **80**, 041404(R) (2009).

[8] T. Ando, J. Phys. Soc. Jpn. **69**, 1757 (2000).

[9] A. De Martino, R. Egger, K. Hallberg, and C.A. Balseiro, Phys. Rev. Lett. **88**, 206402 (2002).

[10] A. De Martino, R. Egger, F. Murphy-Armando, K. Hallberg, J. Phys. Cond. Matt. **16**, S1437 (2004).

[11] L. Chico, M.P. Lopez-Sancho, and M.C. Munoz, Phys. Rev. Lett. **93**, 176402 (2004); Phys. Rev. B **79**, 235423 (2009).

[12] A. De Martino and R. Egger, J. Phys. Cond. Matt. **17**, 5523 (2005).

[13] D. Huertas-Hernando, F. Guinea, and A. Brataas, Phys. Rev. B **74**, 155426 (2006).

[14] J. Zhou, Q. Liang, and J. Dong, Phys. Rev. B **79**, 195427 (2009).

[15] O.M. Auslaender *et al.*, Science **308**, 88 (2005); Y. Jompol *et al.*, Science **325**, 597 (2009).

[16] W. Izumida, K. Sato, and R. Saito, J. Phys. Soc. Jpn. **78**, 074707 (2009).

[17] J.S. Jeong and H.W. Lee, Phys. Rev. B **80**, 075409 (2009).

[18] For reviews, see: T. Ando, J. Phys. Soc. Jpn. **74**, 777 (2005); J.C. Charlier, X. Blase, and S. Roche, Rev. Mod. Phys. **79**, 677 (2007).

[19] A. De Martino, R. Egger, and A.M. Tsvelik, Phys. Rev. Lett. **97**, 076402 (2006).

[20] W. DeGottardi, T.-C. Wei, and S. Vishveshwara, Phys. Rev. B **79**, 205421 (2009).

[21] T. Giamarchi, Quantum Physics in One Dimension (Clarendon Press, Oxford, 2004).

[22] A. Schulz, A. De Martino, P. Ingenhoven, and R. Egger, Phys. Rev. B **79**, 205432 (2009).

[23] A. Schulz, *Interaction and phonon effects in quantum wires with spin-orbit coupling*, Diplomarbeit, Heinrich-Heine-Universität Düsseldorf, 2007.

[24] T. Kimura, K. Kuroki, and H. Aoki, Phys. Rev. B **53**, 9572 (1996).

[25] V. Meden and K. Schönhammer, Phys. Rev. B **46**, 15753 (1992); Phys. Rev. B **47**, 16205 (1993); J. Voit, Phys. Rev. B **47** 6740 (1993).

[26] A.V. Moroz, K.V. Samokhin, and C.H.W. Barnes, Phys. Rev. Lett. **84**, 4164 (2000); Phys. Rev. B **62**, 16900 (2000).

[27] A. De Martino and R. Egger, Europhys. Lett. **56**, 570 (2001).

[28] M. Governale and U. Zülicke, Phys. Rev. B **66**, 073311 (2002).

[29] W. Häusler, Phys. Rev. B **70**, 115313 (2004).

[30] V. Gritsev, G.I. Japaridze, M. Pletyukhov, and D. Baeriswyl, Phys. Rev. Lett. **94**, 137207 (2005).

[31] J. Sun, S. Gangadharaiah, and O.A. Starykh, Phys. Rev. Lett. **98**, 126408 (2007).

[32] I. Zutic, J. Fabian, and S. Das Sarma, Rev. Mod. Phys. **76**, 323 (2004).

[33] S. Datta and B. Das, Appl. Phys. Lett. **56**, 665 (1990).

[34] Y.A. Bychkov and E.I. Rashba, J. Phys. C **17**, 6039 (1984).

[35] M. Governale and U. Zülicke, Phys. Rev. B **66**, 073311 (2002).

[36] M. Governale and U. Zülicke, Solid State Comm. **131**, 581 (2004).

[37] A.V. Moroz, K.V. Samokhin, and C.H.W. Barnes, Phys. Rev. Lett. **84**, 4164 (2000).

[38] A.V. Moroz, K.V. Samokhin, and C.H.W. Barnes, Phys. Rev. B **62**, 16900 (2000).

[39] W. Häusler, Phys. Rev. B **63**, 121310(R) (2001).

[40] A. Iucci, Phys. Rev. B **68**, 075107 (2003).

[41] W. Häusler, Phys. Rev. B **70**, 115313 (2004).

[42] A.V. Moroz and C.H.W. Barnes, Phys. Rev. B **60**, 14272 (1999).

[43] A.V. Moroz and C.H.W. Barnes, Phys. Rev. B **61**, R2464 (2000).

[44] E.A. de Andrada e Silva and G.C. La Rocca, Phys. Rev. B **67**, 165318 (2003).

[45] S.L. Erlingsson, J.C. Egues, and D. Loss, phys. stat. sol. (c) **3**, 4317 (2006).

[46] C.A. Perroni, D. Bercioux, V. Marigliano Ramaglia, and V. Cataudella, J. Phys.: Cond. Matt. **19**, 186227 (2007).

[47] T. Kimura, K. Kuroki, and H. Aoki, Phys. Rev. B **53**, 9572 (1996).

[48] M.A. Ruderman and C. Kittel, Phys. Rev. **96**, 99 (1954); T. Kasuya, Prog. Theor. Phys. **16**, 45 (1956); K. Yosida, Phys. Rev. **106**, 893 (1957).

[49] C. Kittel, Sol. State Phys. **22**, 1 (1968); Y. Yafet, Phys. Rev. B **36**, 3948 (1987).

[50] H. Imamura, P. Bruno, and Y. Utsumi, Phys. Rev. B **69**, 121303(R) (2004).

[51] P. Lyu, N.-N. Liu, and C. Zhang, J. Appl. Phys. **102**, 103910 (2007).

[52] J. Simonin, Phys. Rev. Lett. **97**, 266804 (2006).

[53] R. Egger and H. Schoeller, Phys. Rev. B **54**, 16337 (1996); K. Hallberg and R. Egger, Phys. Rev. B **55**, R8646 (1997).

[54] R. Shankar, *Renormalization Group approach to interacting Fermions*, Rev. Mod. Phys. **66**, 129 (1994).

[55] O.A. Starykh, D.L. Maslov, W. Häusler, and L.I. Glazman, in *Interactions and Quantum Transport Properties of Lower Dimensional Systems*, Lecture Notes in Physics, Springer (Proceedings of the International WEH Workshop, July 1999, Hamburg).

[56] J. Cardy, *Scaling and renormalization in statistical physics*, (Cambridge University Press, 1996).

[57] K.A. Muttalib and V.J. Emery, Phys. Rev. Lett. **57**, 1370 (1986).

[58] W.H.A. Thijssen, D. Djukic, A.F. Otte, R.H. Bremmer, and J.M. van Ruitenbeek, Phys. Rev. Lett. **97**, 226806 (2006).

[59] L.I. Glazman and K.A. Matveev, JETP Lett. **49**, 659 (1989)

[60] J.A. van Dam, Yu.V. Nazarov, E.P.A.M. Bakkers, S. De Franceschi, and L.P. Kouwenhoven, Nature (London) **442**, 667 (2006).

[61] J.-P. Cleuziou, W. Wernsdorfer, V. Bouchiat, T. Ondarcuhu, and M. Monthioux, Nature Nanotechnology **1**, 53 (2006).

[62] M.L. Della Rocca, M. Chauvin, B. Huard, H. Pothier, D. Esteve, and C. Urbina, Phys. Rev. Lett. **99**, 127005 (2007).

[63] H. Shiba and T. Soda, Prog. Theor. Phys. **41**, 25 (1969).

[64] B.I. Spivak and S.A. Kivelson, Phys. Rev. B **43**, 3740 (1991).

[65] O. Zachar, Phys. Rev. B **61**, 95 (2000).

[66] D. Matsumoto, J. Phys. Soc. Jpn. **70**, 492 (2001).

[67] T. Novotný, A. Rossini, and K. Flensberg, Phys. Rev. B **72**, 224502 (2005).

[68] H.I. Jorgensen, T. Novotný, K. Grove-Rasmussen, K. Flensberg, and P.E. Lindelof, Nano Lett. **7**, 2441 (2007).

[69] A.I. Buzdin, Rev. Mod. Phys. **77**, 935 (2005).

[70] F.S. Bergeret, A.F. Volkov, and K.B. Efetov, Rev. Mod. Phys. **77**, 1321 (2005).

[71] J. Sköldberg, T. Löfwander, V.S. Shumeiko, and M. Fogelström, Phys. Rev. Lett. **101**, 087002 (2008).

[72] A. Zazunov, R. Egger, C. Mora, and T. Martin, Phys. Rev. B **73**, 214501 (2006).

[73] A.V. Danilov, S.E. Kubatkin, S.G. Kafanov, K. Flensberg, and T. Bjørnholm, Nano Lett. **6**, 2184 (2006).

[74] S.Y. Quek, M. Kamenetska, M.L. Steigerwald, H.J. Choi, S.G. Louie, M.S. Hybertsen, J.B. Neaton, and L. Venkataraman, preprint arXiv:0901.1139.

[75] A. Donarini, M. Grifoni, and K. Richter, Phys. Rev. Lett. **97**, 166801 (2006).

[76] A. Mitra and A.J. Millis, Phys. Rev. B **76**, 085342 (2007).

[77] P. Lucignano, G.E. Santoro, M. Fabrizio, and E. Tosatti, Phys. Rev. B **78**, 155418 (2008).

[78] H. Bruus and K. Flensberg, *Many-Body Quantum Theory in Condensed Matter Physics*. Oxford Graduate Texts, New York: Oxford University press, 1st ed., 2004

[79] A. Altland and Ben Simons, *Condensed Matter Field Theory*, Cambridge, UK ; New York : Cambridge University Press, 2006.

[80] A.A. Golubov, M.Yu. Kupriyanov, and E. Il'ichev, Rev. Mod. Phys. **76**, 411 (2004).

[81] L.I. Glazman and K.A. Matveev, JETP Lett. **49**, 659 (1989); A.V. Rozhkov and D.P. Arovas, Phys. Rev. Lett. **82**, 2788 (1999); E. Vecino, A. Martín-Rodero, and A.L. Yeyati, Phys. Rev. B **68**, 035105 (2003); F. Siano and R. Egger, Phys. Rev. Lett. **93**, 047002 (2004); M.S. Choi, M. Lee, K. Kang, and W. Belzig, Phys. Rev. B **70**, 020502(R) (2004).

[82] J.X. Zhu, Z. Nussinov, A. Shnirman, and A.V. Balatsky, Phys. Rev. Lett. **92**, 107001 (2004); Z. Nussinov *et al.*, Phys. Rev. B **71**, 214520 (2005); M. Lee, T. Jonckheere, and T. Martin, Phys. Rev. Lett. **101**, 146804 (2008).

[83] A. Zazunov *et al.*, Phys. Rev. Lett. **90**, 087003 (2003); A. Zazunov, V.S. Shumeiko, G. Wendin, and E.N. Bratus', Phys. Rev. B **71**, 214505 (2005).

[84] B. Andrei Bernevig, J. Orenstein, and S.-C. Zhang, Phys. Rev. Lett. **97**, 236601 (2006).

[85] J. Nitta, T. Akazaki, H. Takayanagi, and T. Enoki, Phys. Rev. Lett. **78**, 1335 (1997).

[86] G. Engels, J. Lange, Th. Schäpers, and H. Lüth, Phys. Rev. B **55**, R1958 (1997).

[87] D. Grundler, Phys. Rev. Lett. **84**, 6074 (2000).

[88] Y. Kato, R.C. Myers, A.C. Gossard, and D.D. Awschalom, Nature **427**, 50 (2004).

[89] J. Schäfer, C. Blumenstein, S. Meyer, M. Wisniewski, and R. Claessen, Phys. Rev. Lett. **101**, 236802 (2008).

[90] T. Kaneko, M. Koshino, and T. Ando, Phys. Rev. B **78**, 245303 (2008).

[91] Y.V. Pershin, J.A. Nesteroff, and V. Privman, Phys. Rev. B **69**, 121306(R) (2004).

[92] J. Knobbe and Th. Schäpers, Phys. Rev. B **71**, 035311 (2005).

[93] R.G. Pereira and E. Miranda, Phys. Rev. B **71**, 085318 (2005).

[94] S. Debald and B. Kramer, Phys. Rev. B **71**, 115322 (2005).

[95] L. Serra, D. Sanchez, and R. Lopez, Phys. Rev. B **72**, 235309 (2005).

[96] X.F. Wang, Phys. Rev. B **69**, 035302 (2004).

[97] S. Kettemann, Phys. Rev. Lett. **98**, 176808 (2007).

[98] M. Scheid, M. Kohda, Y. Kunihashi, K. Richter, and J. Nitta, Phys. Rev. Lett. **101**, 266401 (2008).

[99] S. Gangadharaiah, J. Sun, and O.A. Starykh, Phys. Rev. B **78**, 054436 (2008).

[100] Y. Yu, Y. Wen, J. Li, Z. Su, and S.T. Chui, Phys. Rev. B **69**, 153307 (2004).

[101] H.C. Lee and S.R. Eric Yang, Phys. Rev. B **72**, 245338 (2005).

[102] F. Cheng and G. Zhou, J. Phys.: Cond. Matt. **19**, 136215 (2007).

[103] P. Devillard, A. Crepieux, K.I. Imura, and T. Martin, Phys. Rev. B **72**, 041309(R) (2005).

[104] M. Zarea and N. Sandler, Phys. Rev. Lett. **99**, 256804 (2007).

[105] A. Nitzan and M.A. Ratner, Science **300**, 1384 (2003).

[106] N.J. Tao, Nature Nanotechnology **1**, 173 (2006).

[107] A.Yu. Kasumov, R. Deblock, M. Kociak, B. Reulet, H. Bouchiat, I.I. Khodos, Yu.B. Gorbatov, V.T. Volkov, C. Journet, and M. Burghard, Science **284**, 1508 (1999).

[108] A. Morpurgo, J. Kong, C.M. Marcus, and H. Dai, Science **286**, 263 (1999).

[109] B. Reulet, A.Yu. Kasumov, M. Kociak, R. Deblock, I.I. Khodos, Yu.B. Gorbatov, V.T. Volkov, C. Journet, and H. Bouchiat, Phys. Rev. Lett. **85**, 2829 (2000).

[110] M.R. Buitelaar, T. Nussbaumer, and C. Schönenberger, Phys. Rev. Lett. **89**, 256801 (2002).

[111] M.R. Buitelaar, W. Belzig, T. Nussbaumer, B. Babic, C. Bruder, and C. Schönenberger, Phys. Rev. Lett. **91**, 057005 (2003).

[112] Y.-J. Doh, J.A. van Dam, A.L. Roest, E.P.A.M. Bakkers, L.P. Kouwenhoven, and S. De Franceschi, Science **309**, 272 (2005).

[113] A.Yu. Kasumov, K. Tsukagoshi, M. Kawamura, T. Kobayashi, Y. Aoyagi, K. Senba, T. Kodama, H. Nishikawa, I. Ikemoto, K. Kikuchi, V.T. Volkov, Yu.A. Kasumov, R. Deblock, S. Gueron, and H. Bouchiat, Phys. Rev. B **72**, 033414 (2005).

[114] H.I. Jorgensen, K. Grove-Rasmussen, T. Novotný, K. Flensberg, and P.E. Lindelof, Phys. Rev. Lett. **96**, 207003 (2006).

[115] J. Xiang, A. Vidan, M. Tinkham, R.M. Westervelt, and C.M. Lieber, Nature Nanotech. **1**, 208 (2006).

[116] P. Jarillo-Herrero, J.A. van Dam, and L.P. Kouwenhoven, Nature (London) **439**, 953 (2006).

[117] M. Chauvin, P. vom Stein, D. Esteve, C. Urbina, J.C. Cuevas, and A. Levy Yeyati, Phys. Rev. Lett. **99**, 067008 (2007).

[118] A. Eichler, M. Weiss, S. Oberholzer, C. Schönenberger, A. Levy Yeyati, J.C. Cuevas, and A. Martin-Rodero, Phys. Rev. Lett. **99**, 126602 (2007).

[119] T. Sand-Jespersen, J. Paaske, B.M. Andersen, K. Grove-Rasmussen, H.I. Jorgensen, M. Aagesen, C.B. Sorensen, P.E. Lindelof, K. Flensberg, and J. Nygard, Phys. Rev. Lett. **99**, 126603 (2007).

[120] A. Marchenkov, Z. Dai, B. Donehoo, R.H. Barnett, and U. Landman, Nature Nanotech. **2**, 481 (2007).

[121] F. Wu, R. Danneau, P. Queipo, E. Kauppinen, T. Tsuneta, and P.J. Hakonen, Phys. Rev. B **79**, 073404 (2009).

[122] A. Eichler, R. Deblock, M. Weiss, C. Karrasch, V. Meden, C. Schönenberger, and H. Bouchiat, arXiv:0810.1671.

[123] A.V. Rozhkov and D.P. Arovas, Phys. Rev. Lett. **82**, 2788 (1999).

[124] A.A. Clerk and V. Ambegaokar, Phys. Rev. B **61**, 9109 (2000).

[125] E. Vecino, A. Martin-Rodero, and A.L. Yeyati, Phys. Rev. B **68**, 035105 (2003).

[126] F. Siano and R. Egger, Phys. Rev. Lett. **93**, 047002 (2004).

[127] M.S. Choi, M. Lee, K. Kang, and W. Belzig, Phys. Rev. B **70**, 020502(R) (2004).

[128] G. Sellier, T. Kopp, J. Kroha, and Y.S. Barash, Phys. Rev. B **72**, 174502 (2005).

[129] C. Karrasch, A. Oguri, and V. Meden, Phys. Rev. B **77**, 024517 (2008).

[130] T. Meng, P. Simon, and S. Florens, arXiv:0902.1111.

[131] J.X. Zhu, Z. Nussinov, A. Shnirman, and A.V. Balatsky, Phys. Rev. Lett. **92**, 107001 (2004).

[132] Z. Nussinov, A. Shnirman, D.P. Arovas, A.V. Balatsky, and J.X. Zhu, Phys. Rev. B **71**, 214520 (2005).

[133] M. Lee, T. Jonckheere, and T. Martin, Phys. Rev. Lett. **101**, 146804 (2008).

[134] A. Zazunov, D. Feinberg, and T. Martin, Phys. Rev. Lett. **97**, 196801 (2006).

[135] A. Zazunov, A. Schulz, and R. Egger, Phys. Rev. Lett. **102**, 047002 (2009).

[136] N.J. Tao, Nature Nanotechnology **1**, 173 (2006).

[137] A.A. Golubov, M.Yu. Kupriyanov, and E. Il'ichev, Rev. Mod. Phys. **76**, 411 (2004).

[138] A.I. Buzdin, Rev. Mod. Phys. **77**, 935 (2005); F.S. Bergeret, A.F. Volkov, and K.B. Efetov, *ibid.* **77**, 1321 (2005).

[139] T. Novotny, A. Rossini, and K. Flensberg, Phys. Rev. B **72**, 224502 (2005); J. Sköldberg, T. Löfwander, V.S. Shumeiko, and M. Fogelström, Phys. Rev. Lett. **101**, 087002 (2008).

[140] A. Zazunov, R. Egger, C. Mora, and T. Martin, Phys. Rev. B **73**, 214501 (2006); A. Zazunov, D. Feinberg, and T. Martin, Phys. Rev. Lett. **97**, 196801 (2006).

[141] A.V. Danilov *et al.*, Nano Lett. **6**, 2184 (2006).

[142] A. Donarini, M. Grifoni, and K. Richter, Phys. Rev. Lett. **97**, 166801 (2006); A. Mitra and A.J. Millis, Phys. Rev. B **76**, 085342 (2007).

[143] P. Lucignano, G.E. Santoro, M. Fabrizio, and E. Tosatti, Phys. Rev. B **78**, 155418 (2008).

[144] W. Zhang and X. Zhang, Prog. Polymer Sci. **28**, 1271 (2003).

[145] F. Hekking and Yu.V. Nazarov, Phys. Rev. B **44**, 11506 (1991); L.Y. Gorelik *et al.*, Phys. Rev. Lett. **75**, 1162 (1995); D.V. Averin and A. Bardas, *ibid.* **75**, 1831 (1995).

[146] A.L. Yeyati, A. Martín-Rodero, and E. Vecino, Phys. Rev. Lett. **91**, 266802 (2003).

[147] J. Zinn Justin, *Quantum Field Theory and Critical Phenomena,* (Clarendon Press, Oxford, 1996).

[148] I.S.Gradsteyn and I.M. Ryzhik, *Table of Integrals, Series and Products* (Academic Press, 2000).

[149] R. Shankar, Bosonization: *How to make it work for you in condensed matter*, Acta. Phys. Pol. B **26**, 1835 (1995).

Danksagung

An dieser Stelle danke ich allen, die mich beim Anfertigen dieser Arbeit unterstützt haben.
Ich danke Prof. Dr. Reinhold Egger für die Betreuung meiner Arbeit. Durch die vorgeschlagenen Themen konnte ich viele neue physikalische Zusammenhänge verstehen und neue Methode erlernen. Mein Dank auch für seine stete Hilfsbereitschaft und Unterstützung in allen Aspekten dieser Arbeit.
Bei Frau Prof. Dr. Dagmar Bruß bedanke ich mich für die Koreferenz dieser Arbeit.
Ich danke Alessandro De Martino, Alex Zazunov und Roland Hützen für die sorgfältige Durchsicht des Manuskripts.
Ich möchte mich bei allen gegenwärtigen und ehemalige Mitarbeitern meiner Arbeitsgruppe am Institut für Theoretische Physik IV für ihre Hilfsbereitschaft bedanken, vor allem danke ich Alex Zazunov, Roland Hützen, Stephan Weiss und Jens Eckel für die vielen anregenden und nützlichen Diskussionen im Umfeld meiner Arbeit.
Mein besonderer Dank gilt hierbei Alessandro De Martino für viele interessante und bereichernde Diskussionen sowie seine stete Hilfsbereitschaft (*You got five minutes, Alessandro?*).
Bei den restlichen Mitgliedern der Arbeitsgruppe möchte ich mich ebensfalls bedanken: Jens Bremer, Karin Wildhagen, Tomi Panaanen sowie bei meinem Mitbewohner Arthur Hütten.
Ich möchte mich auch bei meinen Freunden Herbert und Oswald bedanken für ihre Kameradschaft und Unterstützung.
Mein besonderer Dank gilt meiner Familie: Meinen Eltern Karin und Wilfried Schulz, und meiner Schwester Susanne für ihre Unterstützung in alle Abschnitten meiner Promotion.

Erklärung

Die hier vorgelegte Dissertation habe ich eigenständig und ohne unerlaubte Hilfe angefertigt. Die Dissertation wurde in der vorgelegten oder ähnlicher Form noch bei keiner anderen Institution eingereicht. Ich habe bisher keine erfolglosen Promotionsversuche unternommen.

Düsseldorf, den 22.05.2010

(Andreas Schulz)